UCGE Reports
Number 20186

Department of Geomatics Engineering

On-The-Fly GPS Ambiguity Resolution with Inertial Aiding

(URL: http://www.geomatics.ucalgary.ca/links/GradTheses.html)

by

Huming Wu

July 2003

THE UNIVERSITY OF CALGARY

On-The-Fly GPS Ambiguity Resolution with Inertial Aiding

by

Huming Wu

A THESIS
SUBMITTED TO THE FACULTY OF GRADUATE STUDIES
IN PARTIAL FULLIMENT OF REQUIREMENTS FOR THE DEGREE OF
MASTER OF SCIENCE

DEPARTMENT OF GEOMATICS ENGINEERING

CALGARY, ALBERTA

JULY, 2003

ABSTRACT

Ambiguity resolution is the key to precise positioning applications with GPS (Global Positioning System) carrier phase measurements. The objective of this research is to investigate the feasibility of integrating high quality inertial data into GPS On-the-Fly (OTF) ambiguity resolution and cycle slip detection. A key factor to an ambiguity search procedure is the accuracy of the float ambiguities. The superior navigation accuracy over the short term provided by a high quality INS (Inertial Navigation System) can improve the precision of the initial float ambiguities, and the integration of inertial data into the ambiguity filtering process can yield more accurate float ambiguities and thus facilitate the integer search procedure. In this thesis, inertial aiding in the FASF (Fast Ambiguity Search Filtering) ambiguity resolution is examined in theory under three INS/GPS integration scenarios: loose and tight coupling integration in a decentralized filter structure, and an augmented master filter integration in a centralized filter structure. The ambiguity dilution precision (ADOP), which measures the accuracy of the float ambiguities and the size of the search space, is investigated. To evaluate the performance of the algorithms proposed in the thesis two data sets are processed and results are analyzed. It is found that the ADOP is significantly reduced with INS data in all three integration schemas as long as the GPS outage period is less than 30 seconds. The time to fix integers is reduced on average 30% - 70% depending on the GPS outage period and the INS/GPS integration strategy. Results also show that tightly coupling and centralized integration outperform the loose coupling approach.

ACKNOWLEDGEMENTS

Firstly, I would like to express my heartfelt thanks and deepest gratitude to my supervisor, Dr. Elizabeth Cannon for her continuous encouragement, guidance and confidence in me throughout my 5-year graduate studies. Without her support, this thesis would not have been possible.

Secondly, I would like to thank Drs. Gérard Lachapelle, Yang Gao and Ed Nowicki, members of my examining committee. Their efforts in reading through this thesis are greatly apprericated.

Thirdly, I would like to take this opportunity to thank Dr. Bruno Scherzinger for his advice on the project, and Applanix Corporation for providing data and funding for this project.

Fourthly, I would like to also thank many fellow students, JiHong Zhang, Ning Luo, JunHan Keong, Xiangxian Liao, Junjie Liu, Rakesh Nayak, Mark Petovello and Jayanta Ray, many of whom have graduated from this department. All of their help and friendship are greatly appreciated.

Finally, and most of all, I would like to thank my parents and especially my wife, Qing, who is always there to support and encourage me.

TABLE OF CONTENTS

LIST OF TABLES

LIST OF FIGURES

LIST OF NOTATION

A, B	Design matrices
$b_i (i = 1,2,3)$	Accelerometer bias vector in the body frame
c	Speed of light
C_l	Covariance matrix of the observations
dt	Satellite clock error
dT	Receiver clock error
$d_i (i = 1,2,3)$	Gyro drift vector in the body frame
d_{ion}	Ionospheric effect
d_{trop}	Tropospheric effect
$d\rho$	Orbital error
E	Skew-symmetric matrix
H	Design matrix
H_0	Null hypothesis
H_1	Alternative hypothesis
p	Pseudorange measurement
P	Error covariance matrix of the state vector
Q	Process noise covariance matrix
R	Measurement covariance matrix
R_b^l	Rotation matrix
$\hat{r}$	Residuals

ϕ	Carrier phase measurement
Φ_k	State transition matrix
ρ	Geometric range between GPS satellite and receiver antenna
λ	Carrier phase wavelength
N	Carrier phase integer ambiguity
ε_p	Pseudorange measurement noise
ε_ϕ	Carrier phase measurement noise
γ	Normal gravity
$\delta\varepsilon_r$	Roll misalignment
$\delta\varepsilon_p$	Pitch misalignment
$\delta\varepsilon_H$	Heading misalignment
$\delta\varphi$	Latitude error
$\delta\lambda$	Longitude error
δh	Height error
δv_n	North velocity error
δv_e	East velocity error
δv_h	Vertical velocity error
x_k	State vector
Ω	Sum of squared residuals
z_k	Measurement vector

LIST OF ABBREVIATIONS

AMF	Augmented Master Filter
2DRMS	Two Dimension Root Mean Square
ADOP	Ambiguity Dilution of Precision
AFM	Ambiguity Function Method
C/A code	Coarse Acquisition Code
DD	Double Difference
DGPS	Differential Global Positioning System
DoD	Department of Defense
DOP	Dilution of Precision
FASF	Fast Ambiguity Search Filtering
FLYKIN	On the Fly Ambiguity Resolution and Kinematic Positioning
GPS	Global Positioning System
IMU	Inertial Measurement Unit
INS	Inertial Navigation System
JPO	Joint Program Office
KF	KALMAN Filter
LAMBDA	Least Squares AMBiguity Decorrelation Adjustment
LS	Least Squares
OTF	On The Fly
P code	Precise Code
RCSR	Recursive Computation of the Search Range
PDOP	Position Dilution of Precision

PRN	Pseudo Random Number
RMS	Root Mean Square
RX	Receiver
SA	Selective Availability
SD	Single Difference
SF	Scale Factor
SOS	Sum of Squares
TEC	Total Electron Content
VCV	Variance-Covariance
WL	Widelane
ZUPT	Zero Velocity Update

CHAPTER 1

INTRODUCTION AND OBJECTIVES

1.1 Background and Objectives

The Navstar Global Positioning System (GPS) is an all–weather, radio frequency (RF) satellite navigation system established by the U.S. Department of Defense (Parkinson et al., 1995). It offers different levels of positioning accuracies with code and carrier phase measurements. When used in differential mode, carrier phase measurements have to be used in order to achieve accuracies at the centimetre level; however, they contain an unknown number of integer cycles called ambiguities. Correct determination of these integer ambiguities is a prerequisite for accurate and reliable positioning.

Ambiguity resolution has been a research area since the 1980s, and it has attracted more researchers after GPS became operational in 1994. A number of techniques have been developed for on–the–fly (OTF) ambiguity resolution, among them are the ambiguity function technique (Remondi, 1984), the LAMBDA method (Teunissen, 1993; 1997), and the fast ambiguity search filter (FASF) technique (Chen, 1993; Chen and Lachapelle, 1994). The major difficulties in fixing ambiguities are twofold. First, resolved ambiguities are integers, which makes it difficult to directly use some standard parameter estimation methods, such as least squares, since the optimization procedure typically results in a float solution (i.e. real-valued ambiguities). Thus a search to find the integers among all potential candidates has to be conducted. The second difficulty in ambiguity resolution is due to the various error sources affecting GPS measurements. Examples of

common error sources include atmosphere effects, multipath and receiver noise, just to name a few. The degradation of GPS measurements makes it difficult to estimate accurate positions and float ambiguity solutions, which can impact the search procedure to fix integers quickly and reliably. However, for many real-time applications, resolving ambiguities reliably and quickly is typically a requirement. These last two requirements are of a conflicting nature since there is usually a trade-off between the time to fix and reliability.

The double difference (DD) technique is usually applied to carrier phase measurements to eliminate or reduce common error sources such as atmospheric effects, orbit errors and the satellite clock bias. Although most common errors are minimized in this mode, errors due to multipath and the atmospheric errors over long baselines, may still be significant. Also in the presence of high dynamics, cycle slips frequently occur due to the loss of phase lock in the receivers which may require the resolution procedure to restart. Cycle slips have to be detected and recovered correctly in order to maintain correct ambiguities. Due to the line-of-sight attribute of GPS signals, it is common that there are situations where there are no GPS measurements available, or the number of observed satellites is less than four, so that no position solution can be achieved. Such cases affect the reliability of using GPS as a stand-alone positioning method.

An Inertial Navigation System (INS) is a self-contained navigation system which does not require any external signals and can thus provide a continuous navigation solution (Britting, 1971). However, the position drifts due to the gyro and accelerometer biases if the INS is operated in stand-alone mode (Britting, 1971). Although the positioning

accuracy from an INS degrades over time, an INS of good quality can offer superior positioning accuracy over the short time, which creates the possibility of including inertial data into GPS ambiguity resolution. Therefore the integration of an INS and GPS can provide a reliable and accurate positioning system (Cannon, 1991). The incorporation of inertial measurements with GPS to resolve ambiguities and to recover cycle slips has been investigated (Schwarz et al, 1994; Skaloud, 1999; Scherzinger, 2000; 2002; Petovello et al, 2001; Petovello 2003). It has been demonstrated that the time and reliability of ambiguity resolution can be improved by including inertial data (Skaloud 1999, Scherzinger 2002, Petovello 2003).

The research of this thesis is aimed to study the feasibility of using navigation grade inertial data to resolve ambiguities within the FASF framework by evaluating the algorithm theoretically and by processing real data sets. The objectives of the research are as follows:

- Investigate the feasibility of INS aiding in GPS ambiguity resolution and cycle slip recovery using different INS/GPS integration architectures. The ambiguity resolution algorithm is based upon the FASF implementation in FLYKIN^{TM} developed at University of Calgary (Chen, 1993).
- Develop a software package based on FLYKIN^{TM} and an INS/GPS integration program developed in the Department of Geomatics Engineering, University of Calgary to implement the proposed method.

- Test and evaluate the effectiveness of the proposed method by processing and analyzing data sets. Sample data sets are provided by the Applanix Corporation, and consist of two land vehicle tests.

1.2 Thesis Outline

The thesis is composed of eight chapters. Chapter 2 gives an overview on the positioning principles of GPS and INS as well as the error sources in GPS positioning. It also describes the algorithm to perform INS coarse and fine alignments. Different INS/GPS integration strategies which are used in the software package are also presented and discussed.

Chapter 3 discusses principles of GPS ambiguity resolution. Different ambiguity search techniques are discussed with a focus on the LAMBDA (Least Squares AMBiguity Decorrelation Adjustment) and FASF methods.

Chapter 4 contains a thorough description of the INS aiding methodology for GPS ambiguity resolution. Three INS aiding approaches in GPS ambiguity resolution are presented from a theoretical point of view, as well as from the implementation aspect within the FASF framework.

Chapter 5 gives a description of the FLYKIN™ based software design. Various program modules as well as the input and output of the software are presented.

Chapter 6 contains a complete description of two tests and INS/GPS integration results to verify the quality of INS/GPS integration algorithms implemented in the software package.

Chapter 7 provides results of ambiguity resolution with inertial aiding using the software package. By analyzing the results the performance of the proposed method is evaluated.

Conclusions and recommendations based on this thesis research are provided in Chapter 8.

CHAPTER 2

GPS AND INS FUNDAMENTALS

2.1 GPS Concepts

2.1.1 Basic Concepts

The Navigation System with Timing And Ranging (NAVSTAR) Global Positioning System (GPS) is a satellite-based radio-navigation system developed and maintained by the Joint Program Office (JPO), which is directed by the U.S. Department of Defense (DoD). The GPS was developed to satisfy requirements for the military forces to accurately and instantaneously determine their position, velocity, and time in a common reference coordinate system anywhere on or near the Earth on a continuous basis (Parkinson et al., 1995). The system is composed of three parts, the space segment consisting of satellites that broadcast signals, the control segment steering the worldwide system and the user segment including the many types of GPS receivers available.

Currently there are twenty-seven satellites (24 + 3 spares) in the Space Segment deployed in six orbital planes with an inclination of 55 degree, an altitude of approximately 20,000 km and a period of about 12 sidereal hours (GPS SPS Performance Standard, 2001). This constellation of satellites provides global and continuous GPS coverage at any time of the day. Each satellite in the constellation continuously broadcasts signals on two L-band carrier phase frequencies, one is L1 frequency at 1575.42 MHz (λ=19 cm) and the other is the L2 frequency at 1227.6 MHz (λ=24 cm). Two pseudo-random noise (PRN) codes, which are used to obtain the pseudorange from each satellite to the receiver, are

modulated onto these two base carriers. The first code, C/A–code (Coarse/Acquisition code) is modulated only on L1, while the second code, P-code (Precise code) is modulated on both the L1 and L2 carriers. In addition to the PRN codes, the navigation message consisting of information such as satellite ephemeris, satellite clock bias and satellite status is also modulated onto the L1 and L2 carriers.

The Control Segment comprises of the Operational Control System that consists of a master control station, worldwide monitor stations, and ground control stations. The main operational task of the control segment is to track the satellites, determine satellite orbits, upload the navigation message, and to control the satellites (GPS SPS Performance Standard, 2001).

The User Segment is basically different types of GPS receivers, which uses the GPS satellite signals to determine user's position, velocity and time. Originally GPS was designated for military use, but since the system was deployed, it has been used in the civilian community for various applications such as conducting land and geodetic control surveys, and fleet management and control in the cities (Hofmann-Wellenhof et al., 1997).

2.1.2 Positioning Principle with GPS Observables

The fundamental GPS observables are pseudorange, carrier phase and the instantaneous Doppler frequency. The pseudorange is measured by comparing the replica of the C/A-code generated in the receiver with the code transmitted from the satellite to determine

the time shift through an autocorrelation analysis. The carrier phase measurement is the accumulated phase offset between the receiver reference signal and the received satellite signal. Therefore the initial number of integer cycles in the carrier phase is unknown (Wells et al., 1987). The unknown integers are the so-called ambiguities.

The basic pseudorange and carrier phase observation equations can be expressed as follows (Lachapelle, 1998):

$$p = \rho + d\rho + c(dt - dT) + d_{ion} + d_{trop} + \varepsilon_p \tag{2.1}$$

$$\phi = \rho + d\rho + c(dt - dT) + \lambda N - d_{ion} + d_{trop} + \varepsilon_\phi \tag{2.2}$$

where

p is the pseudorange measurement (m),

ϕ is the carrier phase measurement (m),

ρ is the range between GPS satellite and receiver (m),

$d\rho$ is the orbital error (m),

c is the speed of light (m/s),

dt is the satellite clock error (s),

dT is the receiver clock error (s),

λ is the carrier phase wavelength (m),

N is the carrier phase integer ambiguities (cycle),

d_{ion} is the ionospheric effect (m),

d_{trop} is the tropospheric effect (m), and

$\varepsilon_p, \varepsilon_\phi$ are the measurement noise and multipath (m) on the pseudorange and carrier phase, respectively.

Due to various error sources in equation (2.1) single point positioning is inaccurate, however, a type of differenced observation can be formed to reduce some common error sources. By subtracting measurements at a reference station from measurements at a user receiver for the same satellite, the satellite clock error, dt, will be removed. Such a single differenced observation also reduces the orbit and atmospheric errors. The positioning equations with the single differenced observation can be formed as follows (Lachapelle, 1998):

$$\Delta p = \Delta\rho + \Delta d\rho - c\Delta dT + \Delta d_{ion} + \Delta d_{trop} + \varepsilon_{\Delta p} \tag{2.3}$$

$$\Delta\phi = \Delta\rho + \Delta d\rho - c\Delta dT + \lambda\Delta N - \Delta d_{ion} + \Delta d_{trop} + \varepsilon_{\Delta\phi} \tag{2.4}$$

where Δ is the single difference (between receivers) operator.

By further taking the difference between measurements from a base satellite and measurements at other satellites, double differenced observations can be obtained. The positioning equations for the double differenced observables are (Lachapelle, 1998):

$$\nabla\Delta p = \nabla\Delta\rho + \nabla\Delta d\rho + \nabla\Delta d_{ion} + \nabla\Delta d_{trop} + \varepsilon_{\nabla\Delta p} \tag{2.5}$$

$$\nabla\Delta\phi = \nabla\Delta\rho + \nabla\Delta d\rho + \lambda\nabla\Delta N - \nabla\Delta d_{ion} + \nabla\Delta d_{trop} + \varepsilon_{\nabla\Delta\phi} \tag{2.6}$$

where ∇ is the single difference (between satellites) operator such that $\nabla\Delta$ is the double difference operator.

The above equations eliminate the satellite and receiver clock errors, and reduce atmospheric and orbital errors as a function of separation between the reference and user receivers.

Equation (2.6) is generally used in applications where a high positioning accuracy is required. However in order to use equation (2.6) the double differenced ambiguity $\nabla\Delta N$ needs to be resolved. Positioning with the fixed ambiguities (integers) has an accuracy at the few centimetre level (Lachapelle et al., 2000). For short baselines (<10 km), the main errors that affect the ambiguity resolution are carrier phase multipath and receiver noise. However ionospheric and atmospheric errors will become significant for long baselines (Lu, 1995; Raquet et al., 1998).

2.1.3 GPS Errors

As indicated in the above section, GPS measurements are subject to many error sources. These error sources are briefly discussed below.

Ionospheric Error

The ionosphere is the layer of the atmosphere ranging from about 50 km to 1000 km where free electrons exist. The ionospheric delay on GPS signals is proportional to the total electron content (TEC) along the signal path and inversely proportional to the squared frequency (Lachapelle, 1998). The equation relating carrier phase error to the ionosphere is given as follows (Lachapelle, 1998):

$$I = -\frac{40.3}{f^2}\text{TEC} \tag{2.7}$$

where

I is error in carrier phase due to ionosphere, and

f is frequency of the L1 or L2 carrier.

The TEC values in the equation depend on the rate of ionization, recombination and transport processes (Skone, 2001). The rate of ionization is a function of the solar activity, which follows cycles of approximately 11 years (Klobuchar, 1996). The value of TEC also varies diurnally. The diurnal maximum occurs at about 2:00 pm local time and and the minimum usually occurs just before the sunrise (Liao, 2000). It has been observed that TEC increases by a factor of three during a solar maximum versus solar minimum (Klobuchar et al., 1995). The latest solar maximum occurred during year 2000-2001. The data set used in this thesis was collected in late 2000, which means ionospheric error should be significant in the data.

The ionospheric effect is correlated with the baseline length between the base and remote receivers. For a large separation between the base station and the remote receiver, the ionospheric effect on GPS positions can be quite significant. The ionosphere error can be on the order of 2-50 metres in single point positioning mode and can be reduced by using the double differential technique to 0.5 – 2 ppm (Lachapelle, 1998). Since the ionospheric delay on GPS carrier frequencies is dispersive, a special linear combinations of L1 and L2 carrier phase measurements can be formed to eliminate the first order of the ionosphere effect (Hofmann-Wellenhof et al., 1997). Recent research has also shown that

the ionosphere delay can be well estimated in a wide area GPS network or a regional GPS network by using interpolation or least squares collocation (Raquet, 1998).

Tropospheric Error

The troposphere is the lowest part of the atmosphere and it reaches a height of about 10 km (Spilker, 1996). It is electrically neutral and non-dispersive for frequencies as high as 15 GHz. The tropospheric delay consists of two parts, the dry and wet components, and is affected by temperature, humidity, and pressure. The dry delay constitutes around 80-90% of the total error and it can be modeled to an accuracy of 1% or better (Raquet, 1998). The wet delay only contributes 10-20% of the total delay, but it is difficult to model accurately. Due to its non-dispersive effect, dual frequency data cannot be used to compute the delay. Various models have been developed to estimate the tropospheric delay, and the best known include the Hopfield model (Hopfield, 1969) and the Saastamoinen model (Saastamoinen, 1973). Similar to the method of handling ionospheric error over the short baselines double differenced observations can be used to reduce the tropospheric effect to 0.1 – 1 ppm (Lachapelle, 1998).

Orbital error

Orbital error is caused by the discrepancies between the actual positions of the satellites and the predicted positions from the broadcast ephemeris. The orbital errors can range from 3 to 8 metres, and by applying the double differential technique, as shown in

Equation (2.5), the orbital errors can be greatly reduced to 0.1-0.5 ppm (Lachapelle, 1998). Precise ephemeris can be used in post-mission applications to achieve better absolute accuracies, which can be less than 10 centimetres (Zumberge and Bertiger, 1996).

Multipath error

Multipath is the phenomena whereby a signal arrives at an antenna via two or more different paths (Ray, 2000). Multipath effects are generally specific to antenna and receiver architectures and depend on the surrounding environment. Multipath affects both the carrier phase and code measurements. Generally code multipath error can be on the order of 0.1-3 metres and is much larger than carrier phase multipath, which typically ranges from 0.1-3 cm (Lachapelle, 1998). In the static mode, multipath is non-Gaussian in nature and shows sinusoidal oscillations due to satellite geometry changes. In the dynamic mode, multipath behaves more randomly because of the combinations of vehicle movement and satellite geometry change. For short baselines, the carrier phase multipath error is usually the most significant error source that affects ambiguity resolution (Shi and Cannon, 1995). Special antenna designs, such as choke rings and multipath limiting antennas, can mitigate multipath effects. Recent research has shown that multipath can be also reduced by using a multi-antenna system along with a Kalman filtering technique (Ray, 2000).

Receiver Noise

Receiver noise is usually caused by high frequency thermal noise and the effects of dynamic stresses on a receiver's tracking loop (Spilker, 1994). It is usually considered as white noise as it is uncorrelated over time. The typical psedorange measurement noise is approximately 0.1 to 3 m on the C/A-code and 0.2 – 2 mm on the carrier phase measurement (Lachapelle, 1998). With differential corrections the receiver noise increases by $\sqrt{2}$, and double differences have a noise amplification of two due to the two differencing steps.

2.2 INS Concepts

Inertial Navigation Systems (INS) made their appearance in commercial aviation in the late sixties and have been extensively used in intercontinental navigation and in-flight control systems (Salychev, 1998). Their distinctive characteristic is the capability for autonomous navigation in any environment. They operate without reference to an external signal and therefore are not affected by atmospheric conditions, line-of-sight obstructions or underwater or underground operation.

The principle of inertial navigation is based on Newton's first and second laws of motion (Britting, 1971). By measuring vehicle acceleration in an inertial frame of reference, integrating it with respect to time and transforming it to the navigation frame, velocity, attitude and position differences in the navigation frame can be obtained. Sensors used to implement such a system are accelerometers that measure specific force and gyroscopes

for the realization of an inertial frame of reference. Since specific force measurements contain the effect of the gravity field of the earth, a gravity model is needed to extract vehicle acceleration from the measurements. Because typical INS employs three translational and three rotational sensors, it can be used for positioning as well as for attitude sensing.

There are three main types of INS, namely the space-stabilized system, the local-level system and the strapdown system (Schmidt, 1978). The INS system used in this research is a strapdown system which is described in the following section.

2.2.1 INS Mechanization

A strapdown navigation system contains three accelerometers and three rate gyroscopes, which measure the projections of specific force and absolute angular velocity, respectively, on their sensitive axes. In the strapdown INS these sensors are fixed in an Inertial Measurement Unit (IMU), and measurements are only available in the body frame. The direction cosine matrix between the body frame and the navigation frame needs to be computed analytically.

In order to realize stand-alone INS navigation, a series of mechanization equations have to be implemented (Schmidt, 1978). Different computational frames can be chosen based on the specific application and INS used (e.g. strapdown, platform). In this thesis, the wander azimuth frame was chosen as the computational frame while the local-level frame

was chosen as the navigation frame (Schwarz and Wei, 1999). The algorithmic flowchart is shown in Figure 2.1.

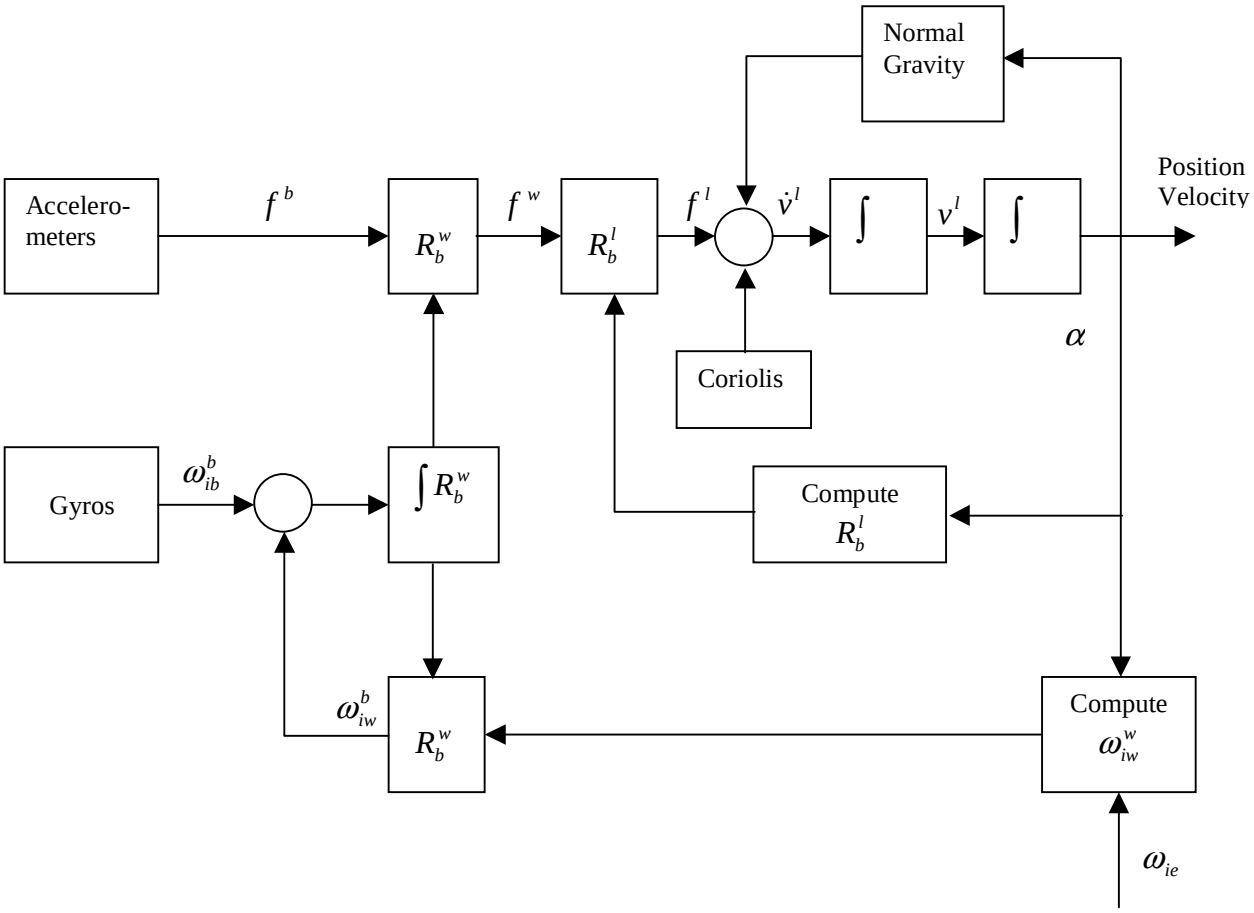

Figure 2.1 Wander Azimuth Frame INS Mechanization (Schwarz and Wei, 1999)

2.2.2 Coarse Alignment

The purpose of the alignment phase is to establish an initial rotation matrix relating the body axes to the wander frame. The body frame in the algorithm adopts right (x) – forward (y) – up (z) axes as demonstrated below:

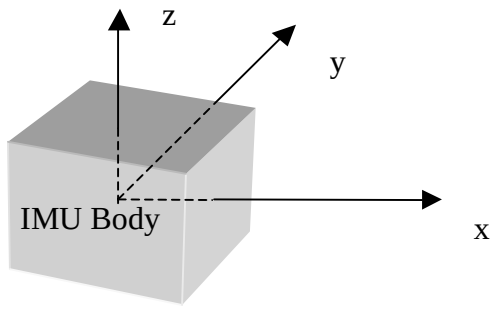

Figure 2.2 Body Axis

An alignment has two steps: coarse alignment and fine alignment. The coarse alignment is to obtain the approximate attitude, which will be fed into the fine alignment procedure to improve the attitude accuracy (Salychev, 1998).

Coarse alignment uses the fact that in static mode the gyros and accelerometers only sense the motion of the earth and the normal gravity and the following are assumed:

a. Pitch, roll and azimuth are small (± several degrees) and the initial wander angle is zero, and
b. The position (φ, λ, h) is known at the time of alignment.

The time of the coarse alignment consists of sixteen four-second periods (thus 64 seconds for the total coarse alignment procedure). The attitude parameters (roll, pitch and azimuth) are updated in a manner shown below:

$$\begin{aligned} Roll_{k+1} &= Roll_k + \delta Roll, \\ Pitch_{k+1} &= Pitch_k + \delta Pitch, \\ Azimuth_{k+1} &= Azimuth_k + \delta Azimuth \end{aligned} \tag{2.8}$$

The initial roll, pitch and azimuth, i.e. $Roll_0, Pitch_0, Azimuth_0$, are assumed to be zero. At the end of each four second interval the update to previous attitudes, i.e. $\delta Roll, \delta Pitch, \delta Azimuth$, are calculated using the summed earth rate and velocities:

$$\begin{aligned} \delta Roll &= \sin^{-1}(-v_x^b / \gamma \Delta t) \\ \delta Pitch &= \sin^{-1}(-v_y^b / \gamma \Delta t) \\ \delta Azimuth &= \tan^{-1}(\sum \theta_x^w / \sum \theta_y^w) \end{aligned} \tag{2.9}$$

where γ is normal gravity and Δt is the sampling interval. v_x, v_y, θ_x^w and θ_y^w are projections of velocity and earth rate in the body frame. For each interval the earth rate is summed by averaging the transformed gyro measurements (body to wander with assumption that the yaw is zero):

$$\sum_{i=1}^{n} \theta_i^w = \frac{1}{n}\theta_i^w + \frac{n-1}{n}\sum_{i=1}^{n-1} \theta_i^w \tag{2.10}$$

where n is the number of epochs and θ_i^w is the earth rate.

However the velocity sums are computed through the INS navigation module. Velocity from the module (in the wander frame) is converted into the body frame. After each four second loop, the updated attitude parameters will be fed into the INS navigation module.

The above process can be considered as one of computationally nulling the velocities in the level frame. The criterion for the completion of the coarse alignment is:

$$v^2 = (v_x^w)^2 + (v_y^w)^2 \cong 0 \tag{2.11}$$

The coarse alignment procedure is shown in Figure 2.3.

2.2.2 Fine Alignment

Results from the coarse alignment are refined through fine alignment to improve their accuracy. Fine alignment is accomplished by a Kalman filter that models the attitude misalignments along with position error, velocity error, accelerometer biases and gyro drifts. It is also assumed that during fine alignment the vehicle is stationary. For details of fine alignment see Wong (1985), for example.

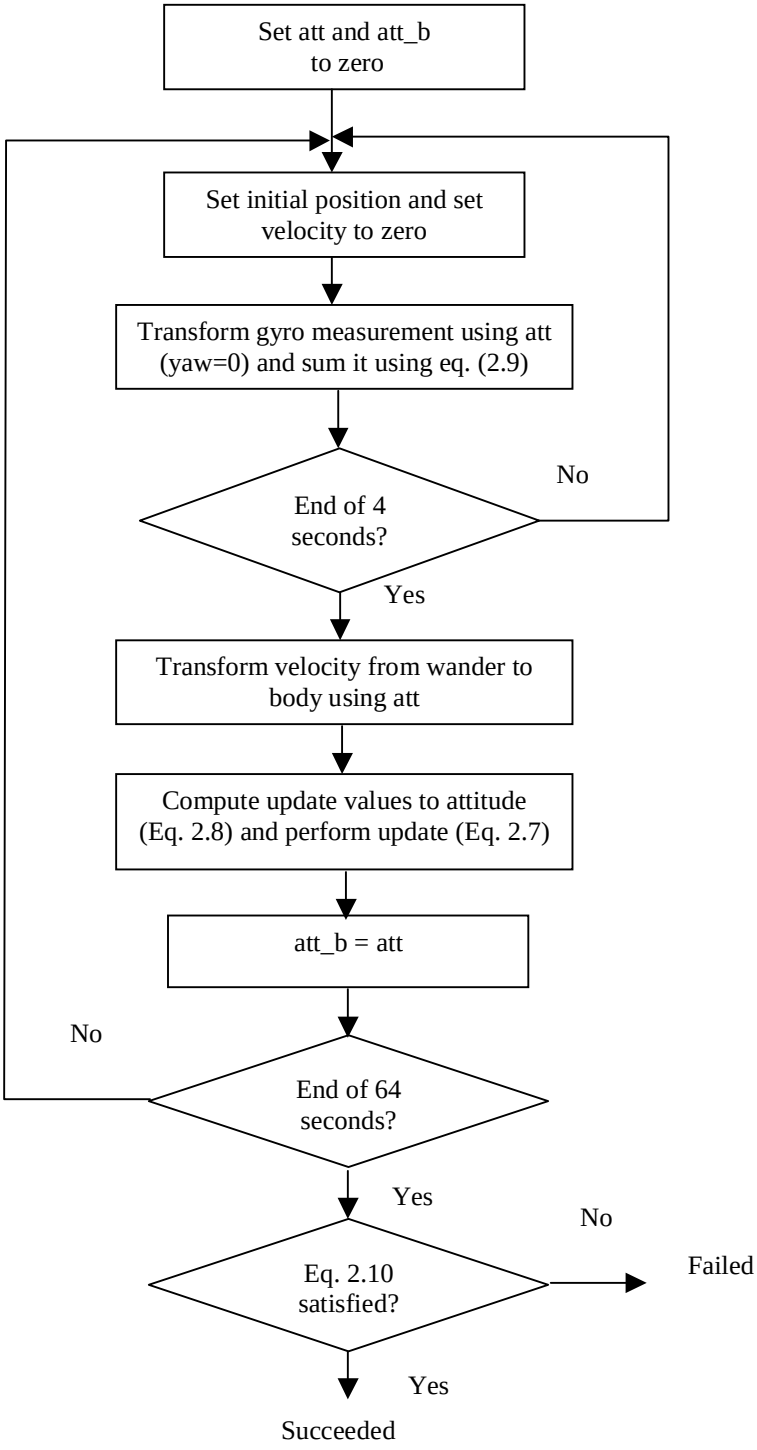

Figure 2.3 Coarse Alignment Process

The fine alignment employs the INS navigation module and Kalman Filter to perform a succession of zero velocity updates. An update interval of 20 seconds was chosen in this case. Below is the description of the filter.

Error Model

The INS states model 15 errors:

$$x = \begin{bmatrix} \delta\varepsilon_r & \delta\varepsilon_p & \delta\varepsilon_h & \delta\varphi & \delta\lambda & \delta v_n & \delta v_e & \delta h & \delta v_u & d_1 & d_2 & d_3 & b_1 & b_2 & b_3 \end{bmatrix}^T \quad (2.12)$$

where

$\delta\varepsilon_r, \delta\varepsilon_p, \delta\varepsilon_H$ are the misalignments (roll, pitch and heading) (radians),

$\delta\varphi, \delta\lambda, \delta h$ are the position errors, i.e. latitude, longitude errors (in radians) and height (m),

$\delta v_n, \delta v_e, \delta v_h$ are the horizontal velocity errors (radian/s) and vertical velocity error (m/s),

d_1, d_2, d_3 is the gyro drift vector in the body frame (deg/hr), and

b_1, b_2, b_3 are the accelerometer bias vector in the body frame (m/s^2).

The system model can then be presented:

$$x_{k+1} = \Phi_k x_k + u_k \quad (2.13)$$

where

Φ_k is the transition matrix, and

u_k is the system disturbance.

Measurement Model (ZUPT)

The measurements are:

$$z_k = \begin{bmatrix} \delta v_n & \delta v_e & \delta v_h \end{bmatrix}_k^T \tag{2.14}$$

where $\delta v_n, \delta v_e$ and δv_h are the summed velocities (m/s) during the ZUPT interval (20 seconds), for the north, east and up directions. The measurement equation is then:

$$z_k = \begin{bmatrix} \ldots & r_1 & 0 & 0 & 0 & \ldots \\ \ldots & 0 & r_2 & 0 & 0 & \ldots \\ \ldots & 0 & 0 & 0 & 1 & \ldots \end{bmatrix} x_k + r_k \tag{2.15}$$

where $r_1 = M + h$ and $r_2 = (N + h)\cos\varphi$.

The first non-zero column is the sixth column in the design matrix. The states corresponding to the non-zero elements (r_1, r_2 and 1) are $\delta v_n, \delta v_e$ (in rad/s) and δv_u (in m/s), respectively.

The filter does a state prediction every one second. At the end of every ten seconds, the predicted error states and its covariance are updated using the measurements. The estimated error states are then used to correct the position, velocity and attitude. The update of the attitude adopts the following linear formula:

$$R_b^l = \hat{R}_b^l (I + E) \tag{2.16}$$

where R_b^l is the rotation matrix relating the body axes to the local-level frame and E is the skew-symmetric matrix of the misalignment states.

A flow-chart of the fine alignment procedure is presented in Figure 2.4.

2.3 INS/GPS Integration

The Kalman filter has been commonly used for INS/GPS integration. Depending on the structure of the filter there are two strategies developed: the decentralized schema and the centralized schema (Gao et al., 1993; Schwarz et al., 1994). In the decentralized strategy two filters, i.e. the GPS filter and the master INS filter, run simultaneously, while in the centralized approach there is only one filter – the master filter. However, in this latter case the state vector in the master filter is augmented to include ambiguity states in the case that ambiguities need to be resolved to achieve high accuracy. The following sections describe the filter structures used in this research and in the software developed for its implementation.

2.3.1 Kalman Filter Structure in the Decentralized Integration Schema

The structure of the INS/GPS integration is shown in Figure 2.5. There are two independent filters running in parallel, i.e. the GPS filter that estimates the GPS navigation solution and its ambiguities, and the master filter that estimates the INS errors.

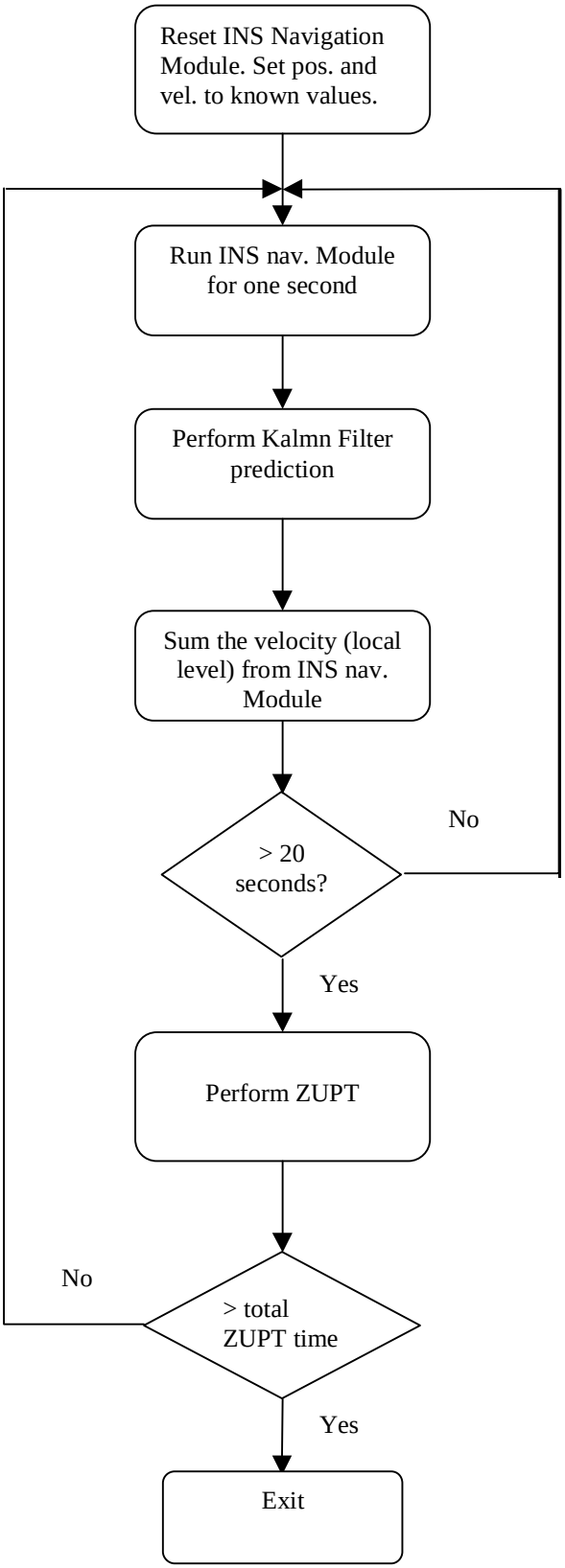

Figure 2.4 Fine Alignment Procedure

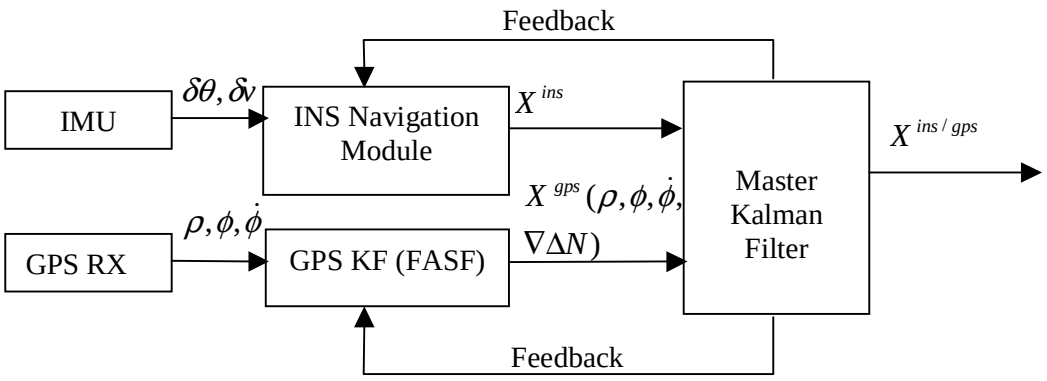

Figure 2.5 INS/GPS Integration Filter Structure

As indicated in the above figure either of two types of GPS information can be fed into the master filter to update the filter's predictions. One is GPS position and velocity, the other is GPS measurements and double differenced ambiguities. The first integration is so-called loose coupling and the latter is referred to as tight coupling (Schwarz, 1994). Measurement equations for each integration type will be described in the following sections.

Feedback to the INS navigation module are velocity and position corrections, gyro drift and accelerometer bias, and it occurs at every epoch when the information is available. It is used to prevent INS error growth. The feedback from the master filter to the GPS Kalman filter, however, is used to correct cycle slips when they occur and/or to assist the GPS filter to fix integers.

GPS Filter

The GPS filter system states are:

$$x^{gps} = [\delta r^{gps}, \delta v^{gps}, \delta\nabla\Delta N]^T \tag{2.17}$$

where

δr^{gps} is the position error vector (m),

δv^{gps} is the velocity error vector (m/s), and

$\delta \nabla \Delta N$ is the double differenced ambiguity correction vector.

The system (discrete) equation is:

$$x_{k+1}^{gps} = \Phi^{gps} x_k^{gps} + u_k^{gps} \tag{2.18}$$

where

Φ^{gps} is the transition matrix, and

u_k^{gps} is the system disturbance.

The transition matrix is:

$$\Phi^{gps} = \begin{bmatrix} 1 & 0 & 0 & \Delta t & 0 & 0 & 0 & 0 & \cdots & 0 \\ 0 & 1 & 0 & 0 & \Delta t & 0 & 0 & 0 & \cdots & 0 \\ 0 & 0 & 1 & 0 & 0 & \Delta t & 0 & 0 & \cdots & 0 \\ 0 & 0 & 0 & 1 & 0 & 0 & 0 & 0 & \cdots & 0 \\ 0 & 0 & 0 & 0 & 1 & 0 & 0 & 0 & \cdots & 0 \\ 0 & 0 & 0 & 0 & 0 & 1 & 0 & 0 & \cdots & 0 \\ 0 & 0 & 0 & 0 & 0 & 0 & 1 & 0 & \cdots & 0 \\ 0 & 0 & 0 & 0 & 0 & 0 & 0 & \ddots & \cdots & 0 \\ \vdots & \vdots & \vdots & \vdots & \vdots & \vdots & \vdots & \vdots & \ddots & \vdots \\ 0 & 0 & 0 & 0 & 0 & 0 & 0 & 0 & \cdots & 1 \end{bmatrix} \tag{2.19}$$

The measurement equations are as follow:

$$\delta \nabla \Delta \Phi_k = A_k \begin{bmatrix} \delta\varphi \\ \delta\lambda \\ \delta h \end{bmatrix}_k + B_k \begin{bmatrix} \nabla \Delta N_1 \\ \vdots \\ \nabla \Delta N_n \end{bmatrix} + r_{1k} \tag{2.20}$$

$$\delta\nabla\Delta\rho_k = A_k \begin{bmatrix} \delta\varphi \\ \delta\lambda \\ \delta h \end{bmatrix}_k + r_{2k} \tag{2.21}$$

where $\delta\nabla\Delta\Phi_k$ is the difference between the measured and approximate double differenced (DD) carrier phase measurements, $\delta\nabla\Delta\rho_k$ is the difference between the measured and approximate DD code measurements, A_k , B_k and C_k are coefficient matrices, and r_{1k} and r_{2k} are measurement noise values for carrier and code measurements, respectively.

Master Filter

The system states are the INS errors (15 states):

$$x^{ins} = [\varepsilon, \delta r^{ins}, \delta v^{ins}, d, b]^T \tag{2.22}$$

where

ε	is the misalignment vector (north, east and up) (rad/s),
δr^{ins}	is the position error vector (m),
δv^{ins}	is the velocity error vector (m/s),
d	is the gyro drift vector (deg/hr), and
b	is the accelerometer bias vector (m/s^2).

The system equation is:

$$x_{k+1}^{ins} = \Phi^{ins} x_k^{ins} + u_k^{ins} \tag{2.23}$$

where

Φ^{ins} is the transition matrix, and

u_k^{ins} is the system disturbance.

For details on the structure of the transition matrix, Φ^{ins}, refer to Schwarz and Wei (1999).

Outputs from the INS navigation module and the GPS filter module form the system measurements to update the master filter's predictions. Depending on what GPS information is used there are two integration modes: loose coupling for GPS position and velocity, and tight coupling for GPS measurements (pseudorange, phase and phase rate) and double differenced ambiguities.

Loose Coupling

The configuration of the loose coupling approach is shown below:

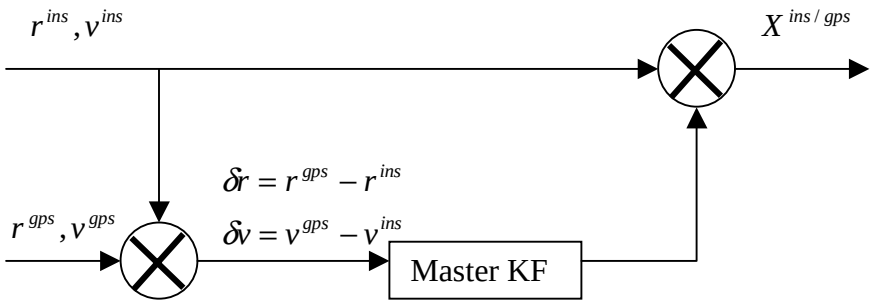

Figure 2.6 Loose Coupling Integration Filter Configuration

The measurement in this configuration is the difference between the INS and GPS navigation solutions. The GPS navigation solution is from the GPS filter as indicated in

Figure 2.6. Since the GPS solution is a referenced source, its accuracy affects the estimation of the master filter.

The measurement equation in this integration mode is:

$$\begin{bmatrix} \delta r \\ \delta v \end{bmatrix}_k = \begin{bmatrix} I_{2X2} & O \\ O & I_{2X2} \end{bmatrix} \begin{bmatrix} \delta r^{ins} \\ \delta v^{ins} \end{bmatrix}_k + r_k \tag{2.24}$$

where I is an identity matrix.

Therefore, in loose coupling, the configuration measurement equation (2.24) and the system model equation (2.23) constitute the Kalman filter. In this integration model, position and velocity from the GPS filter are used as the update information.

Tight Coupling

The configuration for tight coupling is given below:

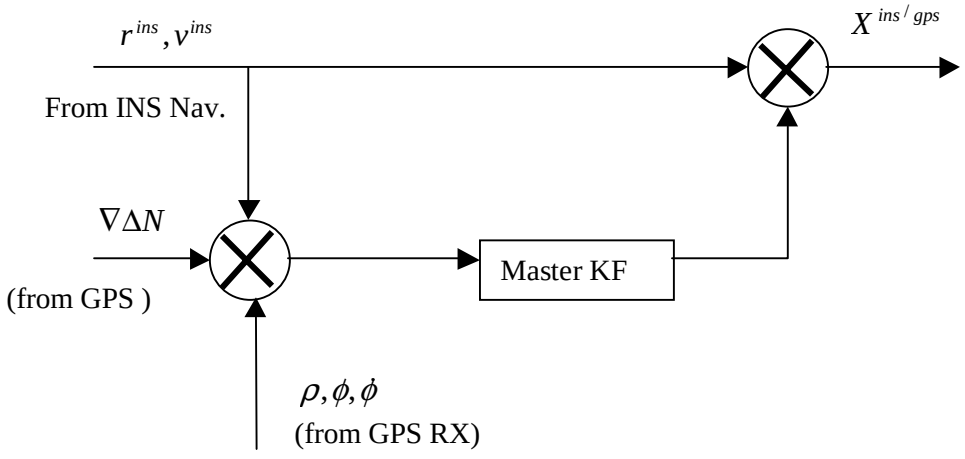

Figure 2.7 Tight Coupling Integration Filter Configuration

The format of the measurement equation is the same as in the GPS filter, but it uses positions from the INS rather than GPS as the approximate position:

$$\delta\nabla\Delta\Phi_k^{ins} = A_k^{ins} r_k^{ins} + B_k^{ins} \begin{bmatrix} \nabla\Delta N_1 \\ \vdots \\ \nabla\Delta N_n \end{bmatrix} + r_{1k} \tag{2.25}$$

$$\delta\nabla\Delta\rho_k^{ins} = A_k^{ins} r_k^{ins} + r_{2k} \tag{2.26}$$

Thus measurement equations (2.25) and (2.26) and system model equation (2.23) form the filter for tight coupling.

2.3.2 Kalman Filter Structure for Centralized Integration

The centralized filter configuration is shown in Figure 2.8 where an augmented master filter (AMF) is constructed to have ambiguities in its state vector.

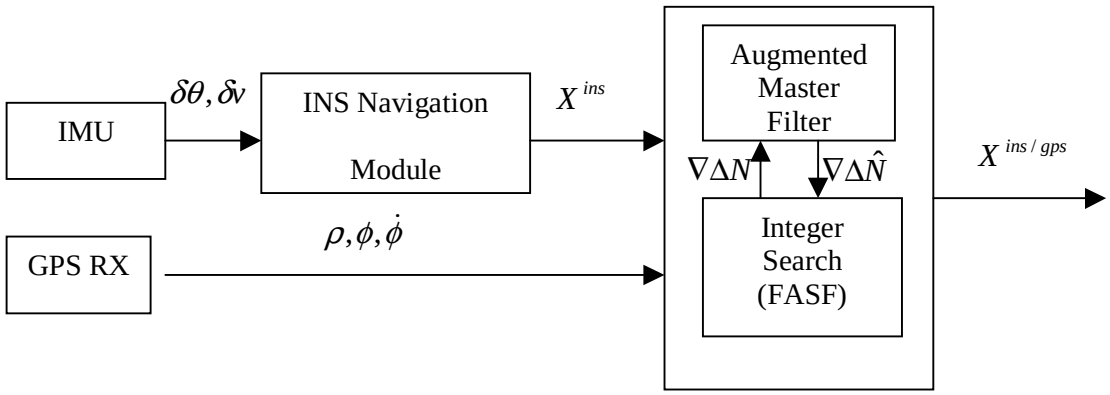

Figure 2.8 Augmented Master Filter (AMF) Configuration

In the above configuration, the AMF also estimates float ambiguities and FASF, merely an integer search module, searches the integers based on the float ambiguities and their

variance-covariance (VCV) information from the AMF. If ambiguities are fixed in FASF, the integers will be fed into the AMF and ambiguity estimation will stop.

The system states are 15 INS errors plus ambiguity errors for all double differences:

$$x = [\varepsilon, \delta r^{ins}, \delta v^{ins}, d, b, \delta \nabla \Delta N]^T \tag{2.27}$$

The system equation is:

$$x_{k+1} = \Phi x_k + u_k \tag{2.28}$$

where

Φ is the augmented transition matrix, and

u_k is the system disturbance.

The augmented transition matrix takes the following format:

$$\Phi = \begin{bmatrix} \Phi^{ins} & 0 \\ 0 & I_{nXn} \end{bmatrix} \tag{2.29}$$

where n is the number of double differenced ambiguities.

The measurements are double differenced pseudorange, phase and phase rate from GPS. Similar to the analysis in Section 2.3.1, the measurement equations are presented below:

$$\delta \nabla \Delta \Phi_k^{ins} = A_k^{ins} r_k^{ins} + B_k^{ins} \begin{bmatrix} \nabla \Delta N_1 \\ \vdots \\ \nabla \Delta N_n \end{bmatrix} + r_{1k} \tag{2.30}$$

$$\delta \nabla \Delta \rho_k^{ins} = A_k^{ins} r_k^{ins} + r_{2k} \tag{2.31}$$

Above measurement equations 2.30 and 2.31 along with system equation 2.28 constitute the filter for centralized integration schema. When comparing to the tight coupling approach, it can be seen that measurement equations are the same but the system state in the centralized integration also includes ambiguities.

CHAPTER 3

GPS AMBIGUITY RESOLUTION

The carrier phase measurement is the most precise GPS signal with which users can achieve positioning accuracies at the centimetre level. However, since a GPS receiver can only measure the fractional part of the phase and integrate the full cycles over time, the unknown integer cycles, the so-called integer ambiguities, must be resolved.

Many ambiguity resolution methods have been proposed. However due to the fact that there are many error sources that deteriorate the phase measurement it is difficult to resolve the integers reliably and quickly. In this chapter, the principles of ambiguity resolution are first discussed. Integer fixing involves three basic steps: float ambiguity estimation, integer search and validation. The least squares method and Kalman filtering technique are discussed in the context of float ambiguity estimation. Two typical integer searching mechanisms, the ambiguity function method and LAMBDA are briefly introduced in the integer ambiguity search. The FASF method developed by Chen (1993) is then studied in detail.

Three basic steps of fixing ambiguities are as follows:

1. Estimation of the float ambiguities and the associated covariance information
2. Integer ambiguity search
3. Integer validation (ratio test or discrimination test)

Float-ambiguity estimation is the first and crucial step to resolve the integers. It offers the approximate ambiguity solution with an uncertainty represented by the estimated variance. Although the estimated ambiguities are the optimal solutions in a statistical sense, which can be provided by some standard estimators like least squares, they are generally not integers. Thus the search procedure is implemented to find the integers within the candidate space which is constructed based upon the float solution and its covariance information from the first step. The discrimination test procedure is then needed to validate the solution.

3.1 Float Ambiguity Estimation

This section introduces two float estimation methods, least squares and the Kalman filter.

3.1.1 Least Squares Estimation

The least squares method is used to estimate a set of unknown parameters from redundant obervables through a known mathematical model. The statement of the least squares estimation in the linear system model is to estimate the parameters, x, in the following equation (Krakiwsky, 1990):

$$l = Ax + r \tag{3.1}$$

where

l is measured observables,

A is the design matrix,

x is the unknown parameter vector, and

r is the vector of measurement residuals.

Under the condition that the following quadratic form must be minimized:

$$\hat{r}^T \mathrm{P}\hat{\mathrm{r}} = \text{minimum} \tag{3.2}$$

where

$\hat{r}$ is the vector of measurement residuals, and

$P = \sigma_0^2 C_l^{-1}$ is the weight matrix. σ_0^{-1} is the *priori* variance factor and C_l^{-1} is the VCV matrix of the measurement errors.

Since the mathematical model relating the carrier phase measurements to the unknown ambiguity parameters is nonlinear as indicated by equation (2.6), the nonlinear relation needs to be linearized in order to apply a least squares estimator. After linearization, the least squares equation for GPS ambiguity estimation using carrier phase measurements is:

$$\delta\nabla\Delta\varphi = A\delta r + B\nabla\Delta N + \varepsilon_{\nabla\Delta\varphi} \tag{3.3}$$

where

$\delta\nabla\Delta\varphi$ is the vector of measured minus computed double difference carrier phase measurement,

δr is the parameter vector containing the increments of the baseline coordinates,

$\nabla\Delta N$ is the double difference ambiguity vector,

A, B are the design matrices, and

$\varepsilon_{\nabla\Delta\varphi}$ is the DD carrier phase measurement errors.

The least squares estimation for equation (3.3) is carried out in an iterative fashion until the correction vector, δr, converges below a threshold, which is close to zero (in the order of 10^{-4}).

The important assumptions behind least squares are that the state vector is constant over one estimation interval and that the measurement errors are Gaussian. The first assumption leads to estimation over a period of static time or on a per epoch basis for a dynamic environment. The second assumption is required to guarantee that the least squares estimate is optimal.

3.1.2 Kalman Filtering

Kalman filtering allows for the state vector to change over time, as is the case for a dynamic system which is typical for GPS kinematic positioning. The Kalman filter prediction and update equations are called the system dynamic model and measurement model, respectively. These two equations are presented below and the filter loop is shown in Figure 3.1(Brown and Hwang, 1995).

The system model is given as:

$$x_{k+1} = \Phi_k x_k + u_k \tag{3.4}$$

where

x_k is the state vector at epoch k,

Φ_k is the discrete transition matrix relating x_k to x_{k+1}, and

u_k is the disturbance vector.

The measurement model is:

$$z_k = H_k x_k + r_k \tag{3.5}$$

where

z_k is the measurement vector at epoch k,

H_k is the coefficient matrix relating the measurement to the state vector at epoch k, and

r_k is the measurement noise vector at epoch k.

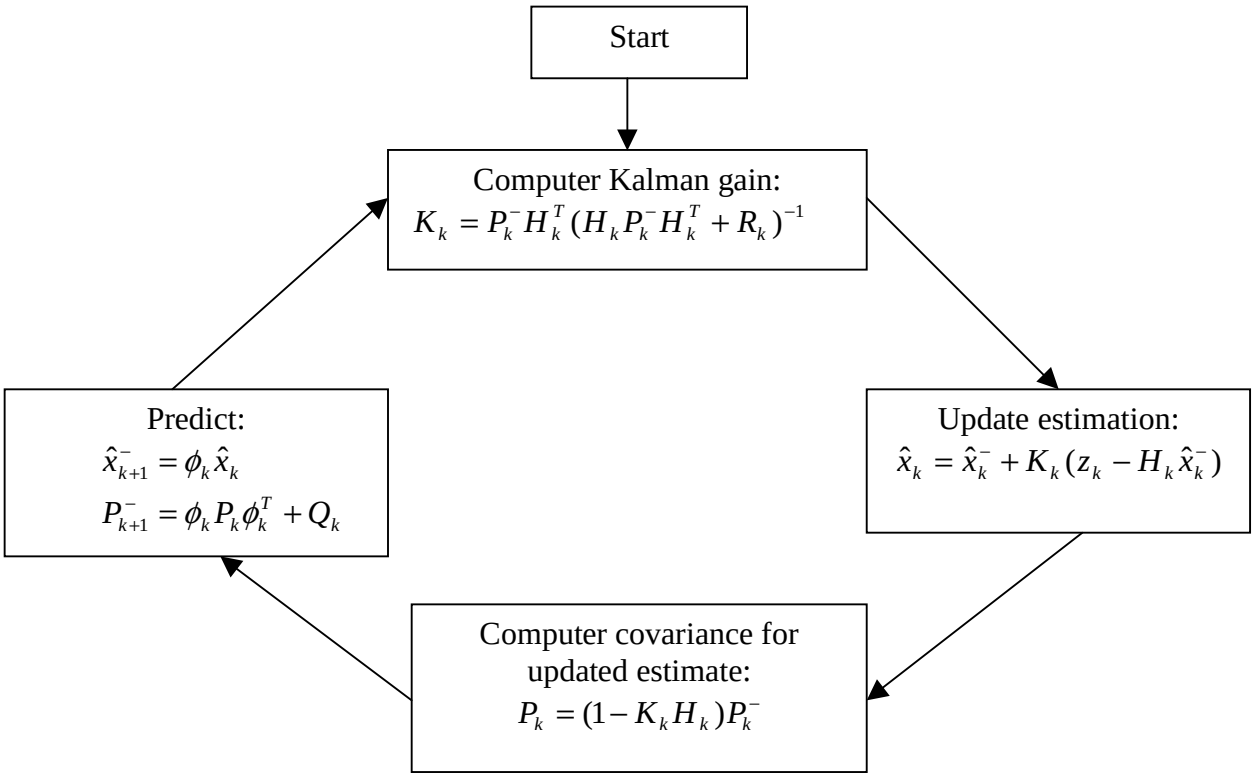

Figure 3.1 Kalman Filtering Flow Chart (Brown and Hwang, 1995)

The system and measurement equations in a GPS filter are described in Section 2.3.1. Since Kalman filter estimation information is carried from the previous epoch to the subsequent epoch, the accuracy of the ambiguities is improved over the estimation period as additional measurements are available for update, which are described in the following sections. As an example, Figure 3.2 shows the estimation of the DD ambiguity for PRNs 5-8 before it is fixed using a sample of GPS data.

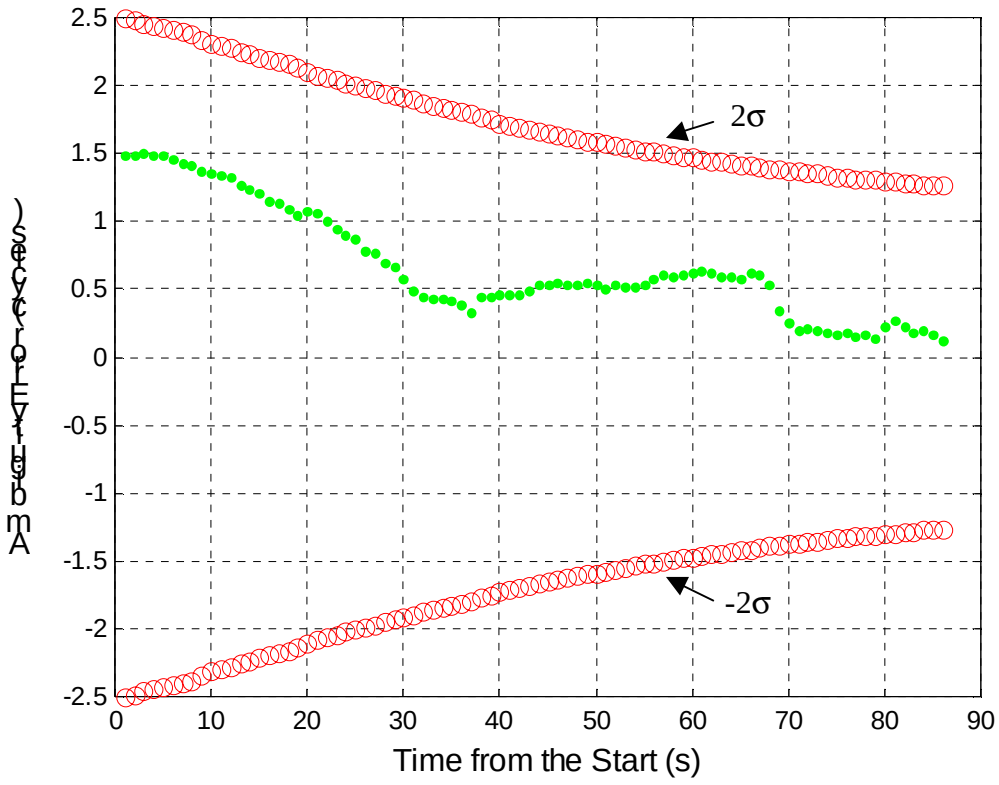

Figure 3.2 Kalman Filter Estimation of Float Ambiguity Std. Deviation for DD PRNs 5-8

3.2 Search Algorithm

Once the float ambiguities and their associated error VCV matrix are obtained, the search can then be performed to find integers. Initial ambiguities, along with their error

covariance, construct a search space and the algorithm basically finds appropriate combinations of integer candidates in this search space. The search can be implemented in either the position or ambiguity domain. This section introduces two well-known search methods that are performed in these two different domains.

3.2.1 Ambiguity Function Method

The ambiguity function method (AFM) was proposed by Counselman and Gourevitch (1981). Remondi (1984, 1990) and Mader (1990) further investigated the concept. Erickson (1992) also studied the reliability and performance of AFM. The principle of the ambiguity function method is to find a set of ambiguity candidates in a cube in the position domain to maximize the following objective function:

$$AFM(x_B, y_B, z_B) = \sum_{k=1}^{n}\sum_{j=1}^{m} \exp[\nabla\Delta\phi_{AB,k}^{j} - \frac{2\pi}{\lambda}\nabla\Delta\rho_{AB,k}^{j}] \tag{3.6}$$

where

A and B are the base and remote stations respectively,

n is the number of epochs,

m is the number of total satellites observed,

$\nabla\Delta\phi_{AB,k}^{j}$ is the double differenced phase measurement for the satellite j at epoch k, and

$\nabla\Delta\rho_{AB,k}^{j}$ is the double differenced code measurement for the satellite j at epoch k.

The AFM procedure is as follows:

1. Calculate the approximate position for the remote station B using differential code measurements,
2. Construct a cube with the approximate coordinates of B obtained in step 1 as its centre and partition the cube into grid points as shown in Figure 3.3. The volume of the cube is determined by standard deviations, e.g. $\pm 4\sigma_x$, $\pm 4\sigma_y$ and $\pm 4\sigma_z$ (Remondi, 1991), which are obtained from the error covariance matrix of the code solution at the first step.
3. Compute the objective function from equation (3.4) for each grid in the position cube. The candidate integers that yield the maximum value should be the desired solution.

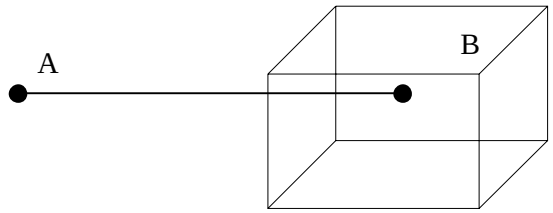

Figure 3.3 Search Cube for the Ambiguity Function Method

Although theoretically the AFM can generate correct integers, the large search volume makes this method generally impractical for real-time applications. As demonstrated by Hofmann-Wellenhof (1997), assuming a $6\text{m} \times 6\text{m} \times 6\text{m}$ cube with a 1 cm grid the number of possible ambiguity candidates reaches $(601)^3 \approx 2.17 \times 10^8$. Erickson (1992) also concluded that, in order to achieve the greatest success, AFM should be used with short baselines (< 10 km) and GPS satellites with high elevations (> 15 °).

3.2.2 LAMBDA Method

Teunissen et al. (1993,1997) document the LAMBDA method which stands for Least-square AMBiguity Decorrelation Adjustment. It is one of the most sophisticated and well-documented ambiguity resolution methods (Jonge et al., 1996). The LAMBDA method applies normal least squares to obtain the float ambiguities, $\nabla\Delta\hat{N}$, and its variance- covariance (VCV) matrix, $Q_{\nabla\Delta\hat{N}}$. The search is then carried out within the search space defined by $\nabla\Delta\hat{N}$ and $Q_{\nabla\Delta\hat{N}}$ to find the integers $\nabla\Delta\breve{N}$ satisfying the following condition:

$$(\nabla\Delta\hat{N} - \nabla\Delta N)^T Q_{\nabla\Delta\hat{N}}^{-1} (\nabla\Delta\hat{N} - \nabla\Delta N) = \text{minimum}, \quad \nabla\Delta N \in Z^n \tag{3.7}$$

Based on the constraint of the integer nature for the solution in equation (3.5) the LAMBDA method is also called the integer least squares adjustment. The ambiguity search space or region is defined as follows:

$$(\nabla\Delta\hat{N} - \nabla\Delta N)^T Q_{\nabla\Delta\hat{N}}^{-1} (\nabla\Delta\hat{N} - \nabla\Delta N) \leq \chi^2 \tag{3.8}$$

where χ^2 is a positive constant and represents the size of the ellipsoidal search region. The region is centred at the float solution, $\nabla\Delta\hat{N}$, and its shape is governed by the variance matrix, $Q_{\nabla\Delta\hat{N}}$. Its size can be controlled by choosing an appropriate value for χ^2 .

Although the search space is given by equation (3.6), it is difficult to implement the search due to the nondiagonality of $Q_{\nabla\Delta\hat{N}}$, which indicates that the float ambiguities are highly correlated in most cases. To facilitate the search and achieve better efficiency, a Z-transformation, which decorrelates the DD ambiguities, is applied to $Q_{\nabla\Delta\hat{N}}$. The transformation makes $Q_{\nabla\Delta\hat{N}}$ nearly diagonal, which means that the ambiguities become almost decorrelated. The transformation is called the LAMBDA decorrelation. After the Z-transformation is applied, the ambiguities as well as the variance matrix are transformed into the Z domain. The search problem is therefore converted into the transformed ambiguity domain. Denoting the transformed ambiguities and the variance matrix as z and Q_z, based on the triangular decomposition of the variance matrix Q_z, the quadratic form of equation (3.6) can then be written as a sum of independent squares in the individual ambiguities (Teunissen, 1993):

$$(\hat{z}-z)^T Q_{\hat{z}}^{-1}(\hat{z}-z)=\sum_{i=1}^{n}(\hat{z}_{i|I}-z_i)^2/\sigma_{z_{i|I}}^2 \tag{3.9}$$

where $\sigma_{z_{i|I}}^2$ is the i^{th} diagonal element in Q_z and it is the conditional variance of ambiguity z_i conditioned on all previous ones ($I=0,1,2,...,i-1$). The notation $\hat{z}_{i|I}$ is used to denote the conditional ambiguity. Using the above quadratic form, the following sequential bounds on the individual ambiguities can be formed:

$$
\begin{aligned}
&(\hat{z}_1 - z_1)^2 \le \sigma_{z_1}^2 \chi^2 \\
&(\hat{z}_{2|1} - z_2)^2 \le \sigma_{z_{2|1}}^2 (\chi^2 - (\hat{z}_1 - z_1)^2 / \sigma_{z_1}^2) \\
&\qquad\qquad \vdots \\
&(\hat{z}_{n|N} - z_n)^2 \le \sigma_{z_{n|N}}^2 (\chi^2 - \sum_{j=1}^{n-1} (\hat{z}_{j|J} - z_j)^2 / \sigma_{z_{j|J}}^2)
\end{aligned}
\qquad (3.10)
$$

A search within all ranges defined by equation (3.10) is then performed. Throughout the search procedure two integer candidate sets with the smallest and the second smallest sum of squared residuals are kept. Afterwards, the ratio of the smallest and the second smallest sum-of-squared (SOS) residuals is calculated and a discrimination test is performed by comparing it with a predefined threshold. If the test passes, the candidate set with the smallest SOS residuals is deemed the integer solution and the integers are then transformed back to the normal ambiguity domain by applying an inverse Z-transformation.

The core part of the LAMBDA method exists in the decorrelation process which simplifies the computation of the minimization equation and reduces the search space. A full discussion on the decorrelation is presented in Section 3.3.2. When comparing the LAMBDA method with the AFM, the LAMBDA method is faster and significantly more efficient (Weisenburger, 1997). The FASF method, to be discussed in the next section, combines the Kalman filter and the LAMBDA decorrelation.

3.3 FASF with LAMBDA Decorrelation

The FASF is an OTF ambiguity search algorithm developed by Chen (1993, 1994a). FASF is a search procedure carried out in the ambiguity domain and the basic theory is

the same as described in the LAMBDA method, i.e. to find the integers satisfying the integer least squares objective function equation (3.5) within the integer candidate space defined by equation (3.8). A Kalman filter is built into FASF to estimate the float ambiguities and the associated VCV matrix. This makes the FASF suitable for real-time applications. Unlike the LAMBDA search, where ambiguity ranges are dynamically calculated through the search procedure, it computes the search range beforehand (Chen, 1994b). This section discusses the FASF filter structure and the search procedure along with the important LAMBDA decorrelation which is adopted in the FASF. Figure 3.4 shows the workflow of the FASF method.

Filter Structure

The system and measurement equations of the filter are as described in Section 2.1. System equation (2.1), along with the measurement equation (2.3), constitutes the Kalman filter in FASF. At each epoch, the float ambiguities and their error covariances are estimated and a search is performed until the integers are obtained. The advantage of using a Kalman filter is that with more measurements available, the estimation of the float solution is more accurate and thus the size of search space is reduced.

3.3.1 LAMBDA Decorrelation

The LAMBDA decorrelation proposed by Teunissen (1994), which facilitates the computation of the search space and reduces the number of ambiguity candidates to be searched and evaluated, is not a prerequisite to perform any ambiguity search to find the integers which must satisfy the minimization problem as given by equation (3.7).

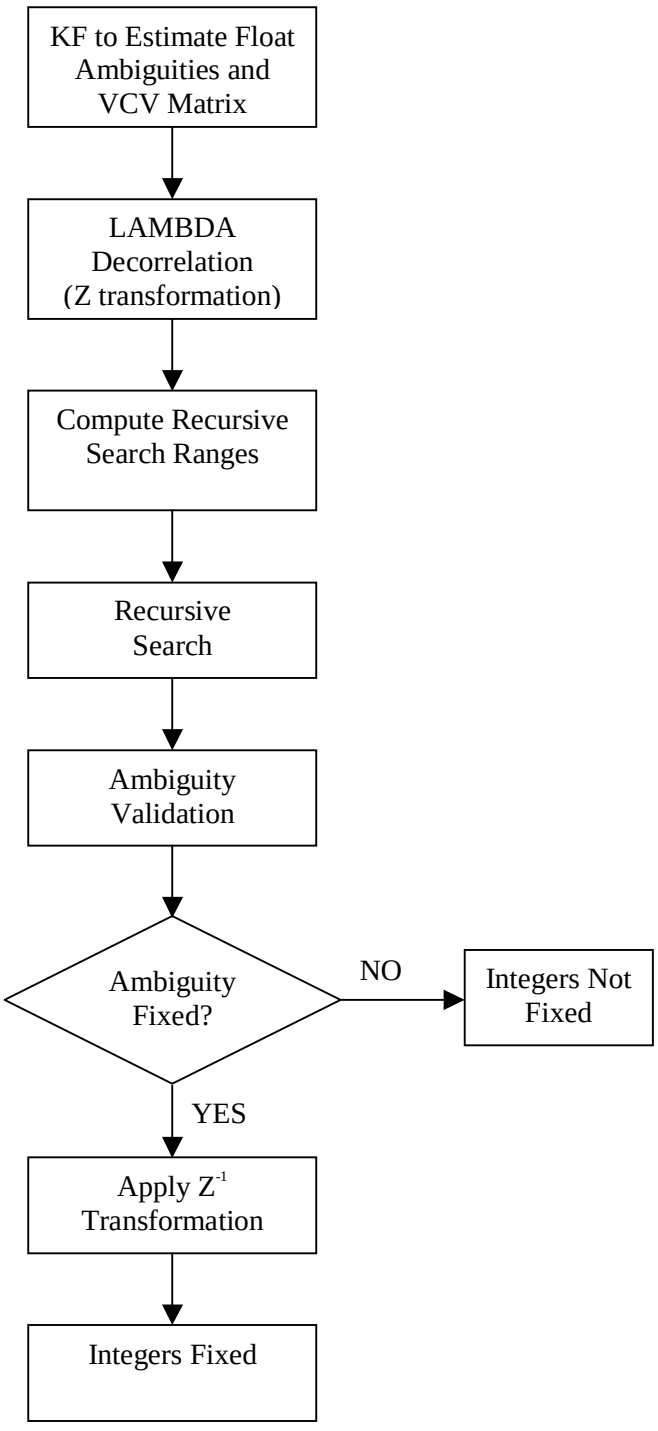

Figure 3.4 FASF Workflow

As indicated earlier, the ambiguity search is aimed to find integer candidates from the search space to minimize equation (3.7). Rewriting the objective function and definition of the search space gives:

$$(\nabla\Delta\hat{N} - \nabla\Delta N)^T Q_{\nabla\Delta\hat{N}}^{-1} (\nabla\Delta\hat{N} - \nabla\Delta N) = \text{minimum}, \quad \nabla\Delta N \in Z^n \tag{3.11}$$

$$(\nabla\Delta\hat{N} - \nabla\Delta N)^T Q_{\nabla\Delta\hat{N}}^{-1} (\nabla\Delta\hat{N} - \nabla\Delta N) \leq \chi^2 \tag{3.12}$$

Expanding the above ambiguity vectors $\nabla\Delta\hat{N}, \nabla\Delta N$ gives the following:

$$\begin{aligned}
&\nabla\Delta N = \begin{bmatrix} \nabla\Delta N_1 & \nabla\Delta N_2 & \cdots & \nabla\Delta N_k \end{bmatrix}^T \\
&\nabla\Delta\hat{N} = \begin{bmatrix} \nabla\Delta\hat{N}_1 & \nabla\Delta\hat{N}_2 & \cdots & \nabla\Delta\hat{N}_k \end{bmatrix}^T \\
&\delta\nabla\Delta N = \begin{bmatrix} \nabla\Delta\hat{N}_1 - \nabla\Delta N_1 & \nabla\Delta\hat{N}_2 - \nabla\Delta N_2 & \cdots & \nabla\Delta\hat{N}_k - \nabla\Delta N_k \end{bmatrix}^T \\
&= \begin{bmatrix} \delta\nabla\Delta N_1 & \delta\nabla\Delta N_2 & \cdots & \delta\nabla\Delta N_k \end{bmatrix}
\end{aligned}$$

It can be observed that if the VCV matrix, $Q_{\nabla\Delta\hat{N}}$, is diagonal, equation (3.11) is reduced to be the sum of independent squares and thus just by 'rounding' the float ambiguities to their nearest integers the correct solution can be obtained. However, due to the correlation among DD ambiguities, $Q_{\nabla\Delta\hat{N}}$ is not diagonal. Thus it is not trivial to iterate candidates in the search ranges defined by equation (3.12). Therefore, the primary aim of introducing a LAMBDA decorrelation is to diagonalize the VCV matrix, which decorrelates DD ambiguities after the transformation. The transformation also has to maintain following properties (Teunissen, 1994):

- It should be volume preserving
- Elements in the transformation matrix must be integers

Due to its second property above, the transformation is called Z-transformation and the domain after the transformation is called Z domain.

To quantify the correlation, the correlation matrix is introduced (Teunissen, 1994):

$$R_{\nabla\Delta\hat{N}} = \left\{diag(Q_{\nabla\Delta\hat{N}})\right\}^{-1/2} Q_{\nabla\Delta\hat{N}} \left\{diag(Q_{\nabla\Delta\hat{N}})\right\}^{-1/2} \tag{3.13}$$

A scalar, which measures the decorrelation and is called the correlation number, can be defined:

$$r_{\nabla\Delta\hat{N}} = \left(\det(R_{\nabla\Delta\hat{N}})\right)^{1/2} \tag{3.14}$$

Substituting (3.13) into equation (3.8) gives the following:

$$r_{\nabla\Delta\hat{N}} = \left(\frac{\det(Q_{\nabla\Delta\hat{N}})}{\det\left\{diag(Q_{\nabla\Delta\hat{N}})\right\}} \right)^{1/2} \tag{3.15}$$

When $Q_{\nabla\Delta\hat{N}}$ is diagonal, $r_{\nabla\Delta\hat{N}}$ is equal to one, otherwise its value is close to zero. By introducing the correlation number, the decorrelation process is now translated into the problem of maximizing $r_{\nabla\Delta\hat{N}}$. From equation (3.15) it can be observed that to maximize $r_{\nabla\Delta\hat{N}}$ is to minimize the denominator in equation (3.15), i.e. the product of diagonal elements in $Q_{\nabla\Delta\hat{N}}$:

$$\prod_{i=1}^{k} \sigma_{\nabla\Delta\hat{N}} = \text{minmum} \tag{3.16}$$

This is the principal of the LAMBDA decorrelation method. It is found that the process of applying the Z-transformation is a process of the conditional least squares adjustment. Namely, the diagonal elements in the transformed matrix Q_z are conditional variances denoting by $\sigma_{z_i \mid z_1, z_{21}, \ldots, z_{1i-1}, z_{1+1}, \ldots z_k}$.

With the DD ambiguities decorrelated, the size of the transformed search space will be reduced as well. Considering the definition of the Ambiguity Dilution of Precision (ADOP) discussed in Section 3.3.5, the following relation between the correlation number and ADOP holds:

$$r_{\nabla\Delta\hat{N}} = \left(\frac{(ADOP)^n}{\det\{diag(Q_{\nabla\Delta\hat{N}})\}} \right)^{1/2} \tag{3.17}$$

As shown the in the equation, as the denominator of the right hand side of equation (3.17) is minimized and the correlation number moves towards one, the ADOP decreases. As is shown later, the ADOP is closely related to the search space such that reducing the ADOP implies a shrinkage of the search space.

Due to the second requirement on the Z-transformation, that elements in the transformation matrix must be integers, $Q_{\nabla\Delta\hat{N}}$ will not be completely diagonal.

Nevertheless, equation (3.11) is approximately translated into one simplified version which is straightforward to implement:

$$\sum_{i=1}^{k} \frac{(\hat{z}_i - z_i)^2}{\sigma_{z_i}^2} = \text{minimum} \tag{3.18}$$

The above equation is the exact objective function to be evaluated throughout the recursive search procedure in FASF.

3.3.2 Search Procedure

The search is performed at each epoch in an attempt to obtain integer ambiguities. The unique feature of FASF exists in its sequential ambiguity search range adjustment, or the Recursive Computation of the Search Range (RCSR) (Chen, 1994). Suppose that the float ambiguities and their error variances at a certain epoch are denoted as $(\Delta\nabla\hat{N}_1, \Delta\nabla\hat{N}_2, ..., \Delta\nabla\hat{N}_n)$ and $(\sigma_{\Delta\nabla\hat{N}_1}, \sigma_{\Delta\nabla\hat{N}_2}, ..., \sigma_{\Delta\nabla\hat{N}_n})$. During the search, the error variance of an ambiguity is adjusted assuming that all remaining ambiguities are fixed. As demonstrated by Lu (1995) such an assumption is equivalent to a constraint in the least squares adjustment and thus mathematically the adjusted error variance and states can be obtained using the following formulas:

$$Q_{\tilde{x}}(n) = Q_{\hat{x}}(n) - q_n q_n^T / (Q_{\hat{x}})_{n,n} \tag{3.19}$$

$$\bar{x}(n) = \hat{x} - q_n (\Delta\nabla\overline{N} - \Delta\nabla\hat{N}) / (Q_{\hat{x}})_{n,n} \tag{3.20}$$

$$\overline{\Omega}(n) = \hat{\Omega} + (\Delta\nabla\overline{N} - \Delta\nabla\hat{N})^2 / (Q_{\hat{x}})_{n,n} \tag{3.21}$$

where

$Q_{\tilde{x}}(n)$ is the error variance matrix after the adjustment,

$Q_{\hat{x}}(n)$ is the error variance matrix before the adjustment,

q_n is the last column in $C_{\hat{x}}$ related to $\Delta\nabla\hat{N}$,

$(Q_{\hat{x}})_{n,n}$ is the diagonal element related to $\Delta\nabla\hat{N}$ in $Q_{\hat{x}}$,

x are the states in the filter $(\delta x, \delta y, \delta z, \Delta\nabla\hat{N}_1, \Delta\nabla\hat{N}_2, ...\Delta\nabla\hat{N}_n)$,

$\hat{x}$ and $\bar{x}$ represent the state before and after adjusted, respectively, and

Ω is the sum of squared (SOS) residuals. $\hat{\Omega}$ and $\overline{\Omega}$ stand for the SOS before and after the adjustment.

Equation (3.19) indicates that the variance after the adjustment is smaller than the original one. This implies that the search range for this ambiguity is reduced. Note that in the LAMBDA decorrelation discussion, it was found that the decorrelation also reduces the search space through the conditional least squares adjustment. Thus two processes exist in FASF to reduce the search space which makes the number of potential integer candidates significantly less than other resolution methods. When comparing FASF with LAMBDA, they share the same reduction scheme at the first stage in the ambiguity search process, which is to decorrelate the ambiguity VCV matrix.

The RCSR in the FASF works backwards. By denoting the adjusted error ambiguity variance as $(\sigma_{\Delta\nabla\bar{N}_1}, \sigma_{\Delta\nabla\bar{N}_2}, ..., \sigma_{\Delta\nabla\bar{N}_n})$, the error variance of the last ambiguity is:

$$\sigma_{\Delta\nabla\bar{N}_n} = \sigma_{\Delta\nabla\hat{N}_n} \tag{3.22}$$

The adjusted error variance of the remaining ambiguities can be computed using equation (3.19). Given the adjusted ambiguities and their error variance, the search range for each ambiguity can be computed as:

$$\Delta\nabla\overline{N}_n - k\sigma_{\Delta\nabla\overline{N}_n} \le \Delta\nabla N_n \le \Delta\nabla\overline{N}_n + k\sigma_{\Delta\nabla\overline{N}_n} \tag{3.23}$$

where k is the scale factor. Depending on the error behaviour in the observations, its value can range from 3 to 10 (Lu, 1995).

Assuming that there are n ambiguities, there will be n levels in which the recursive search procedure will be performed with each ambiguity having its search range representing one level. Search levels can be demonstrated graphically as in Figure 3.5 below:

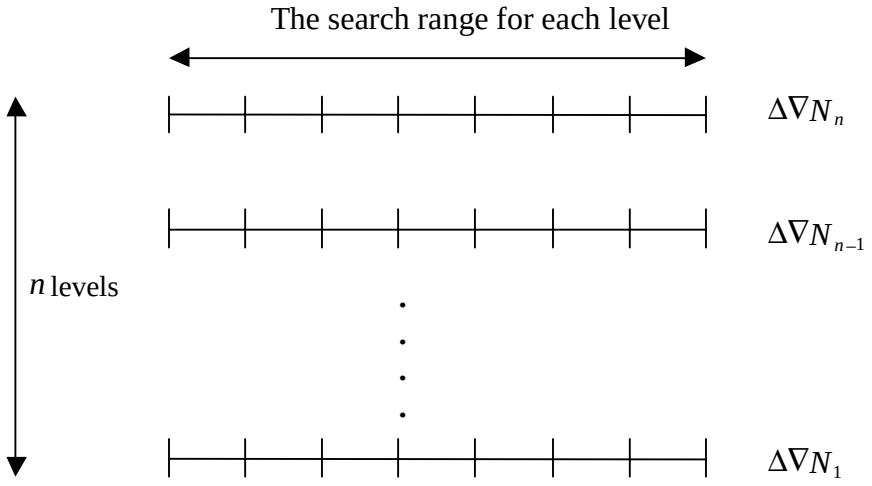

Figure 3.5 FASF Search Levels.

Throughout the recursive search, two sets of candidates consisting of the smallest and the second smallest SOS residuals given by equation (3.18) are obtained. At the end, the discrimination test is on the ratio of the smallest and the second smallest SOS residuals to validate the acceptability. The ratio test is discussed in the next section.

3.3.3 Quality Control

The quality control process has two purposes. One is to guarantee with some likelihood that the solution from the recursive search procedure is correct through a statistical test called the discrimination or ratio test. The other aim is to further validate integers at each epoch over the period after the integer is fixed. The validation test at this stage is the residual test.

Ratio Test

This validation test evaluates the ratio between the SOS residuals of the best and second best integer sets against a threshold. Based on equation (3.13), the SOS is defined as the following in FASF:

$$\Omega = \sum_{i=1}^{n} (\nabla\Delta\hat{N}_i - \nabla\Delta N_i)^2 / Q_{i|1,\ldots,j\neq i,\ldots,n} \tag{3.24}$$

where

Ω is the sum of squared residuals,

$\nabla\Delta\hat{N}, \nabla\Delta N$ are float ambiguity and integer candidate, respectively, and

$Q_{i|1,\ldots,j\neq i,\ldots,n}$ is the conditional variance of ambiguity i assuming that the rest ambiguities are fixed.

The ratio test is:

$$\frac{\Omega_{second\ smallest}}{\Omega_{smallest}} > \tau \tag{3.25}$$

where τ is a threshold. This threshold will be discussed shortly in the following paragraphs.

The ratio calculated on the left hand side of equation (3.25) is a random variable. The test can then be translated into hypothesis testing with two hypotheses, the null hypothesis denoted by H_0 and the alternative hypothesis denoted by H_1:

H_0 : the best solution is correct

H_1 : the best solution is incorrect

Given a threshold (the critical value) if the test for equation (3.25) passes, H_0 would not be rejected and the set of ambiguity candidates with the smallest SOS would be selected as the correct solution. Otherwise H_0 would be rejected. The rationale behind the validation test is that the SOS of the correct integers should be significantly larger than the SOS of the second best solution. This also implies that the likelihood of the best solution should be sufficiently different from the likelihood of the second best solution if enough geometry information is accumulated over time. If the difference is not sufficient the evidence of accepting the best solution would not be conclusive. Figure 3.6 shows the SOS of two sets of ambiguity candidates from a sample of GPS data. In this figure, the SOS of the wrong ambiguities (the second best) diverges as the geometry changes over times while the the SOS of the correct ambiguities (the best) converges. This makes the

ratio between these two SOSs reach the threshold, which in this case is 4, resulting in the integer resolution.

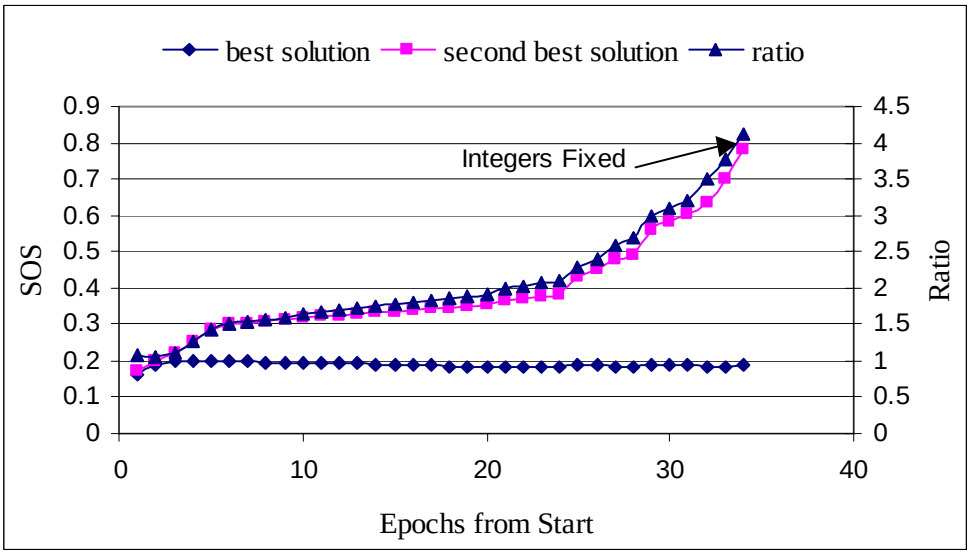

Figure 3.6 SOS Values of the Correct Ambiguities and Incorrect Ambiguities

In some of the literatures (Abidin, 1993; Rochacher and Mervart, 1996), the ratio is said to be a Fisher distribution. Lu (1995) states that this is not correct since the denominator and numerator are clearly correlated. Nevertheless, theoretically the threshold can be chosen with some significance level. In the case of an F-distribution the critical value or threshold can be determined based on the significance level, α, and the degrees of freedom of the system. The ratio test however can lead to incorrect results, i.e. the null hypothesis H_0 may fail to reject while it is false and a type II error is committed. A Type I error, in which H_0 is rejected while it is true, can also be committed and it causes the search procedure to take longer time to resolve integers. The ratio used in this research is 4. To further validate the integers which are deemed correct based on the ratio test, the residual check is performed.

Residual Check

The residual test is to further check whether the 'fixed' integers are correct or not. The rationale behind the residual check is that if the ambiguities are incorrectly fixed the measurement residuals will be large, or they will increase over the time as the geometry changes. The residuals are calculated using the following formula:

$$r = \Delta\nabla\hat{\rho} + \lambda\nabla\Delta N - \nabla\Delta\varphi \tag{3.26}$$

where $\nabla\Delta\hat{\rho}$ is the computed DD range between receivers and satellites using the fixed solution. The misclosure given by equation (3.26) is then used to carry out the test:

$$\begin{aligned} r &\le \tau_1 \\ r &\le \tau_2 \end{aligned} \tag{3.27}$$

where τ_1 and τ_2 are two thresholds and $\tau_1 < \tau_2$. τ_1 is used to detect small errors while τ_2 is designated for large errors or blunders. In FLYKIN™, the empirical values of these two thresholds (τ_1 and τ_2) are 3.5 cm and 5 cm for 'short' baselines (< 1000 m), and 5 cm and 7 cm for the 'long' baselines (>1000 m), respectively. A flowchart of the residual check is shown in Figure 3.7.

3.4 Ambiguity Dilution of Precision (ADOP) and Ambiguity Search Space

The ADOP is a scalar measurement which represents the accuracy of the float ambiguities and the size of the integer search space (Teunissen, 1997). Its value is defined as follows:

$$ADOP = (\det Q_a)^{\frac{1}{2n}} \tag{3.28}$$

where Q_a is the VCV matrix of the float ambiguities at a given epoch.

Theoretically the ADOP is invariant under volume preserving transformations such as the Z-transformation (Teunissen, 1995). The computation of equation (3.28) is not an easy task. An alternative method to compute the ADOP is:

$$\det Q_a = \prod_{i=1}^{n} \sigma^2_{\hat{N}_{i|1,\ldots,n-1}} \tag{3.29}$$

where $\sigma_{\hat{N}_{i|1,\ldots,n-1}}$ is the conditional variance of ambiguity $\hat{N}_i$ after LAMBDA decorrelation.

Teunissen (1997a) presents a closed form of the ADOP in a least squares estimation for the L1 only case as:

$$ADOP_{L1} = m^{\frac{1}{2(m-1)}} \sqrt{\frac{\sigma^2_{\phi_1}}{k\lambda_1^2}} \left(1 + \frac{\sigma^2_{\rho_1}}{\sigma^2_{\phi_1}}\right)^{\frac{1}{2}} \tag{3.30}$$

where

- m is the number of satellites ,
- k is the number of samples,
- λ_1 is the wave length,
- σ_{ρ_1} is the standard deviation of the code measurement, and
- σ_{ϕ_1} is the standard deviation of the carrier phase measurement.

Equation (3.30) shows that there is no dependency on the reference satellite, or the geometry. Generally the ADOP depends on the following factors (Teunissen, 1997a):

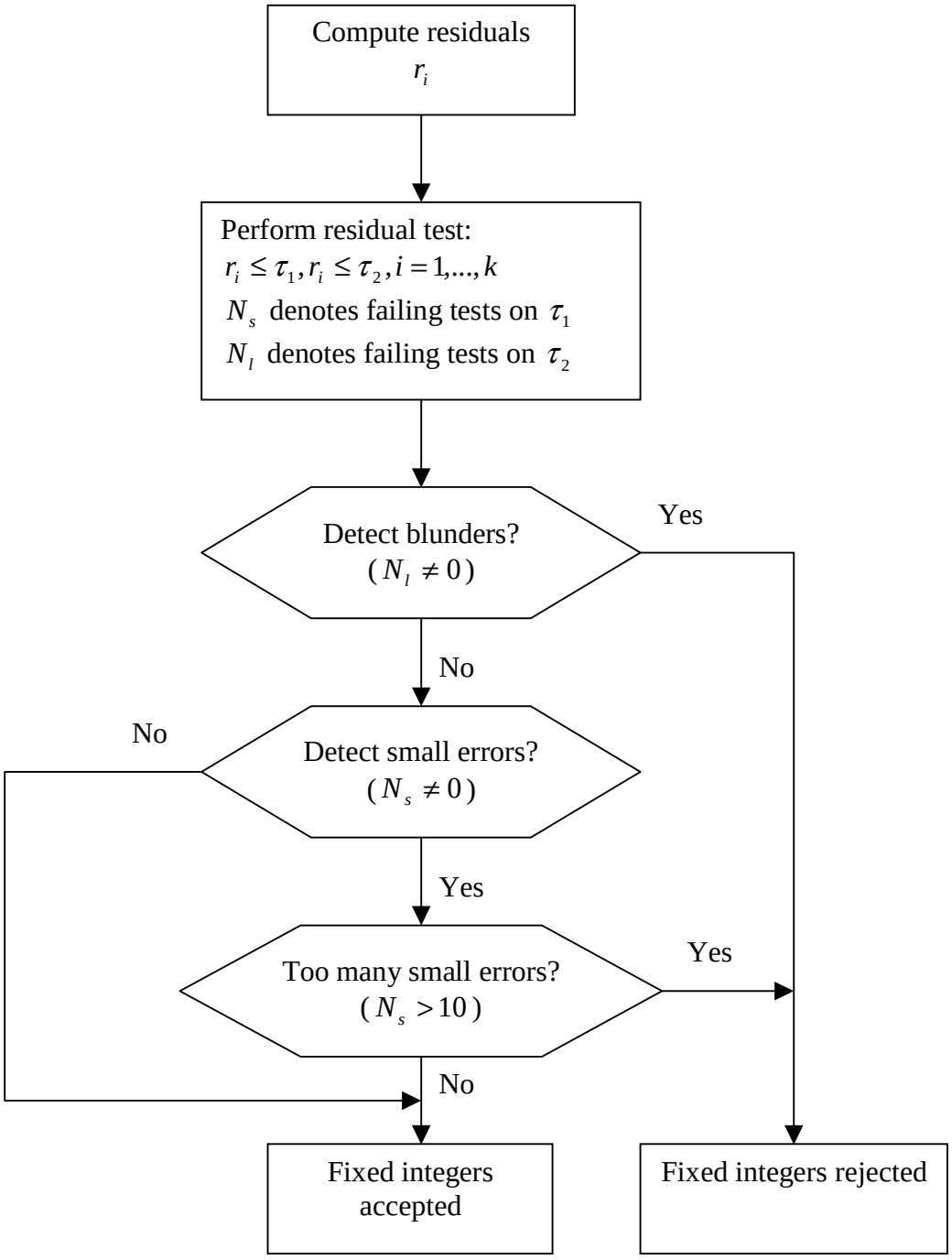

Figure 3.7 Residual Test

1. The number of satellites observed.
2. The accuracy of the code and carrier phase measurements.
3. Measurement redundancy.

The closed form for dual frequency is (Teunissen, 1997):

$$ADOP_{L1,L2} = m^{\frac{1}{2(m-1)}} \sqrt{\frac{\sigma_{\phi_1}\sigma_{\phi 2}}{k\lambda_1\lambda_2}(1+\frac{\sigma_{\phi_1}^2\sigma_{\phi_2}^2}{\sigma_{\rho_1}^2\sigma_{\rho_2}^2}\frac{\sigma_{\rho_1}^2+\sigma_{\rho_2}^2}{\sigma_{\phi_1}^2+\sigma_{\phi_2}^2})^{\frac{1}{2}}} \tag{3.31}$$

where

m is the number of satellites,

k is the number of samples,

λ_1, λ_2 are the wavelengths of L1 and L2, respectively,

$\sigma_{\rho_1}, \sigma_{\rho_2}$ are the standard deviations of L1 and L2 code measurements, respectively, and

$\sigma_{\phi_1}, \sigma_{\phi_2}$ are the standard deviations of L1 and L2 carrier phase measurements, respectively.

A comparison of equations (3.30) and (3.31) shows that the dual frequency ADOP is smaller than that of L1 because of the inclusion of L2 measurements. This, in theory, explains why generally time to resolve integers is generally faster when there are L2 measurements present in the filter.

In FASF the actual number of ambiguity candidates to be searched is dynamic depending on the covariance matrix of the float ambiguities from the filter and the ambiguity validation procedure (e.g. the maximum number of candidates to be processed). However, the ADOP can provide information on the size of the search space. The search space volume can be obtained using the following formula:

$$V_n = k^n ADOP^n \tag{3.32}$$

where

V_n is the number of integer candidates in the search space where there are n satellites, and

k is the scale (expansion) factor used in computing search range in FASF procedure.

CHAPTER 4

AMBIGUITY RESOLUTION WITH INS AIDING

This chapter investigates the feasibility of using inertial data to aid OTF ambiguity resolution in a modified FASF framework. Three approaches to assist GPS ambiguity resolution are studied in this chapter. The implementation of each of them depends on different INS/GPS integration schemes. The approaches that are studied are:

- INS bridging in a decentralized filter configuration
- Adding an INS navigation solution as a reference or measurement to the GPS filter to enhance the GPS measurement update in a decentralized filter configuration. This is called INS measurement aiding.
- Augmenting the INS master filter to have ambiguity states in the centralized filter configuration.

The first approach feeds an INS navigation solution as initial information in the GPS filter before ambiguity estimation. The INS measurement aiding approach adds the INS navigation solutions to the measurement equations in the GPS filter to update the prediction. It is clear that the centralized integration approach naturally has the aiding capability of the third method since ambiguities are part of the state vector. The following subsections discuss each of these aiding approaches.

4.1 Ambiguity Resolution with INS Bridging

FASF restarts the ambiguity estimation and search procedure to determine new ambiguities after cycle slips and less than four satellites available or when GPS outages occur since the filter loses the fixed integer solution. Figure 4.1 shows a flowchart of ambiguity fixing with consideration of GPS outages.

The information gained on the ambiguity prior to the outage is completely lost in the filter reset. As shown in Figure 4.2 the ambiguity estimates during phase B will not incorporate any information from phase A. In GPS-only positioning at the starting point of phase B, i.e. once the receiver reacquires satellites, the initial position is computed using standard least squares with DD code measurements. The initial float ambiguities are calculated with the following formula using code and carrier phase measurements:

$$\nabla\Delta\hat{N}_0 = \frac{\nabla\Delta\phi - \nabla\Delta\rho}{\lambda} \tag{4.1}$$

where

$\nabla\Delta\hat{N}_0$ is the double differenced initial ambiguities (cycles),

$\nabla\Delta\phi$ is the double differenced carrier phase measurement (metres), and

$\nabla\Delta\rho$ is the double differenced pseudorange (metres)

However the initial positions and float ambiguities calculated from GPS measurements may not be accurate. The accuracy will depend on the vehicle dynamics and many other

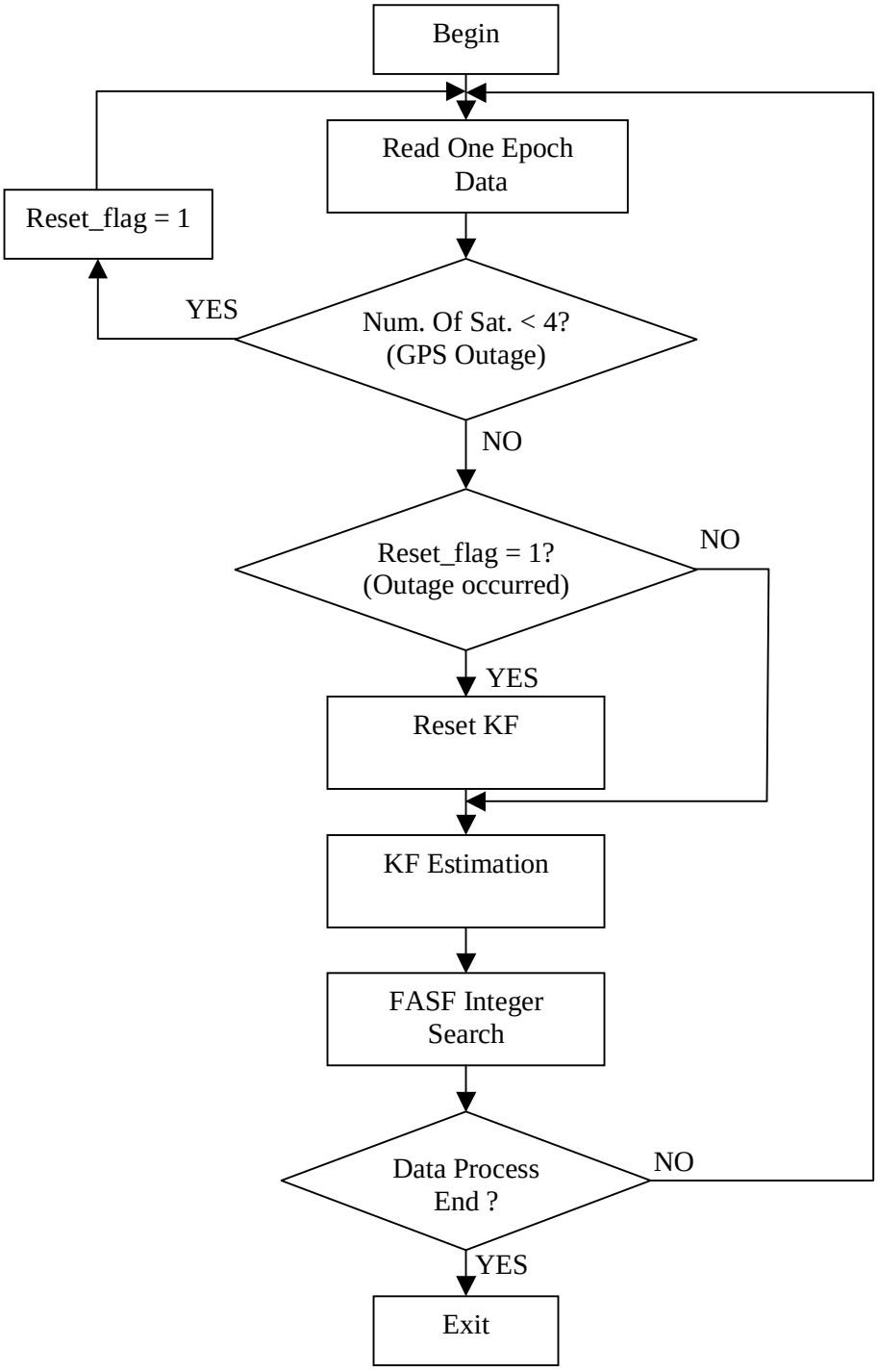

Figure 4.1 Ambiguity Resolution with GPS Outage

surrounding factors (e.g. multipath and receiver noise) which can affect GPS measurements adversely. Since an INS is a self-contained navigation system which does not require any external signals, it can fill the outage and act as a bridge to carry previous estimation information into phase B.

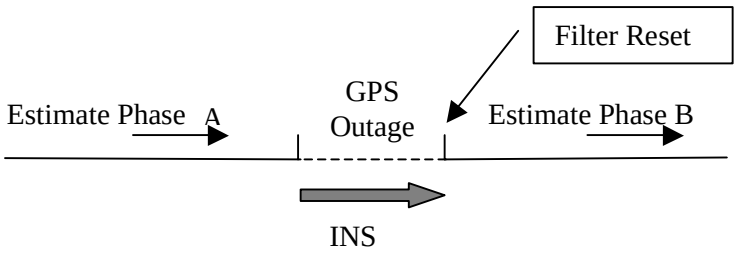

Figure 4.2 GPS Filter Reset and INS Bridging During a GPS Outage

The aiding mechanism in the decentralized integration is shown in Figure 4.3. With this aiding approach, the state error prediction in the master filter is still performed during the GPS outage and the INS output continues to be corrected with the predicted errors. Once the outage ends, the position and velocity along with their associated covariance matrix information from the INS is used to initialize the GPS filter. The initial ambiguities are calculated using the following equation:

$$\nabla\Delta\hat{N}_0 = \frac{\nabla\Delta\varphi - \nabla\Delta\hat{\rho}}{\lambda} \tag{4.2}$$

where $\nabla\Delta\hat{\rho}$ is the computed double-difference pseudorange based on the predicted INS position. By replacing the measured pseudorange with the more accurate predicted measurement, the code multipath error and receiver noise are potentially removed. Typically the code multipath ranges from 0.2 and 3 m while the code noise from 0.1 to

3m (Lachapelle, 1998). These errors are quite significant and will affect the ambiguity estimation accuracy and thus degrade the time to fix integers in the FASF search procedure. After the outage, and when ambiguity integers are fixed, navigation solutions or measurements and integers are fedback to the INS filter to perform the update. The dashed line in the figure represents this feedback.

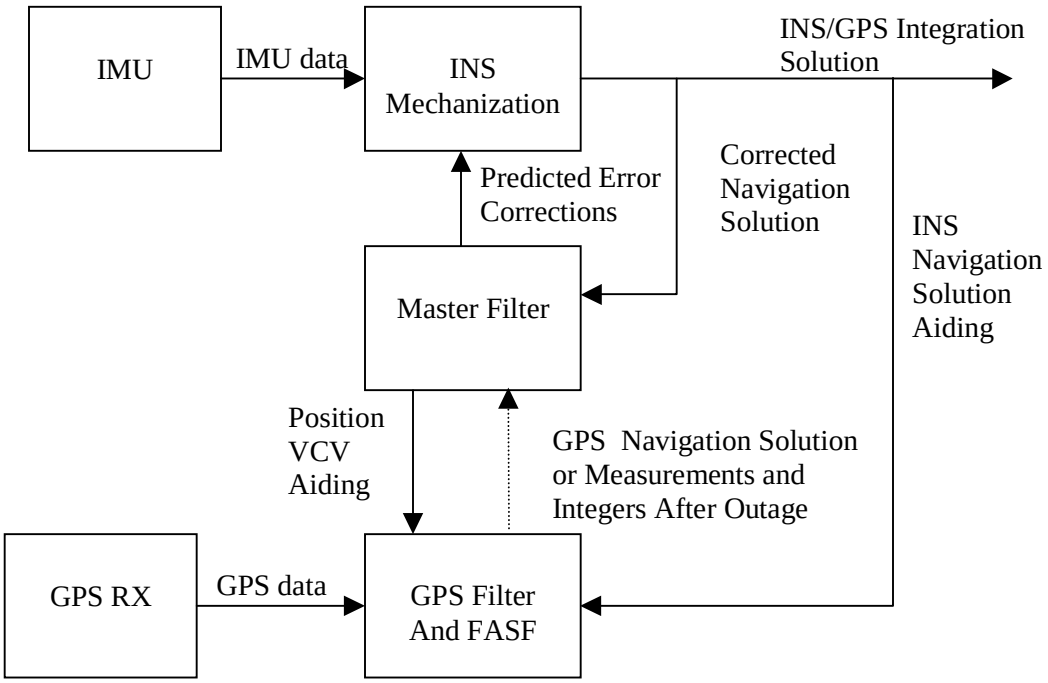

Figure 4.3 INS Navigation Aiding in a Decentralized INS/GPS Integration Filter

4.2 Ambiguity Resolution with INS Measurement Aiding

As described in Section 2.3.3, in a tightly coupled integration using a decentralized filter structure, the GPS carrier phase and code measurements along with GPS integer ambiguities are fed into the master filter which estimates the INS errors. The GPS filter

(or local filter) runs independently of the master filter to estimate ambiguities. In the case that the GPS filter loses its integers when there are GPS outages (or when the residual consistency check fails) the filter needs to restart ambiguity estimation and search. The aiding mechanism is the same as that demonstrated in Figure 4.3. During float ambiguity estimation, the navigation solution from the INS in stand-alone mode along with the covariance matrix from the master filter are used as additional measurement information in the GPS filter update equation.

Denoting the position from the INS output at k epoch as r_k^{ins}, gives:

$$r_k^{ins} = r_k + \Delta r_k \tag{4.3}$$

where $r_k = [\varphi \quad \lambda \quad h]_k^T$, and Δr_k are INS position errors.

This gives:

$$r_k^{ins} - r_k^0 = r_k + \Delta r_k - r_k^0 = r_k - r_k^0 + \Delta r_k = \delta r_k + \Delta r_k = \begin{bmatrix} \delta\varphi \\ \delta\lambda \\ \delta h \end{bmatrix}_k + \Delta r_k \tag{4.4}$$

or alternatively.:

$$\left[r_k^{ins} - r_k^0\right] = \begin{bmatrix} \delta\varphi \\ \delta\lambda \\ \delta h \end{bmatrix}_k + r_{3k} \tag{4.5}$$

Equation (4.5) can then be used to update the FASF's prediction along with its original measurement equations (2.19) and (2.20).

4.3 Augmentation of Master Filter to Assist Ambiguity Resolution

In the centralized INS/GPS integration structure as indicated in Figure 2.8, the master filter is augmented to have ambiguity states. By modeling the ambiguity states into the master filter's state vector, the IMU automatically contributes to ambiguity estimation. In this configuration, the Kalman filter is removed from the FASF and thus only the search algorithm remains. Basically the filters i.e. the FASF filter and the master filter, are merged together into one filter and all functions in the GPS navigation module are removed. Cycle slip detection is integrated into the aiding module using the inertial data. The inertial aiding in cycle slip detection is discussed in Section 4.6, and the ambiguity resolution aiding mechanism is shown in Figure 4.4.

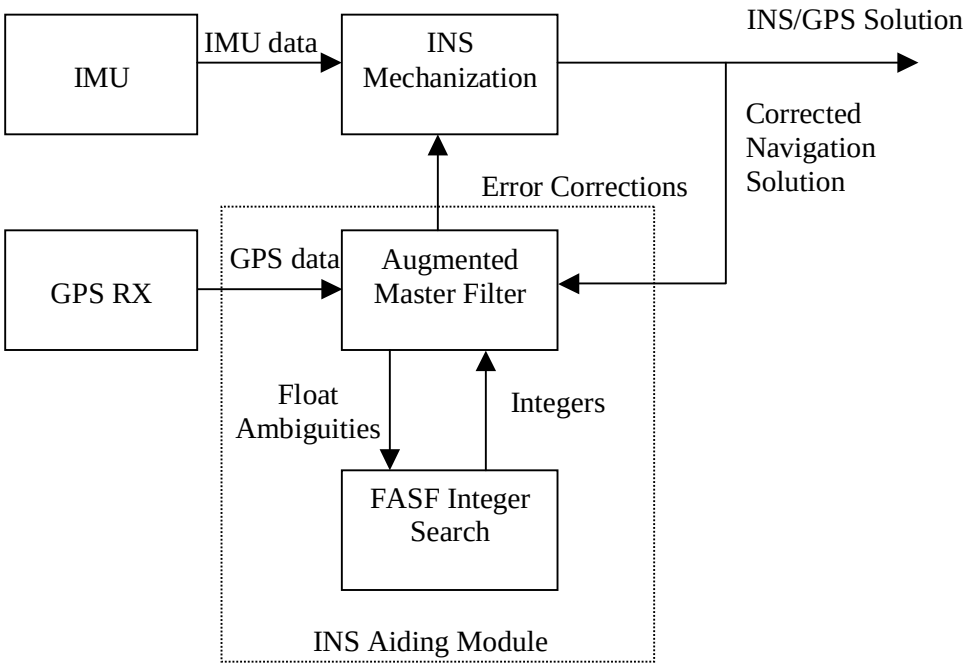

Figure 4.4 INS Aiding in the Centralized INS/GPS Integration Filter

With this aiding approach, the augmented master filter (AMF) will estimate the float ambiguities and the FASF search procedure takes the estimated float ambiguities along with their covariance matrix to perform a normal search. Once the integers are fixed the AMF will stop ambiguity estimation.

4.4 Summary of INS Aiding Approaches in Ambiguity Resolution

The three ambiguity resolution approaches with INS data require a navigation solution from the INS stand-alone navigation module, and the first two approaches require additional error predictions from the master filter. Thus, the feasibility of using these three mechanisms depends on the quality of the INS equipment and the period of INS stand-alone navigation. The advantage of using an INS solution in ambiguity resolution only occurs when the accuracy of the INS solution is better than the DGPS code solution. The feasibility relies on the INS to provide a superior accuracy over the short term. Figure 4.5 shows a position drift of a high quality IMU during a 10-second snapshot period. The INS data is from the HG-1050 INS, which is a navigation- grade INS to be further discussed in Chapter 6.

Although GPS does not have such a linear error growth behaviour, it typically cannot achieve such accuracy with double differenced pseudorange measurements. The self-contained features of the INS also provide a reliable information source. By incorporating an accurate INS bridging solution into FASF, more accurate information is obtained to perform its subsequent estimation and thus the time to fix integers and the reliability can be potentially improved.

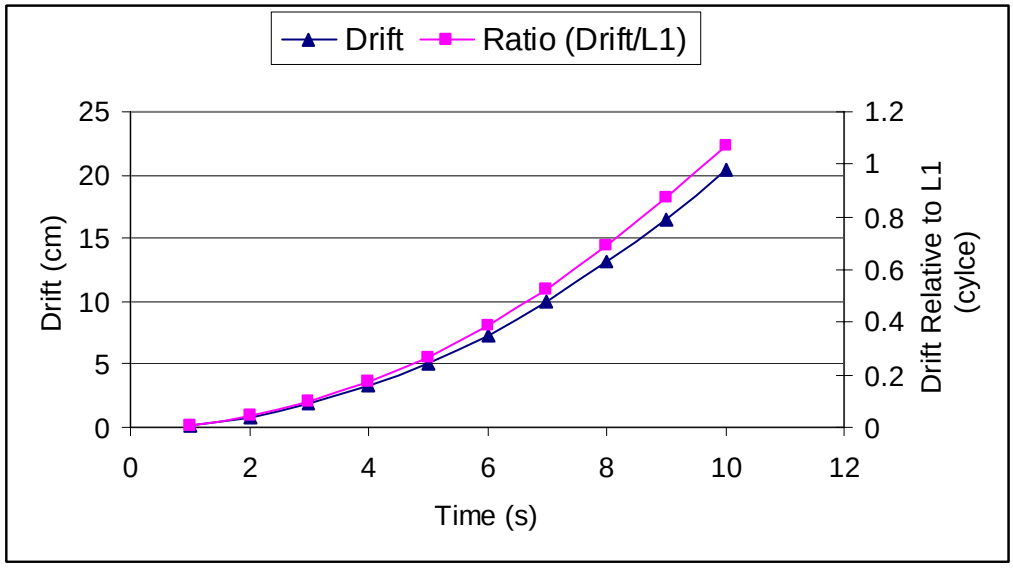

Figure 4.5 INS Position Drift (Horizontal Error), 10 seconds

The first approach, so-called INS navigation aiding, is primarily useful in GPS outages where there is no GPS available or the number of satellites available is insufficient (i.e. less than four) such that the GPS navigation module cannot fix the receiver's position. This approach is simplistic and easy to implement since it does not require any change to the system model.

The INS measurement aiding approach may not be suitable for GPS outages with a relatively long period of time because the INS is already in stand-alone navigation mode during the GPS outage and its navigation solution may not be sufficiently good to be added in the GPS filter as an additional piece of measurement information after the outage due to the linear position error drift of the INS stand-alone solution. However, INS measurement aiding would be suitable very short-period GPS outages or cases when the GPS filter loses the integers because of cycle slips or failure of the residual checks. In these cases, the INS drift will not be significant since the INS measurement incorporation

in the GPS filter starts almost immediately after INS stand-alone navigation mode. This approach requires the modification of the measurement equations in the GPS filter and it is obviously more complicated than INS navigation aiding.

The third approach, the augmented master filter, is a very different INS/GPS integration architecture from the first two approaches. It reduces the complexity of having two parallel Kalman filters. INS aiding in ambiguity resolution is automatically accomplished through the float ambiguity estimation in the augmented state vector. This approach is also subject to the INS drift during its stand-alone navigation mode.

4.5 Float Ambiguity Accuracy and ADOP with INS Aiding

In previous sections, the incorporation of an INS navigation solution into the GPS filter, as an additional piece of information, is studied. The key to this integration is whether it can improve the accuracy of the estimated float ambiguity since the accuracy is directly related to the FASF search procedure as indicated earlier. In other words, it needs to be determined if the inertial data can reduce the ADOP magnitude and thus shrink the ambiguity search space. A float ambiguity with poorer accuracy will increase the time to fix integers and also reduce the reliability of fixing. This section explores the effect of inertial data over the accuracy of the float ambiguity as well as the ADOP in the least squares framework.

Assuming there are n observations and k satellites (except the base satellite), the system of equations which contains the double-differenced code, carrier phase and INS navigation solution are:

$$\begin{aligned} \delta r^{ins} &= H\delta r + \varepsilon_{ins} \\ \delta\nabla\Delta\rho &= A\delta r + \varepsilon_{\nabla\Delta\rho} \\ \delta\nabla\Delta\varphi &= A\delta r + \lambda B\nabla\Delta N + \varepsilon_{\nabla\Delta\varphi} \end{aligned} \tag{4.6}$$

where

δr^{ins} is the difference between INS position and the nominal position, i.e. the INS 'measurement' vector ($3n\times 1$),

$\delta\nabla\Delta\rho$ is the vector ($nk\times 1$) of measured minus computed double difference code measurement,

$\delta\nabla\Delta\varphi$ is the vector ($nk\times 1$) of measured minus computed double difference carrier phase measurement,

δr is the parameter vector (3×1) that contains the increments of the baseline coordinates,

$\nabla\Delta N$ is the double difference ambiguity vector ($k\times 1$),

H is a design matrix ($3n\times 3$),

A is a design matrix ($nk\times 3$),

B is a design matrix ($nk\times k$) of the ambiguity state vector, and

$\varepsilon_{ins}, \varepsilon_{\nabla\Delta\rho}, \varepsilon_{\nabla\Delta\varphi}$ are the measurement noises of the INS, DD code and carrier phase measurements, respectively.

The design matrices H and B take following special forms:

$$H = \begin{bmatrix} 1 & 0 & 0 \\ 0 & 1 & 0 \\ 0 & 0 & 1 \\ 1 & 0 & 0 \\ 0 & 1 & 0 \\ 0 & 0 & 1 \\ \vdots & \vdots & \vdots \end{bmatrix} = \begin{bmatrix} I_3 & I_3 & \cdots \end{bmatrix}^{\tau} \tag{4.7}$$

$$B = \begin{bmatrix} I_k & I_k & \cdots \end{bmatrix}^{\tau} \tag{4.8}$$

Rearranging equation (4.6) into a vector form gives:

$$\underbrace{\begin{bmatrix} \delta r^{ins} \\ \delta \nabla \Delta \rho \\ \delta \nabla \Delta \varphi \end{bmatrix}}_{y} = \underbrace{\begin{bmatrix} H & O \\ A & O \\ A & \lambda B \end{bmatrix}}_{B} \underbrace{\begin{bmatrix} \delta r \\ \nabla \Delta N \end{bmatrix}}_{b} + \underbrace{\begin{bmatrix} \varepsilon_{ins} \\ \varepsilon_{\nabla \Delta \rho} \\ \varepsilon_{\nabla \Delta \varphi} \end{bmatrix}}_{\varepsilon} \tag{4.9}$$

or the more simplistic form:

$$y = Bb + \varepsilon \tag{4.10}$$

The closed form of the least squares solution to the above normal equation can readily be obtained. However, what is of interest is the VCV matrix of the estimated parameters. The VCV matrix can be obtained based on standard least squares adjustment theory (Krakiwsky, 1990):

$$\begin{bmatrix} Q_{\delta r} & Q_{\delta r, \nabla \Delta N} \\ Q_{\nabla \Delta N, \delta r} & Q_{\nabla \Delta N} \end{bmatrix} = \left(B' R_{\varepsilon}^{-1} B \right)^{-1} \tag{4.11}$$

where R_{ε}^{-1} is the inverse of VCV matrix of measurement errors ε.

What is needed to resolve is the VCV matrix for the DD ambiguities, i.e. $Q_{\nabla\Delta N}$. The following closed form of the DD ambiguity vector VCV matrix can be obtained (for a full derivation see Appendix A):

$$Q_{\nabla\Delta N} = \frac{1}{\lambda^2}[R^*_{\nabla\Delta\varphi} + R^*_{\nabla\Delta\varphi}B'R^{-1}_{\nabla\Delta\varphi}[H'R^{-1}_{ins}H + A'R^{-1}_{\nabla\Delta\rho}A]^{-1}A'R^{-1}_{\nabla\Delta\varphi}BR^*_{\nabla\Delta\varphi}] \quad (4.12)$$

where

$R_{\nabla\Delta\varphi}$ is the VCV of the DD carrier phase measurement errors

$R_{\nabla\Delta\rho}$ is the VCV of the DD code measurement errors,

R_{ins} is the VCV of the INS navigation errors, and

$R^*_{\nabla\Delta\varphi}$ is the $k \times k$ matrix that is the linear combinations of $R^{-1}_{\nabla\Delta\varphi}$. See derivation in the Appendix A.

If there is no inertial data present in the system equations, the same technique can be used to obtain the corresponding VCV matrix of the DD ambiguities as follows:

$$Q^*_{\nabla\Delta N} = \frac{1}{\lambda^2}[R^*_{\nabla\Delta\varphi} + R^*_{\nabla\Delta\varphi}B'R^{-1}_{\nabla\Delta\varphi}[A'R^{-1}_{\nabla\Delta\rho}A]^{-1}A'R^{-1}_{\nabla\Delta\varphi}BR^*_{\nabla\Delta\varphi}] \quad (4.13)$$

All VCV matrices and their corresponding inverse forms are positive definite matrices. The special form, $R^*_{\nabla\Delta\varphi}$, is a positive definite matrix as well. By comparing equations (4.13) and (4.12) it is intuitive that the following condition is satisfied:

$$\det Q_{\nabla\Delta N} < \det Q^{*}_{\nabla\Delta N} \tag{4.14}$$

The analysis of the VCV matrix of the DD ambiguities indicates that the incorporation of the inertial data improves the accuracy of the float ambiguities and reduces the search space. This result will be shown with real data in Chapter 7.

4.6 Cycle Slip Detection and Recovery with INS Aiding

Cycle slip detection and repair is an important strategy for quality control in GPS navigation with carrier phase measurements. In the case when only GPS is available, the detection of cycle slips and recovery can be performed with the aid of the Doppler measurements (Cannon, 2002). The algorithm basically predicts the carrier phase measurement and compares it with the actual observation. The predicted carrier phase can be calculated using the following equation:

$$\phi_{k+1} = \phi_k + \frac{\dot{\phi}_k + \dot{\phi}_{k+1}}{2}\Delta t \tag{4.15}$$

where

ϕ is the carrier phase measurement,

$\dot{\phi}$ is the carrier phase rate,

k is the epoch where measurement is made, and

Δt is the time interval between two consecutive epochs.

The accuracy of this method largely depends on the vehicle dynamics. It assumes that the vehicle's velocity is constant during the interval Δt which may not be true in reality, especially when the vehicle makes a turn or accelerates. This method may also not be able to detect small cycle slips. The typical magnitude of cycle slips that can be detected and recovered with this method is 10 cycles under normal vehicle dynamics (Cannon, 1994).

During INS/GPS integration, the INS can be used to predict the vehicle's position which has better accuracy since the INS has very good short-term positioning accuracy. A double differenced carrier phase can then be computed based on the INS output and a difference can be calculated by comparing the calculated double differenced carrier phase and the measured one using the following formula:

$$\delta = \frac{\Delta\nabla\rho}{\lambda} - \Delta\nabla\phi \tag{4.16}$$

where

δ is the difference between the predicted and measured double-difference carrier phase in cycles,

$\Delta\nabla\rho$ is the computed double-difference pseudorange in meters based on INS predicted position, and

$\Delta\nabla\phi$ is the measured double-difference carrier phase (cycles).

With δ computed, a threshold can then be applied to determine whether a cycle slip occurs or not. The threshold should not be large in order to reliably detect small cycle slips. The threshold also needs to be adjusted depending on the quality of INS and the vehicle's dynamics.

CHAPTER 5

INS/GPS INTEGRATION SOFTWARE

A software package, INSGPS, which demonstrates the methodologies discussed in the previous chapter, was developed. It is based on the existing ambiguity resolution program FLYKIN™ and INS/GPS software which only used code measurements in the integration. This chapter describes the structure of the newly developed program and various modules as well as its input and output.

5.1 Software Modules

As shown in Figure 5.1 there are three high level modules, i.e. the INS navigation module, the GPS navigation module and the INS/GPS integration module. These three modules work together in different data processing modes such as INS-only, GPS-only or INS/GPS.

The following sections give the details of each module.

5.1.1 INS Navigation Module

The INS navigation module performs the coarse and fine alignments to obtain the initial orientation relating the INS body frame to the wander frame and subsequently to resolve the INS mechanization equations in the wander coordinate system to obtain positions and

velocities. Figure 5.2 shows the INS navigation module. As indicated in the flowchart, vertical channel assistance from the GPS navigation module is required.

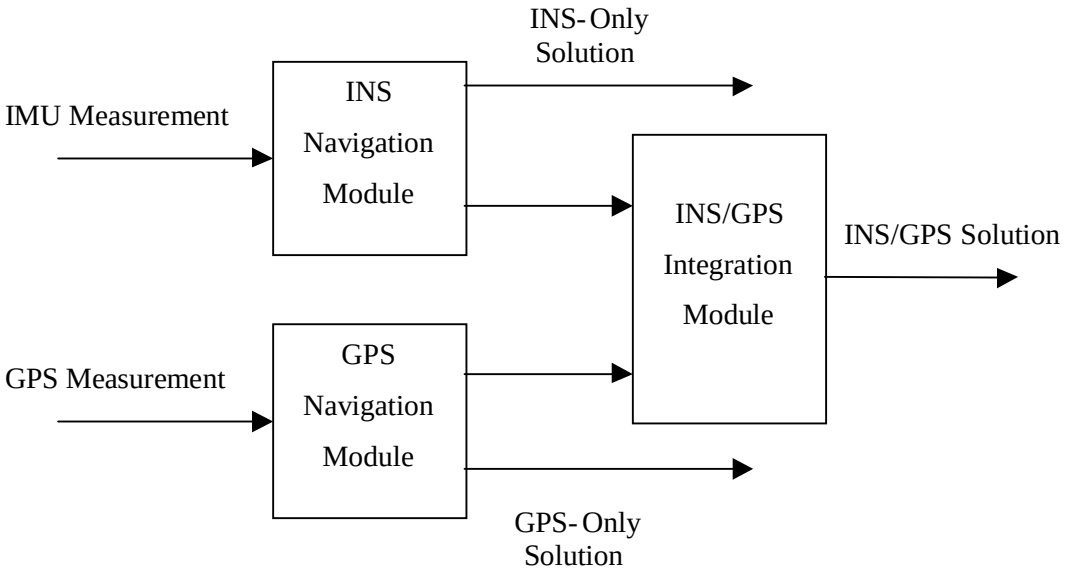

Figure 5.1 High Level Software Modules

The coarse alignment contains 16 iterations and in each iteration the alignment procedure processes four seconds of data. The period of the coarse alignment is thus 64 seconds. Fine alignment needs a time specification from the input option file indicating the window of the INS data to perform the fine alignment. After these two steps, the program enters the INS mechanization module to compute positions and velocities with raw measurements from the gyros and accelerometers. The INS navigation module exits when there is no external data available for processing.

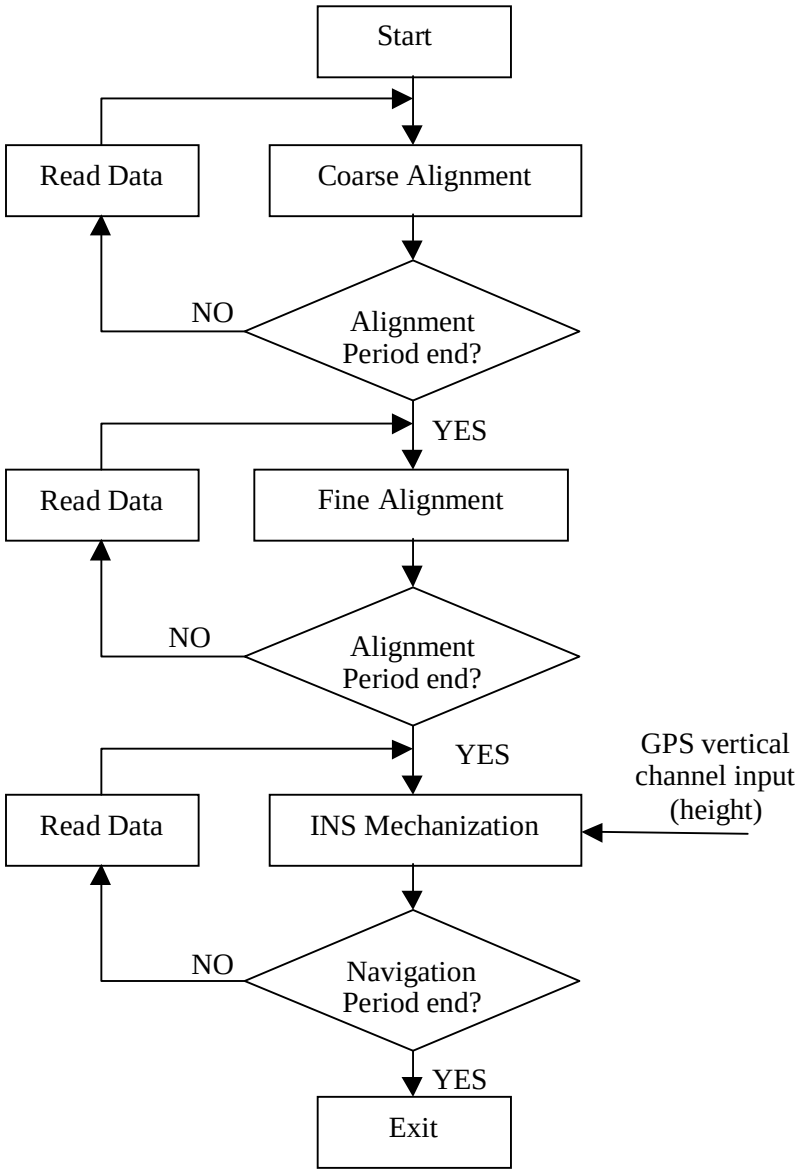

Figure 5.2 INS Navigation Module

5.1.2 GPS Navigation Module

The GPS navigation module computes the receiver's positions and velocities as well as resolves ambiguities along with their variances based on the code and carrier phase

measurements. The ambiguity resolution method – FASF, is implemented in the navigation module to resolve integers. Figure 5.3 shows a flow chart of the GPS navigation module.

In FASF, a Kalman filter is first used to estimate float ambiguities and the LAMBDA transformation is then performed. The recursive search procedure is carried out within the transformed search space. During the search, if the number of ambiguity candidates is more than 2000 the search exits. The number 2000 is an empirical value built in FLYKIN^{TM} to reduce the search time. FASF keeps track of two ambiguity candidates whose SOS residuals are the smallest and the second smallest among all the candidates in the search space. After the search, the ratio of SOS residuals of the two candidates are calculated and compared with a threshold. If the computed value is lager than the threshold, the ambiguity candidate with the smallest SOS residuals is considered the correct solution. The navigation module uses the fixed integers to calculate positions and velocities after the integers are resolved. Otherwise the module uses the estimated float ambiguities to compute the so-called float solution, which has a poorer accuracy compared to the fixed solution.

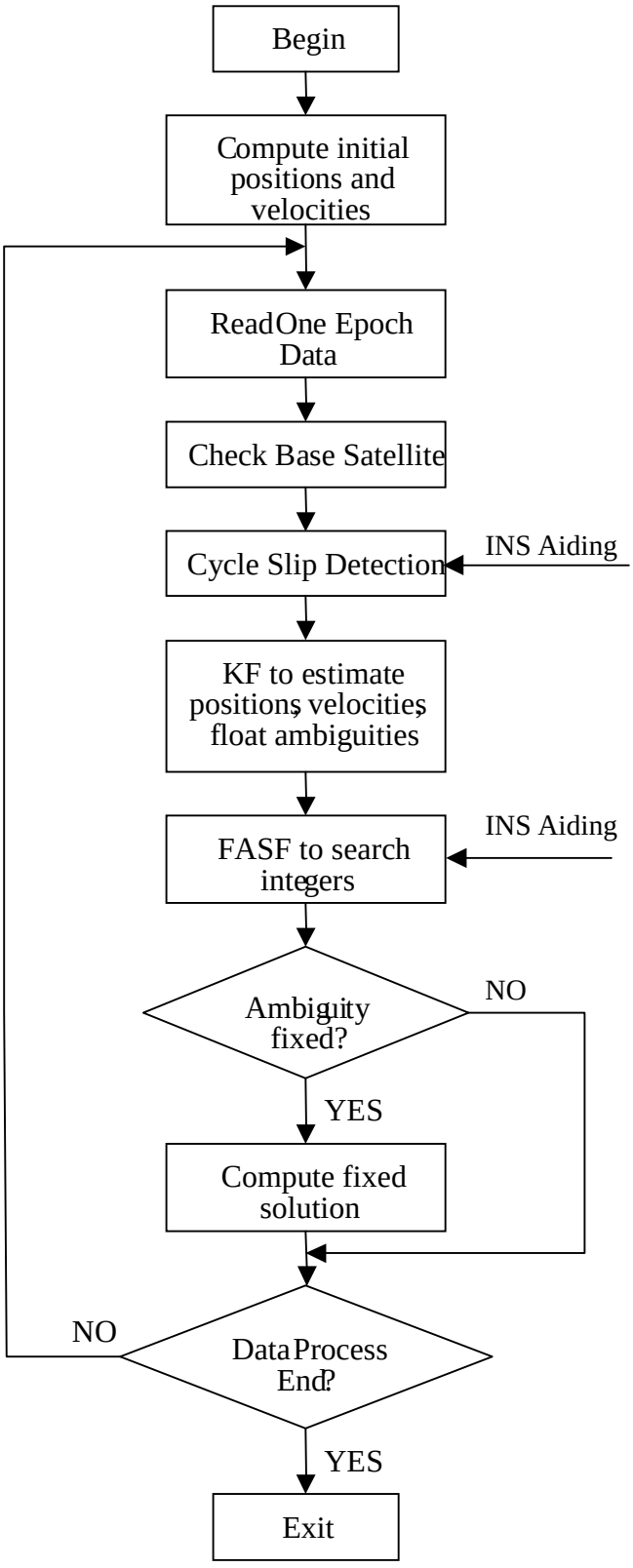

Figure 5.3 GPS Navigation Module

5.1.3 INS/GPS Integration Module

The INS/GPS integration module combines information from the GPS navigation module to update the predictions of the 15 error states in the INS Kalman filter. However, the information from the GPS navigation module is different depending on the integration approach, i.e. whether it is loose coupling or tight coupling. In the loose coupling configuration, the navigation solution from the GPS navigation module is used as a reference and the difference between the GPS and INS solutions are used as measurements to update the prediction in the master filter. In the tight coupling configuration, however, the code and carrier phase measurements from the GPS receivers, and the ambiguities from the GPS navigation module, are required to update the prediction. A flowchart for the INS integration module is shown in Figure 5.4.

5.2 Augmented INS/GPS Integration Module

The augmented integration configuration does not require the GPS navigation module. Since the ambiguity error states are added to the master filter. The error states in the master filter are the 15 standard INS errors plus the errors of all the double differenced GPS ambiguities. The measurements are DD code, carrier phase and phase rate (Doppler) from the GPS receivers.

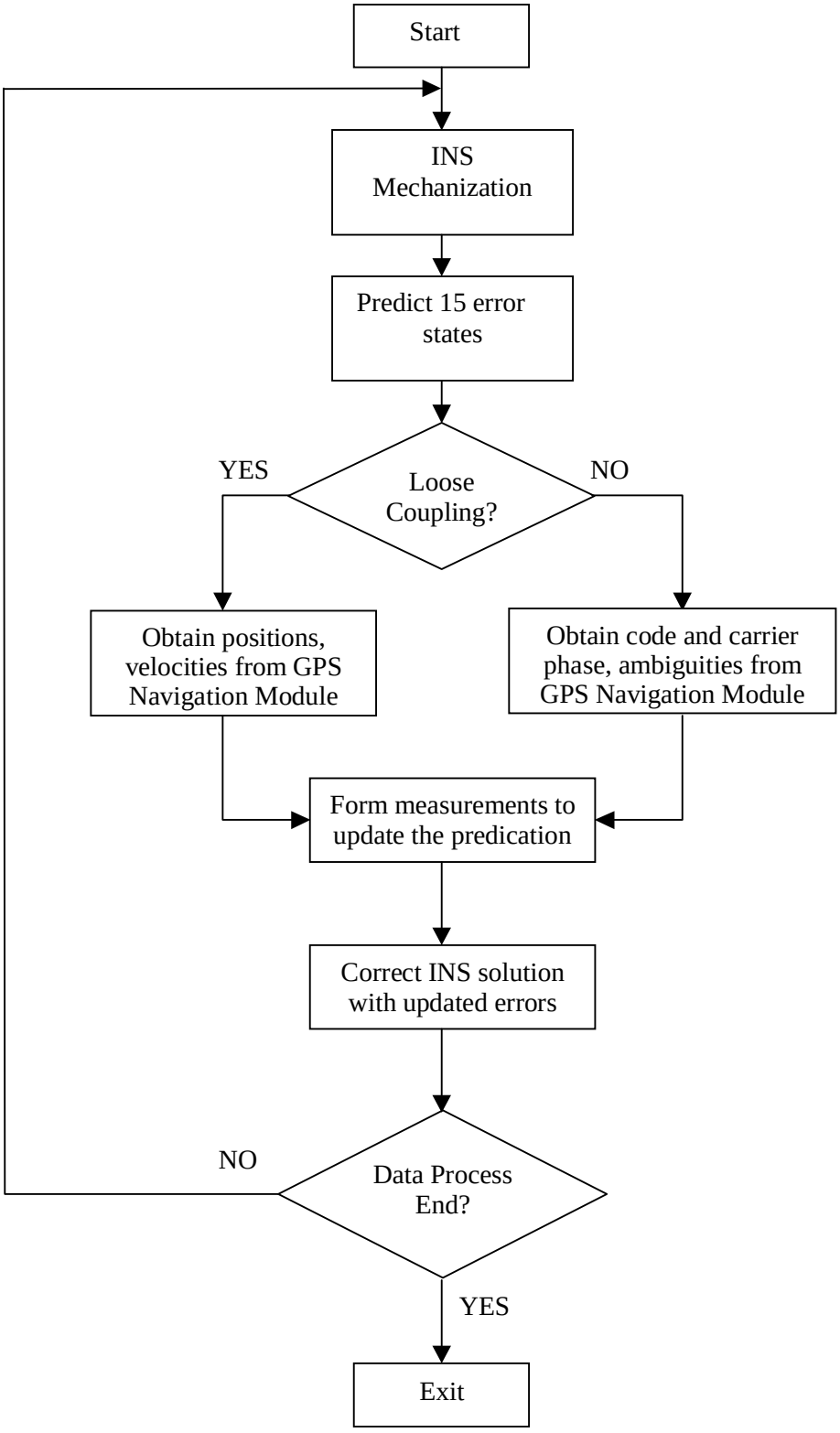

Figure 5.4 INS/GPS Integration Module

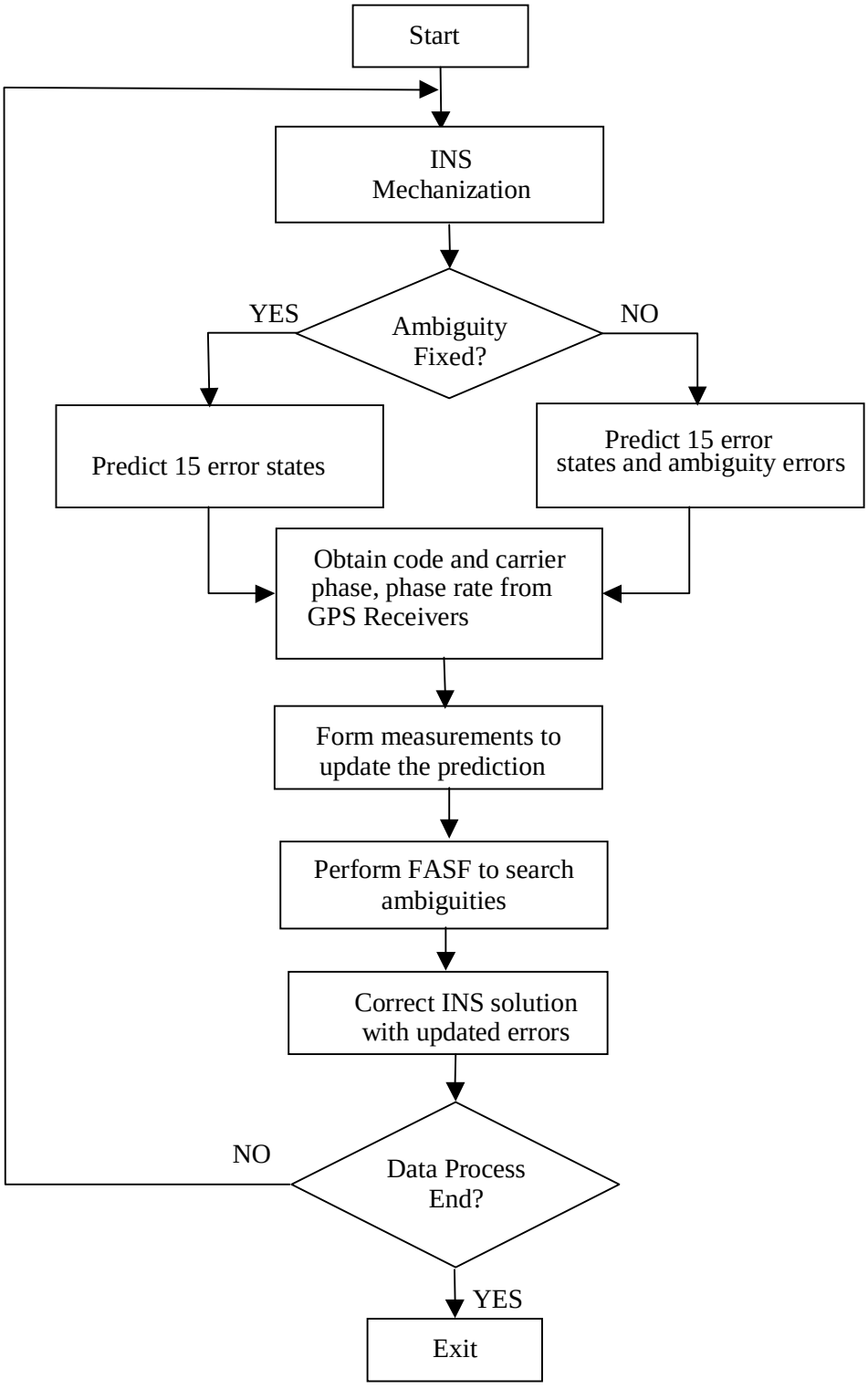

Figure 5.5 Augmented INS/GPS Integration Module

5.3 Software Input and Output

The INS/GPS integration program can run in five modes in terms of data processing, i.e. INS-only, GPS-only, INS/GPS loose coupling, and INS/GPS tight coupling 1 and 2. INS-only mode means INS stand-alone navigation where no integration with GPS is performed. However GPS data is still required to provide vertical channel assistance to the INS navigation module. The GPS-only mode only requires GPS data and the INS navigation module is not involved. The rest of the modes invoke INS/GPS integration with the Kalman filtering mechanism depending on the coupling scheme.

Four data files are required as the data input to run the program:

- Raw GPS measurement data of the base station
- Raw GPS measurement data of the rover station
- Ephemeris data of satellites recorded in the base station
- Raw INS data of the rover station

Data files, along with the input option file, provide all input information to run the program. The program also creates four output files:

- GPS navigation solution (.GPS)
- GPS ambiguity resolution results (.AMB)
- GPS cycle slip detection summary (.SLP)
- INS coarse and fine alignment results (.ALG; except GPS-Only)
- INS navigation solution (.INS; INS-Only) or INS/GPS integration solution (.INS; except GPS-Only)

Conceptually the information in the option file can be grouped into the following three sections:

- GPS data specification
- INS data specification
- Miscellaneous

Details on above specifications are presented in Tables B.1 to B.3 in Appendix B. The format of all output files is summarized in Table B.4 in Appendix B.

CHAPTER 6

TEST DESCRIPTIONS

Two van tests are discussed in this chapter. The first van test denoted as Van Test I, is a short baseline test conducted with lower dynamics while the second test, denoted as Van Test II, is performed over a longer baseline and with higher dynamics. Results from the developed software under different integration scenarios are presented in this chapter to verify the quality of GPS-only, INS-only and INS/GPS navigation modules described in Chapter 5.

6.1 Van Test I

This test was conducted by Applanix Corporation on August 13, 2000 in the area of Richmond Hill, Ontario. The test trajectory comprised a drive along streets near the Applanix building. The vehicle used in the test was a GMC Rally. The GPS receivers used in the base and rover stations were the NovAtel Millennium receivers, and the data rate of the GPS receiver was set at 1 Hz. The IMU was the Honeywell HG1050, which uses Honeywell GG1342 RLGs and Sundstrand QA-2000 accelerometers. Table 6.1 shows the IMU's error characteristics. The data rate of the HG1050 INS was 50 Hz. The IMU and the GPS antenna were mounted on the top of the vehicle. The coordinate system of the IMU with respect to the vehicle is defined as forward (X – axis), right (Y – axis) and down (Z – axis) as shown in Figure 6.1. The lever arms of the IMU with respect to GPS antenna centre are defined as in Table 6.2. The van trajectory from GPS-only navigation mode is shown in Figure 6.2. The time latency caused by data transmission

can cause significant errors to INS/GPS integration (Petovello, 2003). However, measurement time between GPS and INS was synchronized by Applanix Corporation when the data was provided.

Table 6.1 Honeywell HG1050 Error Characteristics

Errors	Values
Accelerometer bias	50 μg
Accelerometer scale factor error	200 ppm
Gyro bias	0.007 deg/hr
Gyro scale factor error	20 ppm
Gyro random walk	0.005 deg/$\sqrt{\text{hr}}$

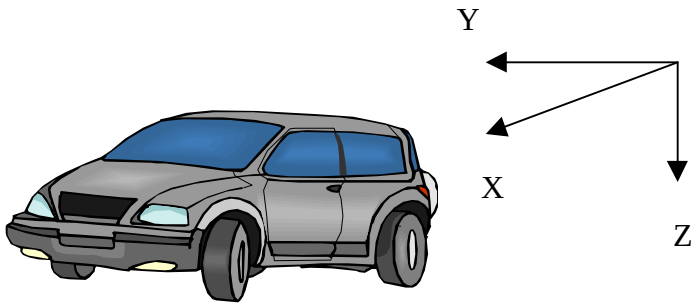

Figure 6.1 IMU Orientation with Respect to the Van.

Table 6.2 Lever Arm of IMU GPS Antenna Centre

X (m)	Y (m)	Z (m)
2.96	0.31	-1.78

6.2 Van Test II

The second test was conducted by Applanix Corporation (on October 23, 2000) in the same area as Van Test I. The equipment used in this test was the same as in Van Test I except that the receiver in the vehicle was a Trimble SE4000.

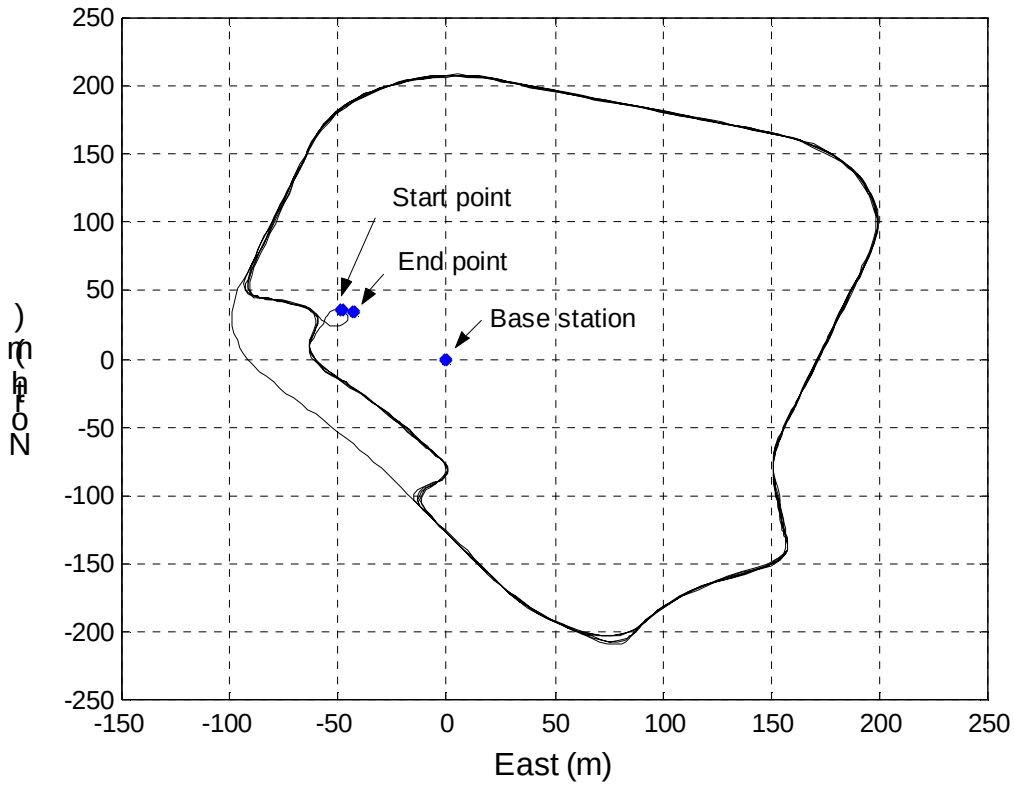

Figure 6.2 Van Trajectory, Van Test I

The data rate of the IMU was also 50 Hz and 1 Hz for the GPS receivers. Figure 6.3 shows the van trajectory during the test. The IMU orientation with respect to the van and the lever arm configuration were the same as in the first test. The measurement time

between GPS and INS for this test was also synchronized when the data was provided by Applanix Corporation.

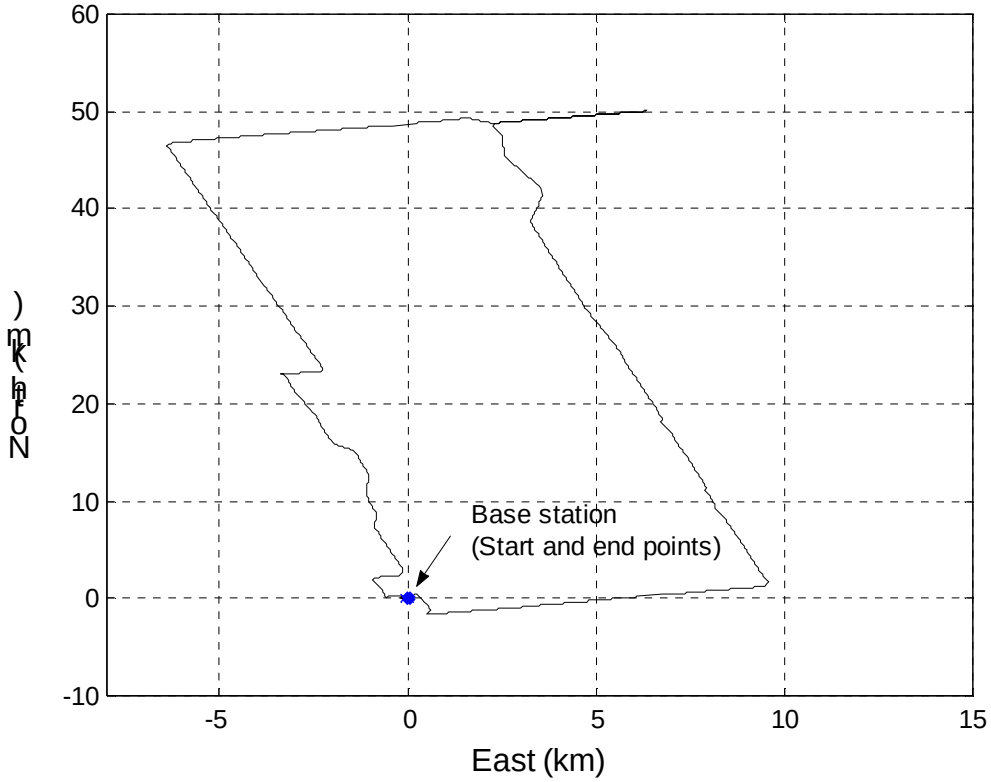

Figure 6.3 Van Trajectory, Van Test II

6.3 GPS Kinematic Solution

This section provides the GPS solution (GPS-only mode with L1) from the software for both tests. The results are a good indication of the dynamics and geometries during the tests that are closely related to ambiguity resolution. Under higher dynamics, the tracking performance of the receiver can be affected and thus cycle slips can occur more frequently than a van test with lower dynamics. This will subsequently affect the ability

of the ambiguity resolution process to resolve the correct integers in a timely and reliable way.

6.3.1 Van Test I

Figure 6.4 shows the baseline variation during the van test, and the plot indicates that the baseline does not exceed 240 m. The speed profile presented in Figure 6.5 shows that the test had moderate dynamics. As shown in Figure 6.6, the number of satellites tracked by the remote receiver during the test changes frequently due to surrounding buildings which block signals from GPS satellites. However, there were no cycle slips detected primarily because the test had very low dynamics. Ambiguities were fixed to integers during the most of the test as shown in Figure 6.8. The cutoff elevation is 7.5 degree.

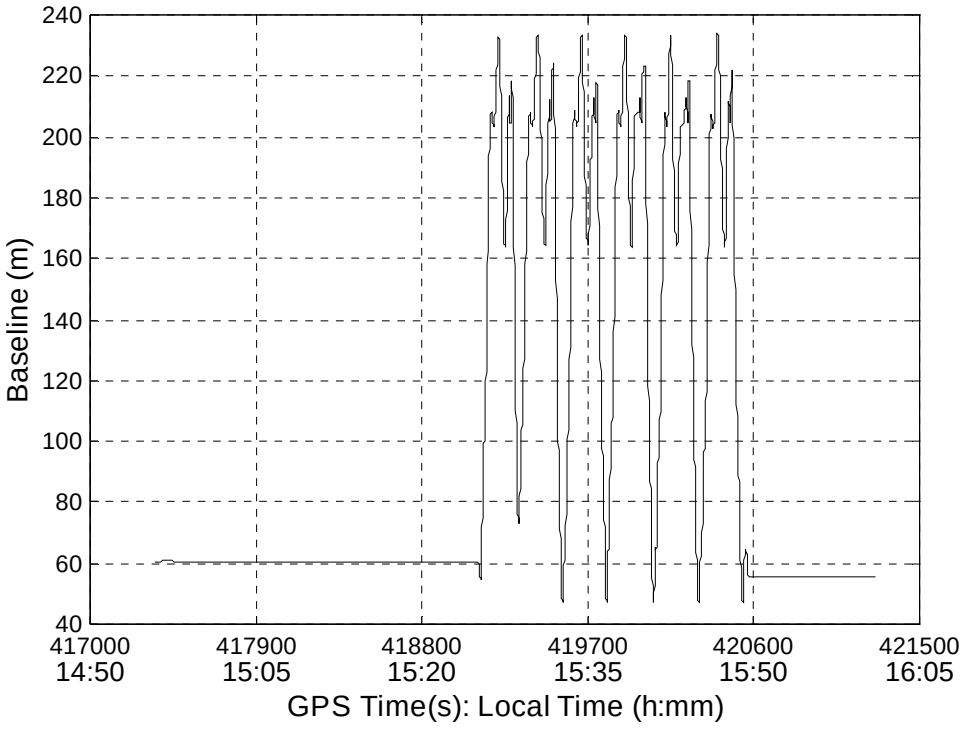

Figure 6.4 Baseline Variation, Van Test I

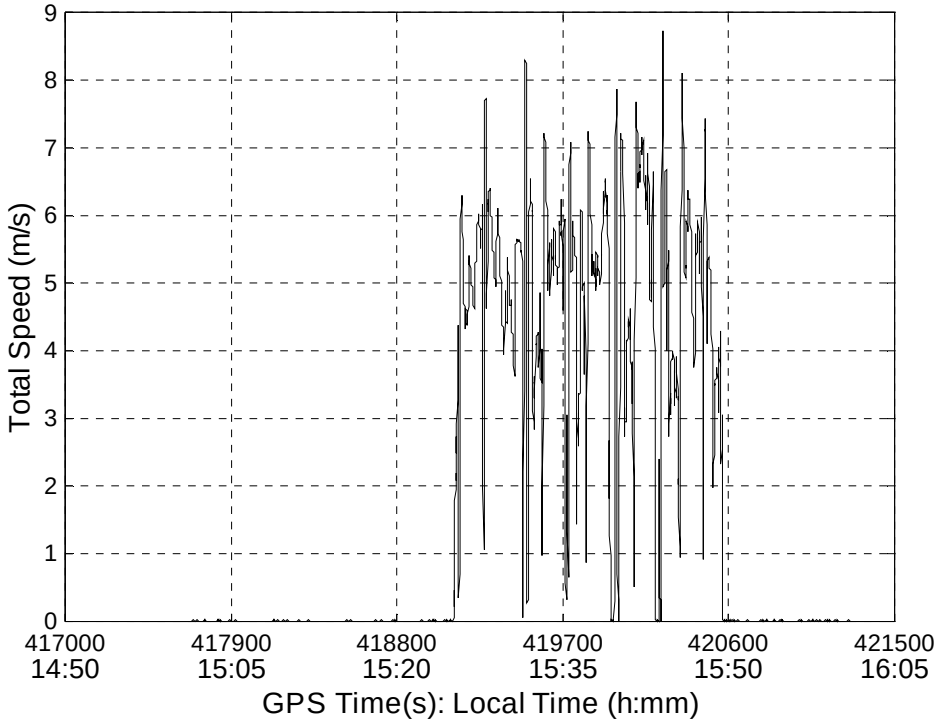

Figure 6.5 Speed Profile, Van Test I

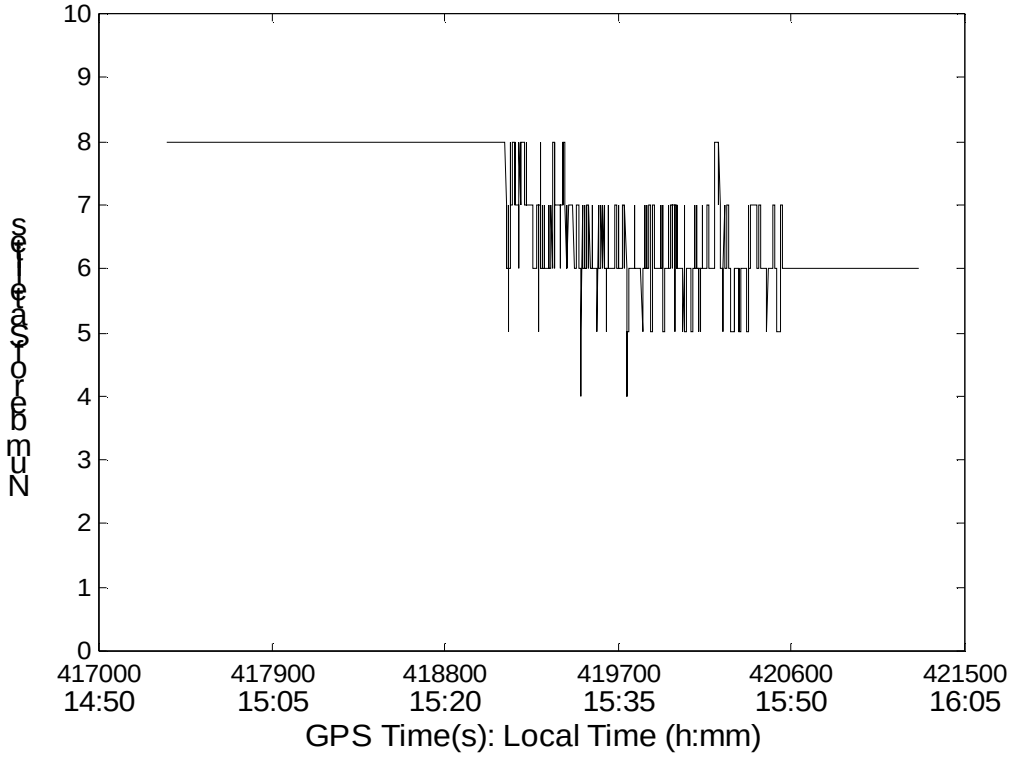

Figure 6.6 Numer of Satellites vs. Time, Van Test I

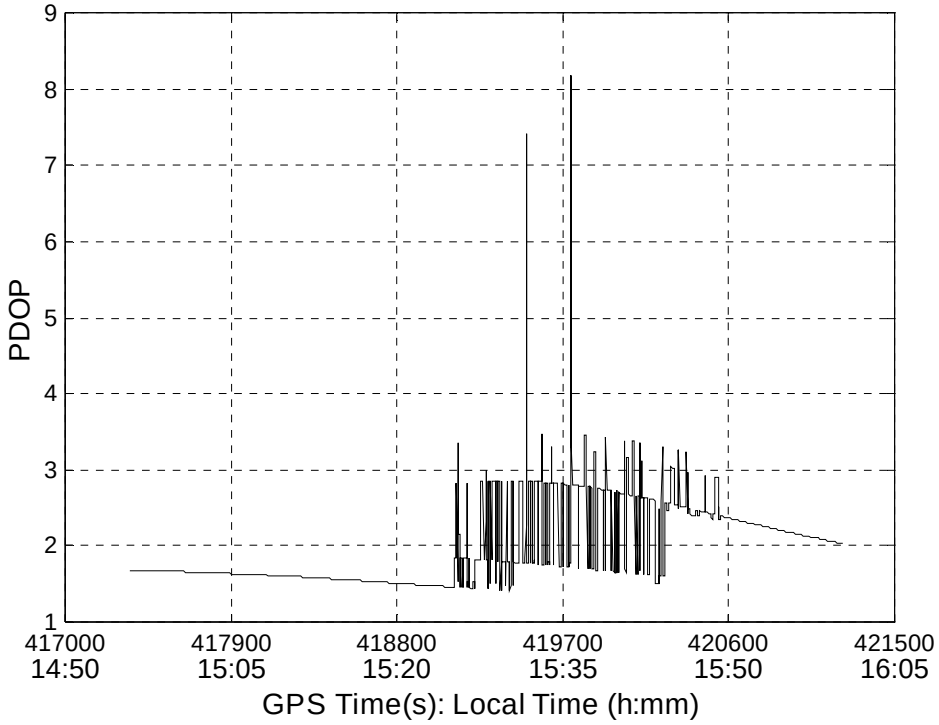

Figure 6.7 PDOP vs. Time, Van Test I

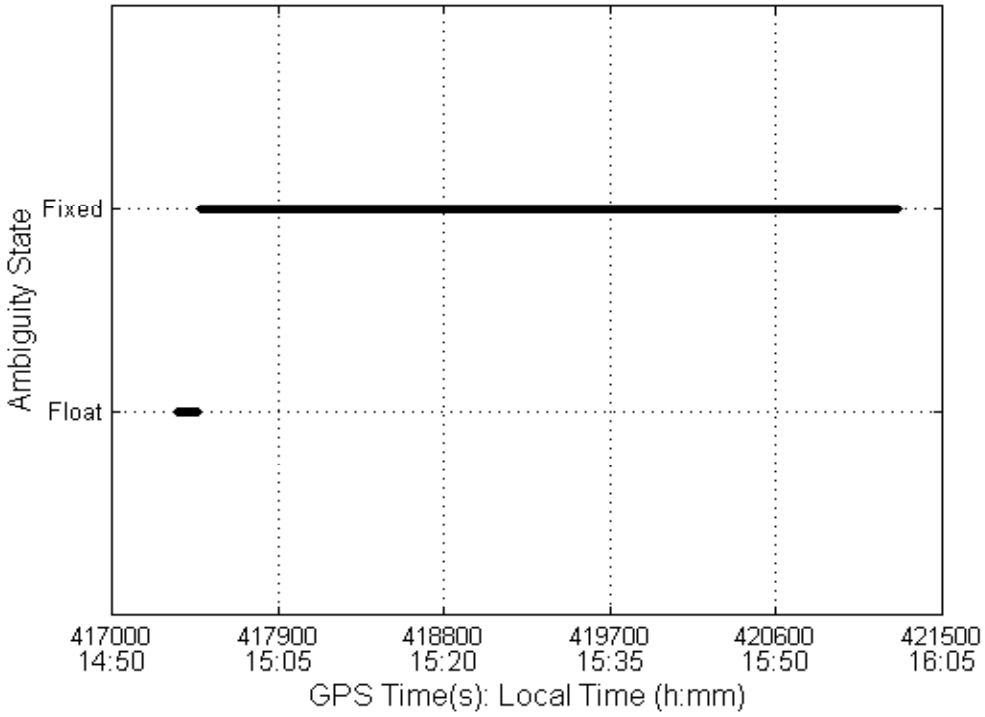

Figure 6.8 Ambiguity Resolution Over Time, Van Test I

For this test, as shown in Figure 6.8, the majority of the initial ambiguities are maintained through out the whole trajectory with only a few of the satellites needing to recompute their ambiguities. Therefore, the position accuracy is quite high. In order to assess the impact of error sources, carrier phase residuals are plotted in Figure 6.9 when ambiguities are fixed. Since this test is a short baseline test, the atomospheric errors should not be significant. The residual magnitude along with its pattern in Figure 6.9 indicates that the major error sources are multipath and noise.

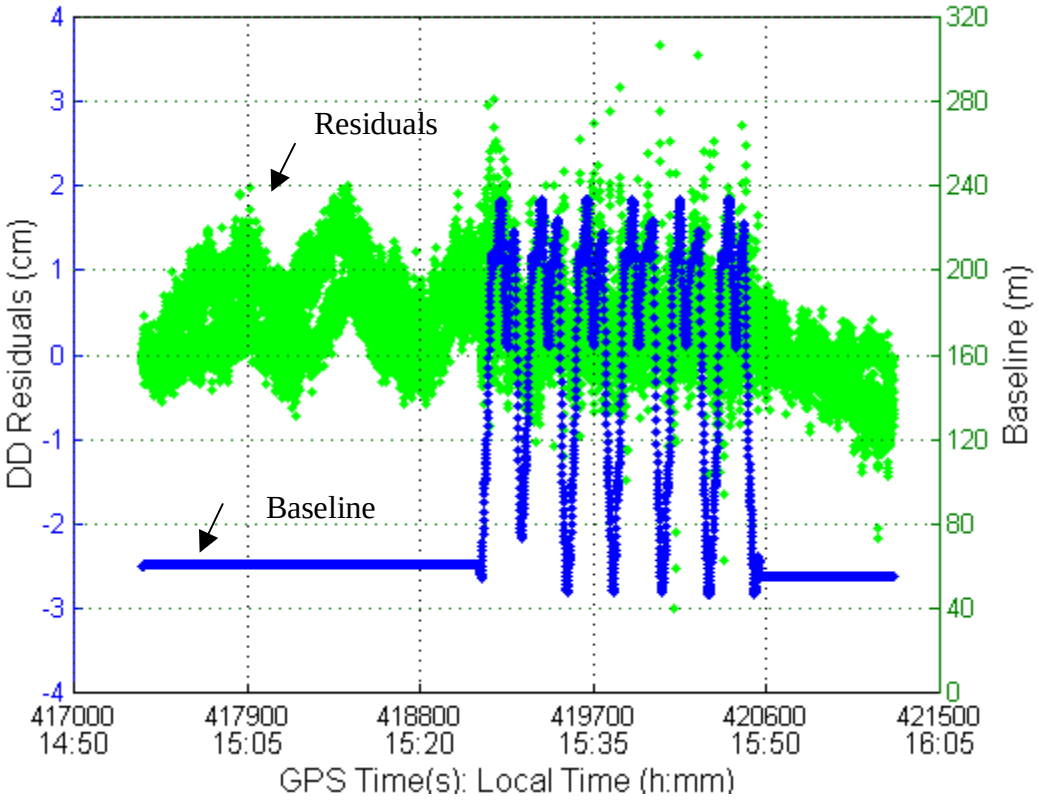

Figure 6.9 DD Carrier Phase Residuals, L1, Van Test I

The double difference ionosphere errors with L1 and L2 data is presented in Figure 6.10 below.

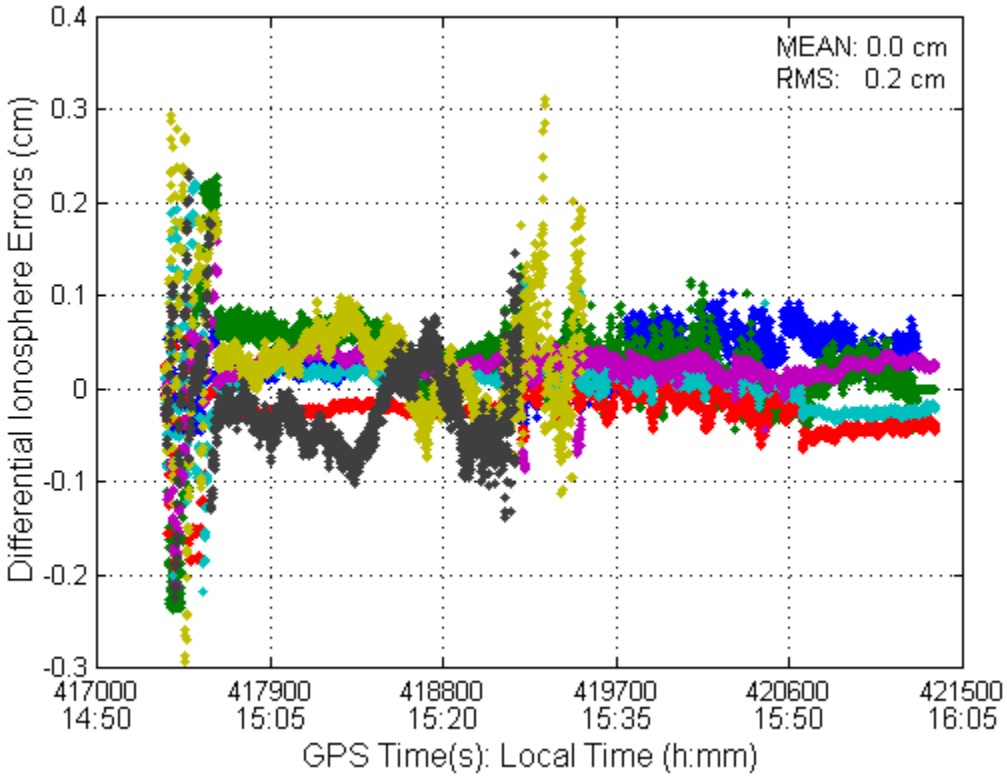

Figure 6.10 Differential Ionosphere Errors, Van Test I

6.3.2 Van Test II

The baseline variation presented in Figure 6.11 indicates that this is a relatively long baseline test. The speed profile is shown in Figure 6.12 and it is relatively higher than that of the first test. It can be seen that the dynamics are higher in this test and also there are a few sudden stops during the test. Cycle slips occurr at various times for all satellites as shown in Figure 6.15. The PDOP is plotted in Figure 6.14, and comparing with the

PDOP in Van Test I, it can be seen that this test has slightly poorer geometry. The spikes in Figure 6.14 are caused by the loss of satellites. The cutoff elevation for this data is 7.5 degree as well.

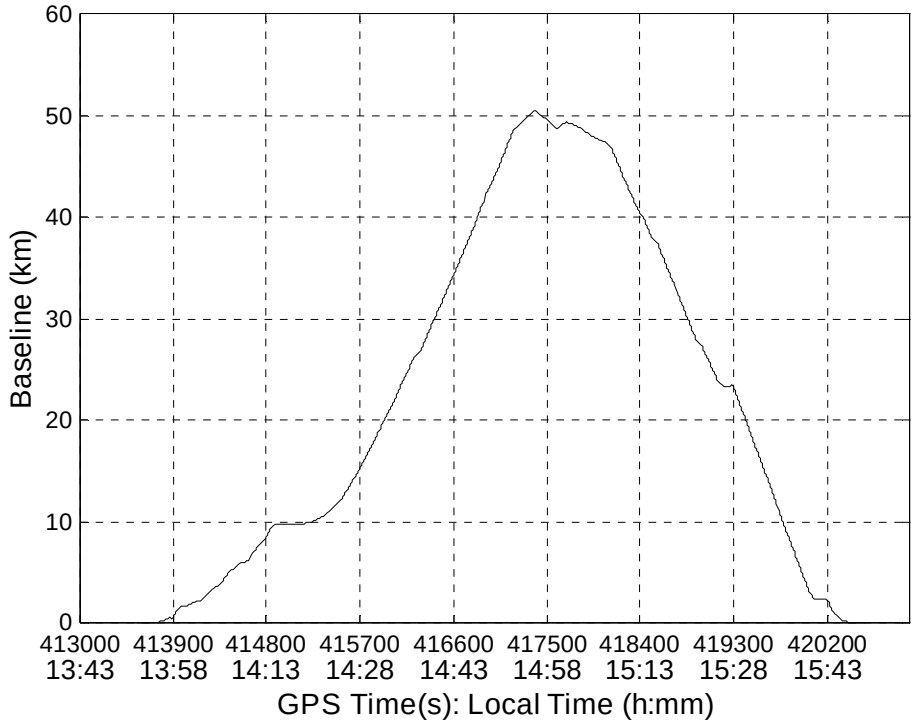

Figure 6.11 Baseline Variation, Van Test II

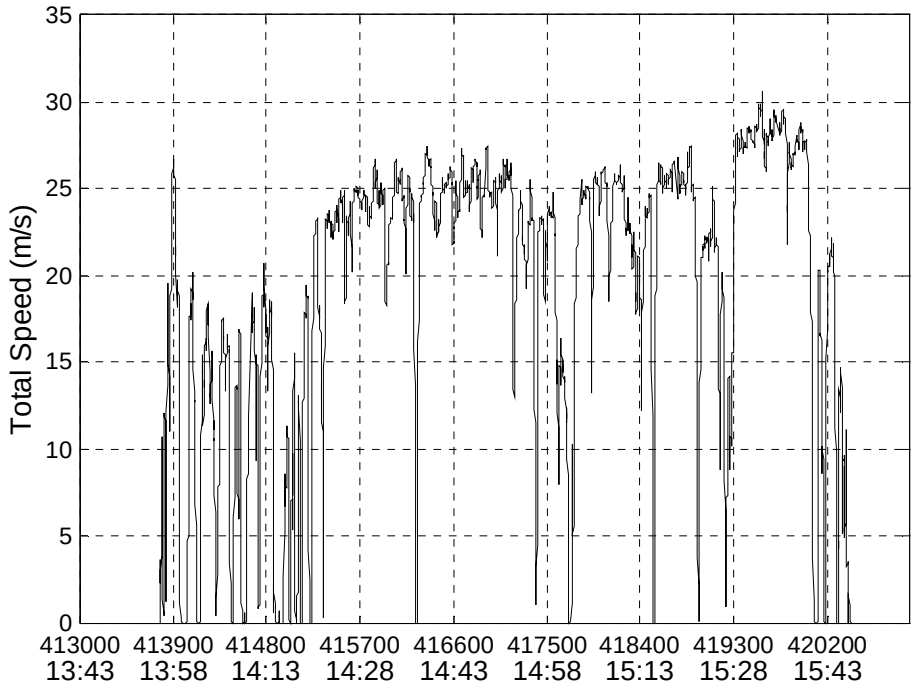

Figure 6.12 Speed Profile, Van Test II

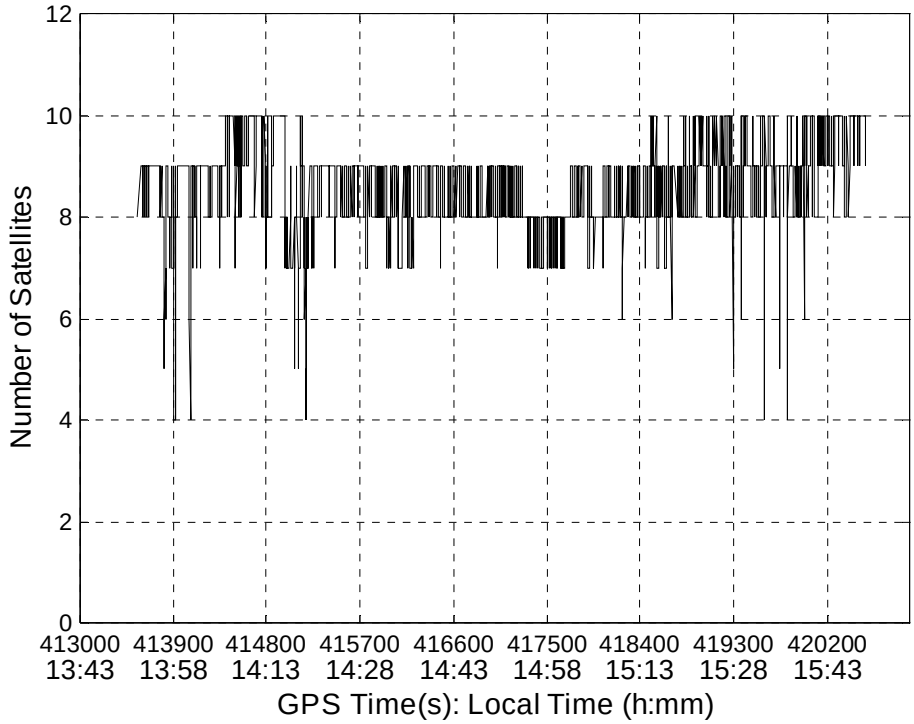

Figure 6.13 Number of Satellites versus Time, Van Test II

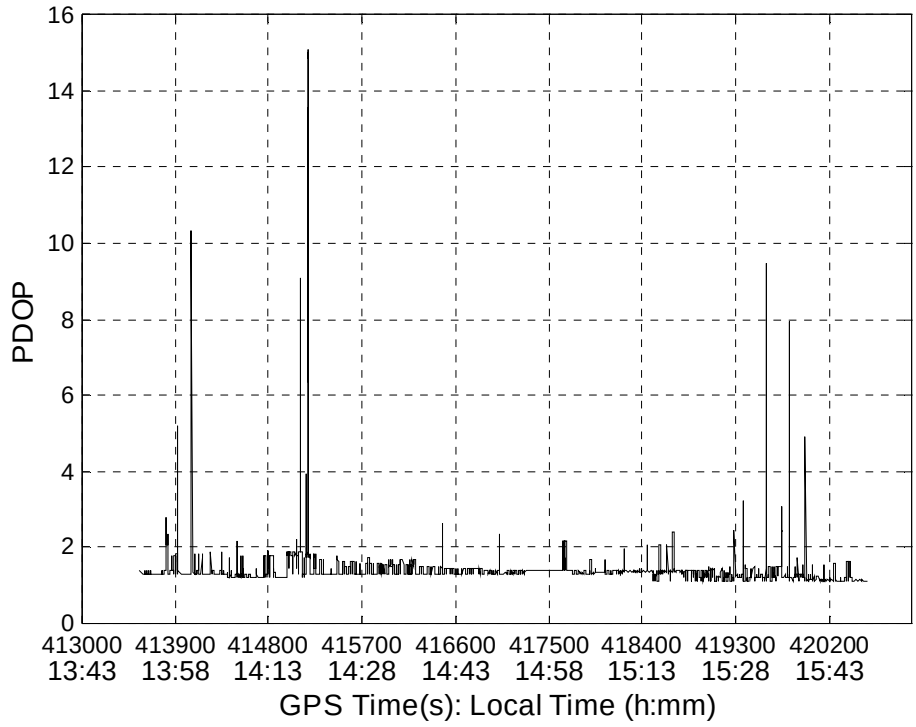

Figure 6.14 PDOP versus Time, Van Test II

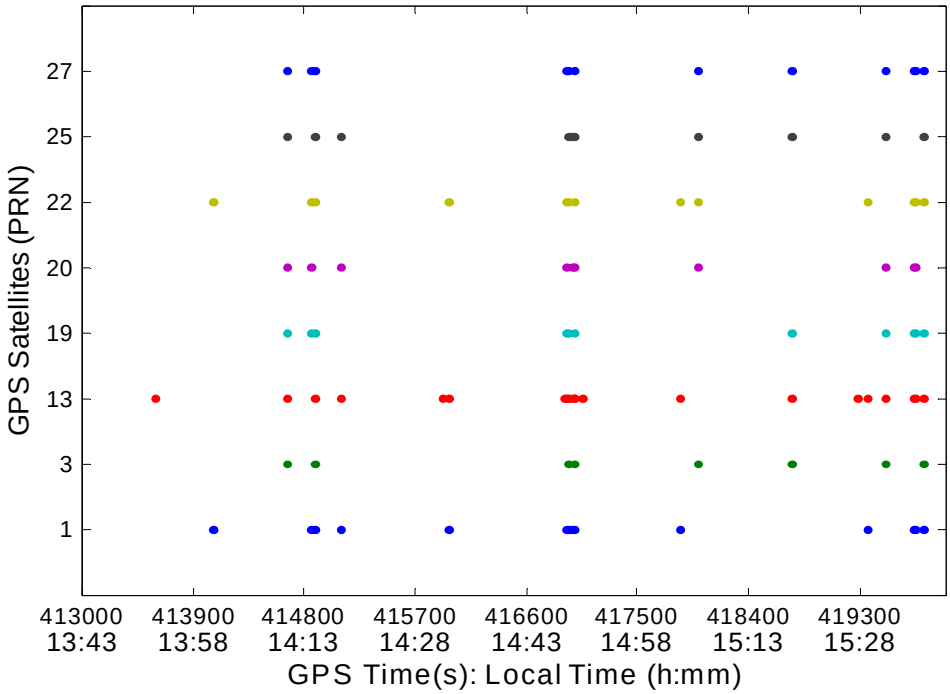

Figure 6.15 Cycle slips versus Time, Van Test II

Carrier phase residuals of those satellites with fixed ambiguities are fixed are plotted in Figure 6.16 below. The figure only shows the part of the trajectory with baselines less than 20 km. When the baseline goes above 20 km Flykin™ cannot fix ambiguities. Also in the figure there is a gap between GPS time 414622 and 414668 s, and this is because during this period all satellites lost their fixed ambiguities. When comparing Figures 6.16 and 6.9, the residual magnitude is larger in Van Test II. This indicates that the atomospheric error has more impact on this van test.

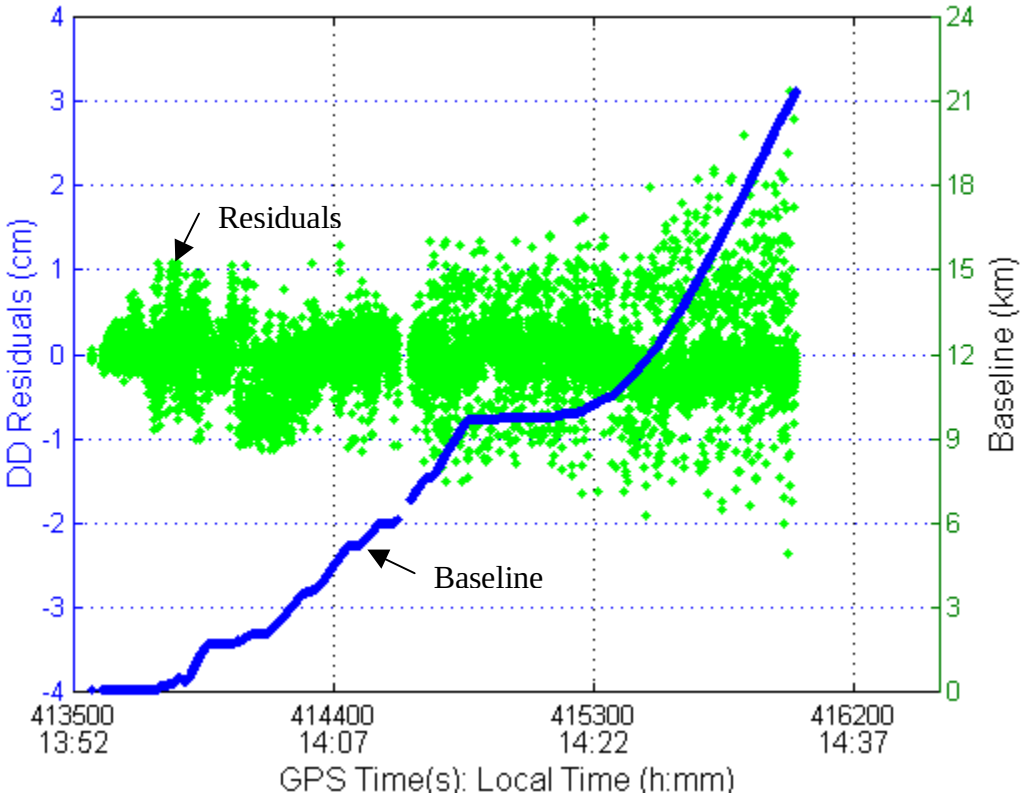

Figure 6.16 DD Carrier Phase Residuals, L1, Van Test II

The double differencel ionosphere errors for this test with L1 and L2 measurements is shown in Figure 6.17 below. When comparing this figure to Figure 10, it can be seen that the magnitude of ionosphere errors is larger than Van Test I's. This is consistent with the residual analysis.

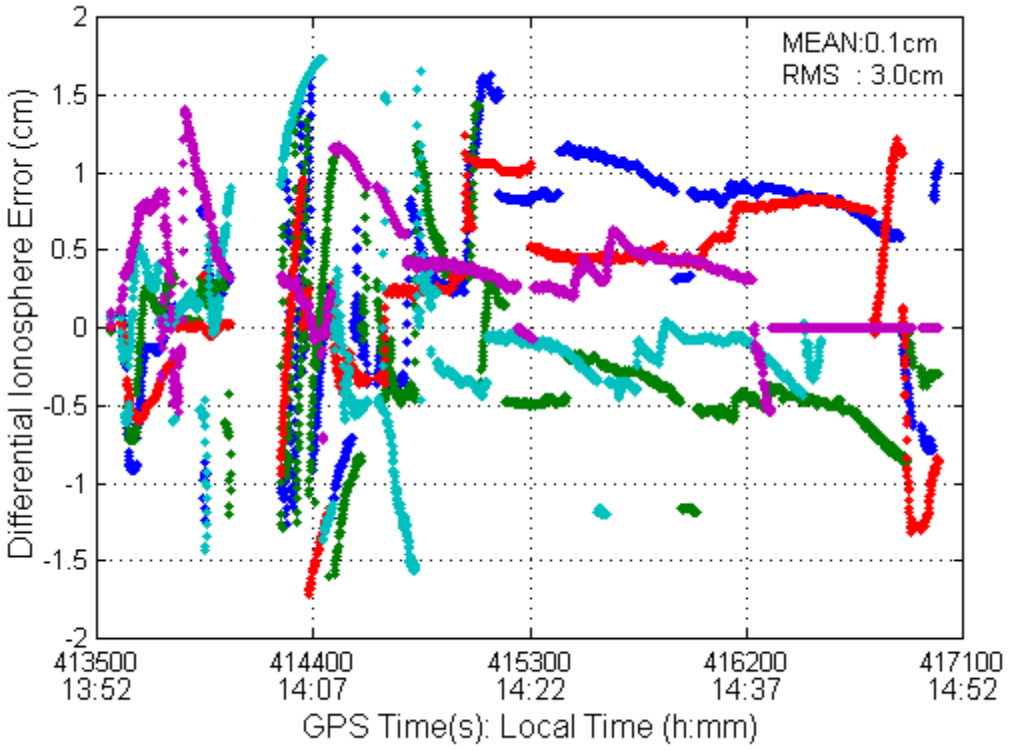

Figure 6.17 Differential Ionosphere Errors, Van Test II

6.4 INS Solution

This section presents the results from the INS stand-alone navigation solution for the two van tests. The attitude profiles show the maneuvers of the vehicles during the tests. The INS drift is derived by comparing the INS stand-alone solution with the solution from GPS -only mode. The drift is a good indication of the quality of the IMU used.

6.4.1 Van Test I

Figures 6.18 through 6.20 show the results from INS stand-alone navigation. The position drift and the velocity error growth presented in Figures 6.19 and 6.20 are fairly reasonable given the quality of the IMU (0.007 degrees per hour).

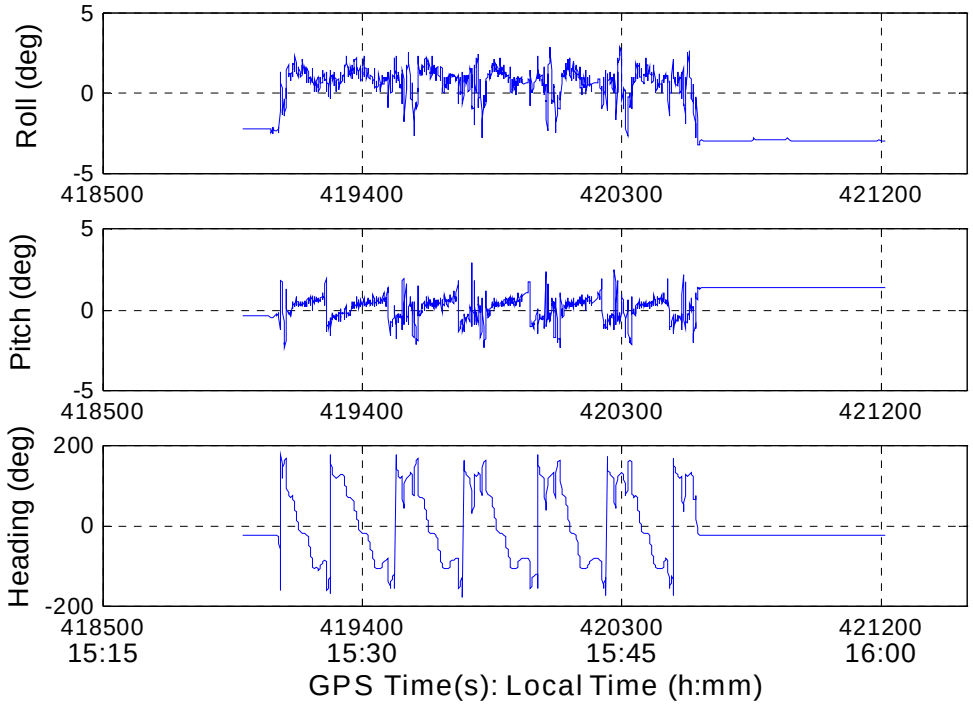

Figure 6.18 Attitude Profile, Van Test I

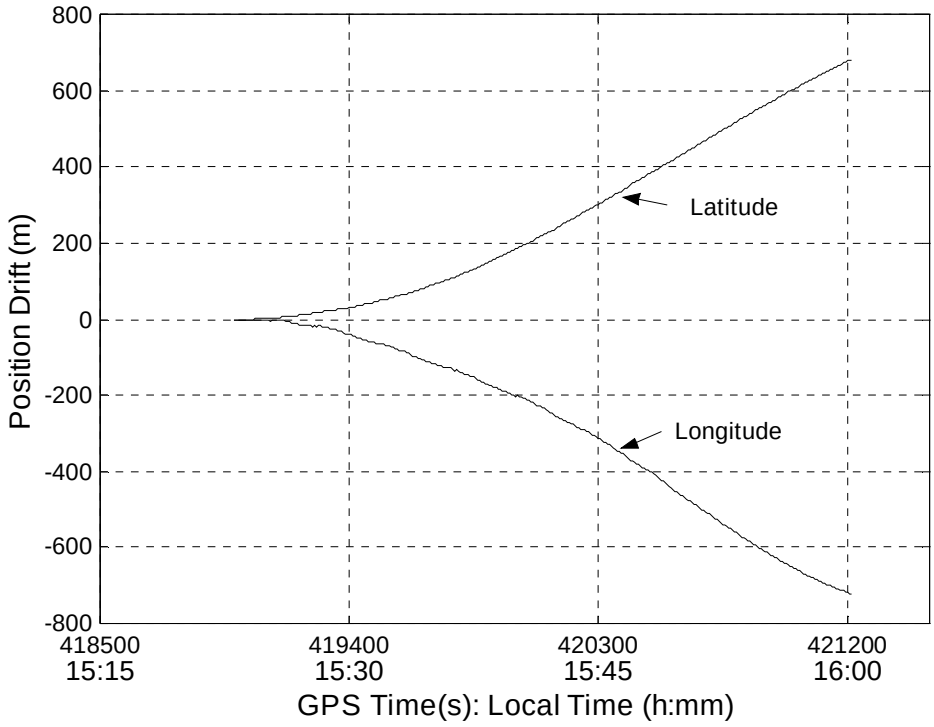

Figure 6.19 INS Position Drift, Van Test I

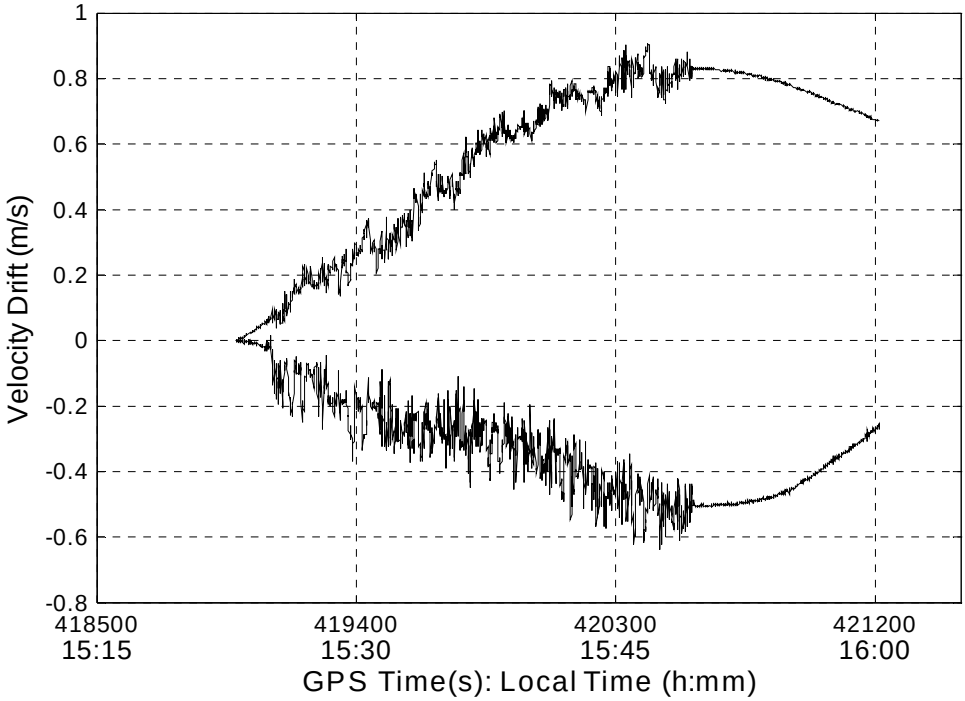

Figure 6.20 INS Velocity Drift, Van Test I

6.4.2 Van Test II

Figures 6.21 through 6.23 show results for the second van test. This test lasts about two hours, and the Schuler pattern is well indicated in Figures 6.22 and 6.23.

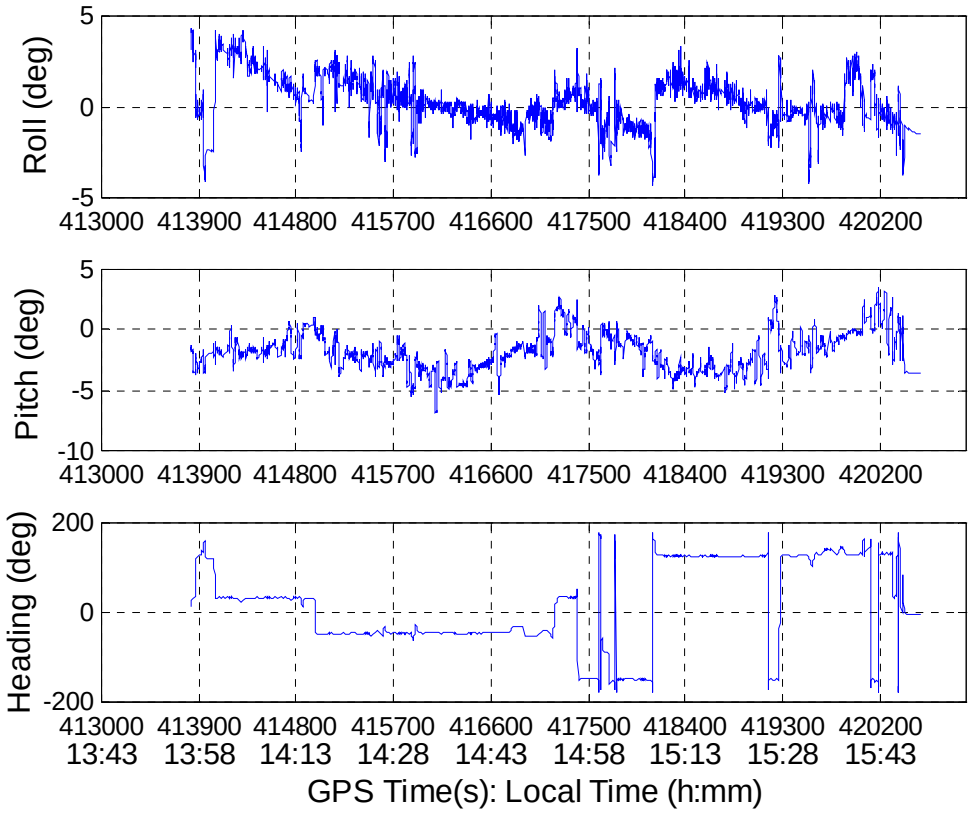

Figure 6.21 Attitude Profile, Van Test II

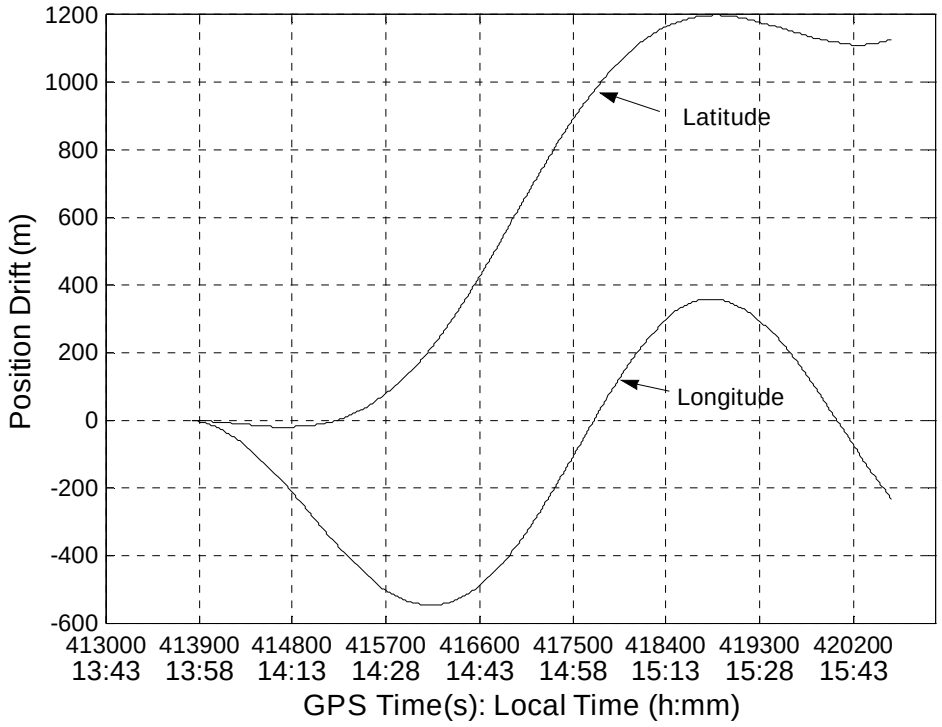

Figure 6.22 INS Position Drift, Van Test II

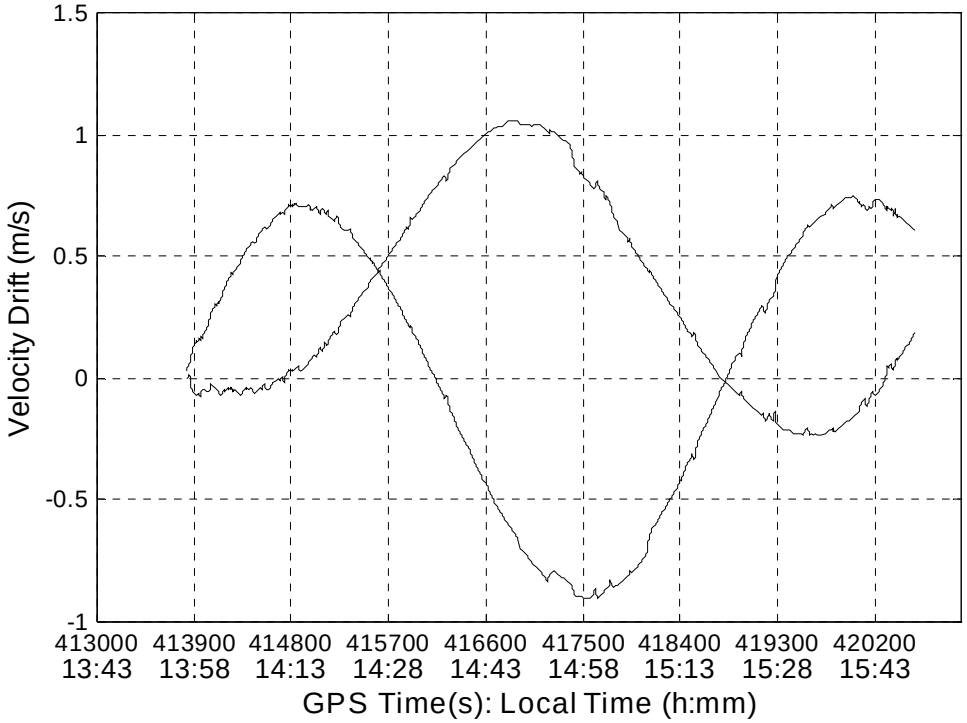

Figure 6.23 Velocity Position Drift, Van Test II

6.5 INS/GPS Integration Solution

Results from the three INS/GPS integration schemes are presented to evaluate the integration performance. Position and velocity errors from the tightly coupled integration for the first test (Van Test I) are plotted in Figures 6.24 and 6.25. However, data sets from both tests are processed using all three integration schemes, i.e. loose coupling and tight coupling in a decentralized filter structure and centralized integration. Error statistics from different integration structures are summarized in Tables 6.3 and 6.4. GPS results are used as a reference to compute error statistics. Loose coupling uses position and velocity from the GPS navigation module to update the error predictions in the master filter.

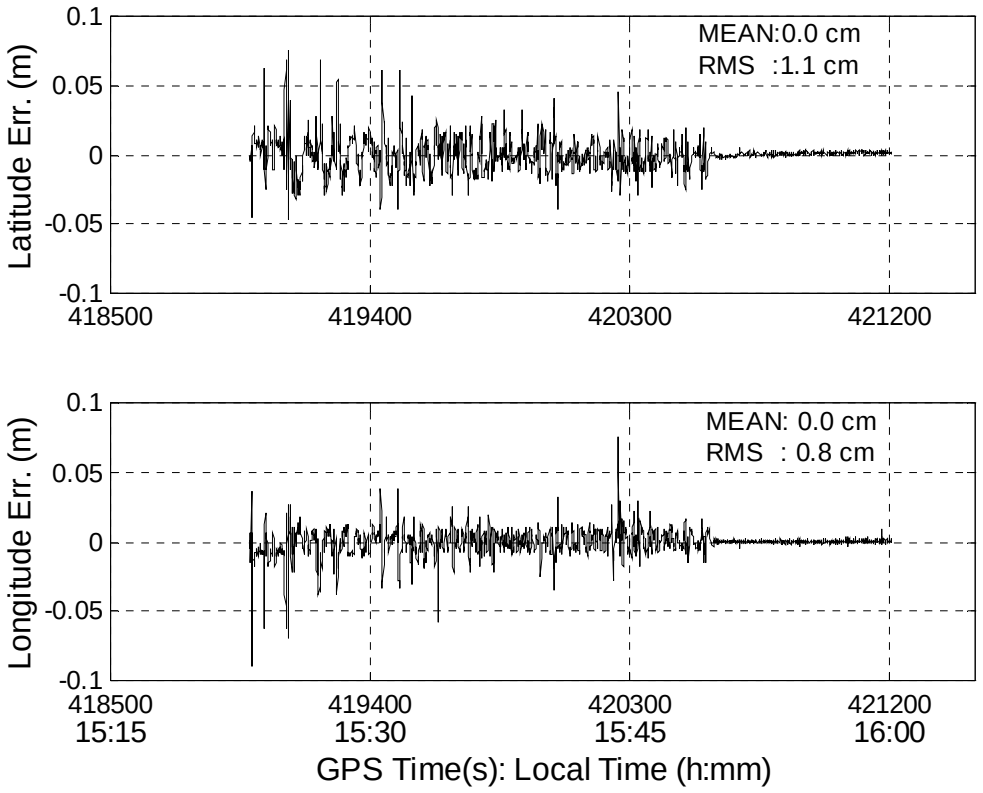

Figure 6.24 Position Error, INS/GPS, Tight Coupling, Van Test I

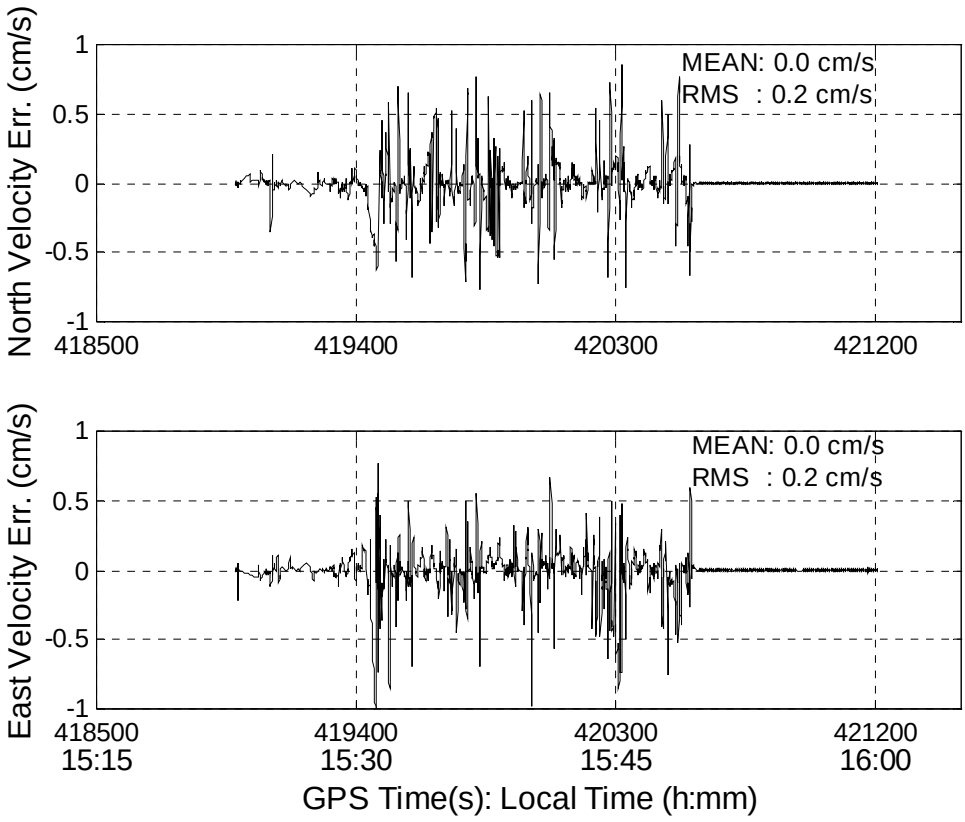

Figure 6.25 Velocity Error, INS/GPS Tight Coupling, Van Test I

Table 6.3 Error Statistics, Van Test I

Errors / Integration Strategies	Latitude (cm)		Longitude (cm)		North Velocity (cm/s)		South Velocity (cm/s)	
	Mean	RMS	Mean	RMS	Mean	RMS	Mean	RMS
Loose Coupling	-0.1	1.3	0.1	1.0	0.0	0.3	0.0	0.3
Tight Coupling	0.0	1.1	0.0	0.8	0.0	0.2	0.0	0.2
Centralized Integration	0.0	1.0	0.0	0.8	-0.1	0.2	0.0	0.2

Table 6.4 Error Statistics, Van Test II

Errors / Integration Strategies	Latitude (cm)		Longitude (cm)		North Velocity (cm/s)		South Velocity (cm/s)	
	Mean	RMS	Mean	RMS	Mean	RMS	Mean	RMS
Loose Coupling	-0.1	2.1	0.0	1.8	-0.1	0.5	0.0	0.6
Tight Coupling	-0.1	1.6	0.0	1.5	0.0	0.3	0.0	0.4
Centralized Integration	0.0	1.5	0.1	1.2	0.0	0.3	0.0	0.2

Figure 6.26, a comparison of the 2DRMS for the three integrations for Van Test I, shows that, although the RMS difference of positions and velocities for these three integrations is not significant, the tight coupling and centralized integration have slightly better performance. As discussed in Section 2.3, in loose coupling, the position and velocity from the GPS filter is mostly correlated over time and this violates the optimization assumption in the filtering process and thus affects the filtering performance. However, code and phase measurements from GPS receivers are used directly in the tight coupling and the centralized integration.

When comparing results of Van Test I and II, it can be seen that RMS values for Van Test II are slightly higher. As shown in Section 6.3.2, the second test is a long baseline and it has more dynamics. During the second test, there are also constant cycle slips.

Results of this Chapter verify the algorithm of INS/GPS integrations. In the next chapter the results of using INS data to aid GPS ambiguity resolution will be analyzed.

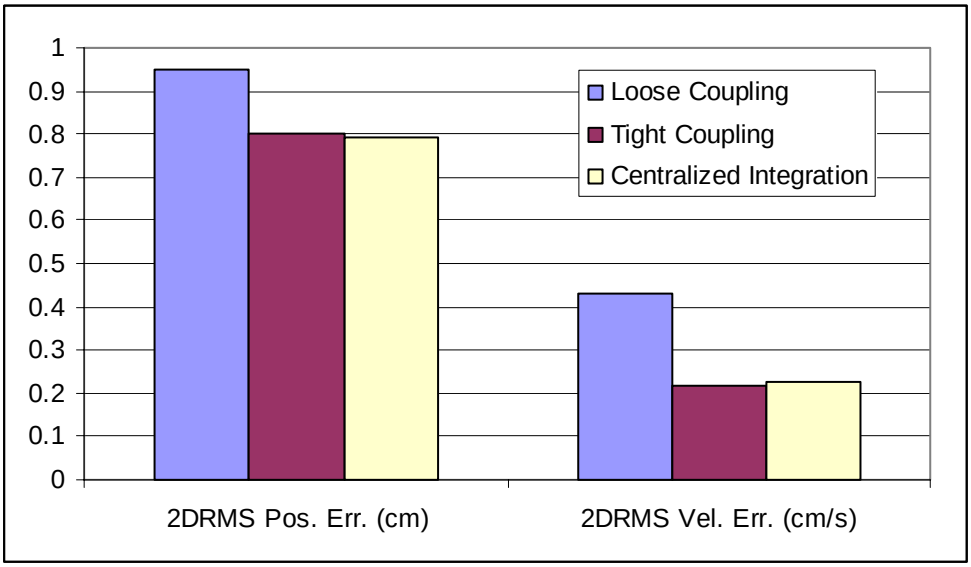

Figure 6.26 Integration Performance, Van Test I

CHAPTER 7

TEST RESULTS AND ANALYSIS

Results from two van tests for ambiguity resolution with INS aiding are presented and analyzed in this chapter. Tests are used to prove the concept and methodology developed in previous chapters. The benefits of integrating inertial data into GPS ambiguity resolution are examined in these two test cases.

7.1 Test Design

In order to investigate the effect of INS aiding on GPS ambiguity resolution, a GPS outage is simulated by taking out GPS measurements during the outage period. Two outage scenarios are simulated, a complete outage where there are no GPS measurements available, and a partial outage where there are less than three satellites available. Three outage cases are simulated. Different outage periods are designed such that the improvement with using INS in GPS ambiguity resolution can be seen from the best case to a poorer case. The first outage period is very short so that the INS can continue to deliver positions with superior accuracy. This type of outage has the maximum benefit of using the INS to assist GPS to fix integers due to the accurate position seed from the INS. The second outage period is moderately short, in which positions from the INS are less accurate. However, the position drift from the INS should not be significantly degraded, and there should be still some improvement. The third period is relatively long, such that the position from the INS is degraded and INS aiding shows no improvement in

ambiguity resolution. Based on the quality of the IMU used in the test these three outage periods are:

- 10 – second outage
- 30 – second outage
- 60 – second outage

Position drifts from INS during above outage periods will be discussed shortly.

The key values with and without INS aiding in each case to study are:

- The time to fix the integers indicating the performance of the search procedure
- The ADOP indicating the accuracy of the float ambiguities and the search space

As indicated previously, the purpose of simulating multiple outage periods is to study the ability of INS aiding to assist integer resolution under different conditions. Generally, the longer the outage, the poorer the IMU accuracy. It is expected that a longer outage will reduce the effect of INS aiding. Ten GPS outages were simulated for each outage period. In tight coupling, once there are no GPS measurements available, the master filter performs pure prediction and the INS solution is corrected using the predictions from the master filter. For a complete GPS outage, the master filters in the loose coupling and centralized integration schemes have the same behaviour. However under a partial outage, for the tight coupling and centralized integration schemes, the measurements from the available GPS satellites are fed into the master filter to update the prediction. Therefore, it is expected that the position error in partial outages is smaller than that in full outages.

Figures 1 and 2 below show individual outages in the trajectories of Van I and II. Each mark represents a GPS outage.

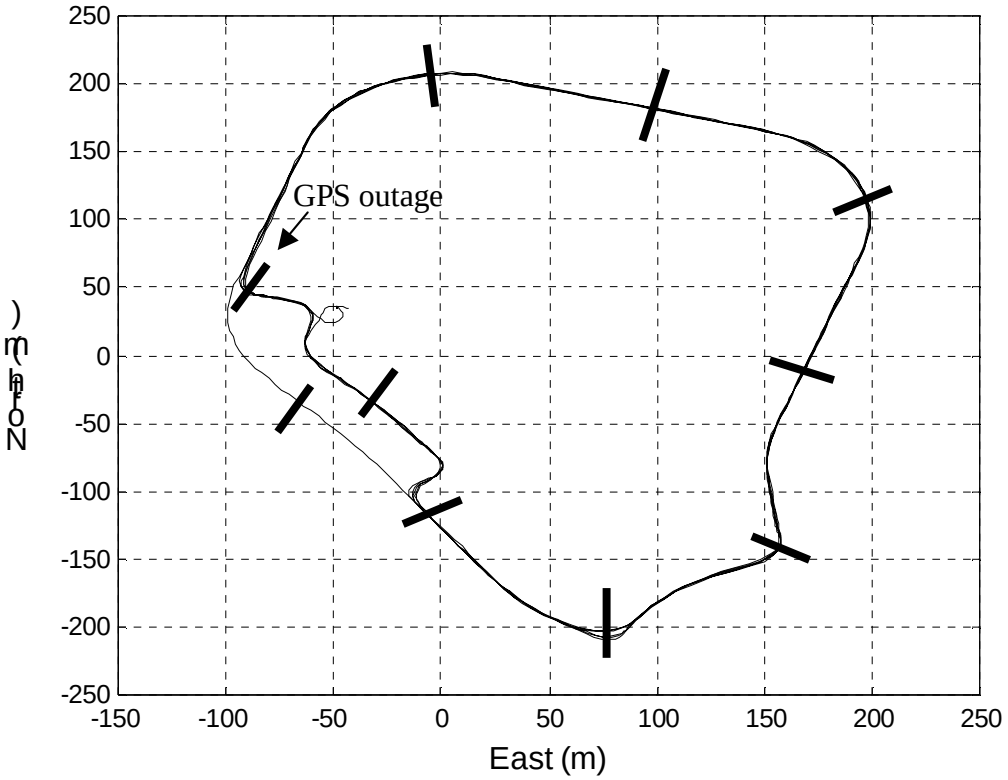

Figure 7.1 GPS Outage Locations, Van Test I

Figures 7.3 through 7.5 show the INS drifts during the ten complete outages for the tightly coupled integration for Van Test I. All outages are labeled by the sequence numbers on the top of the position drifts.

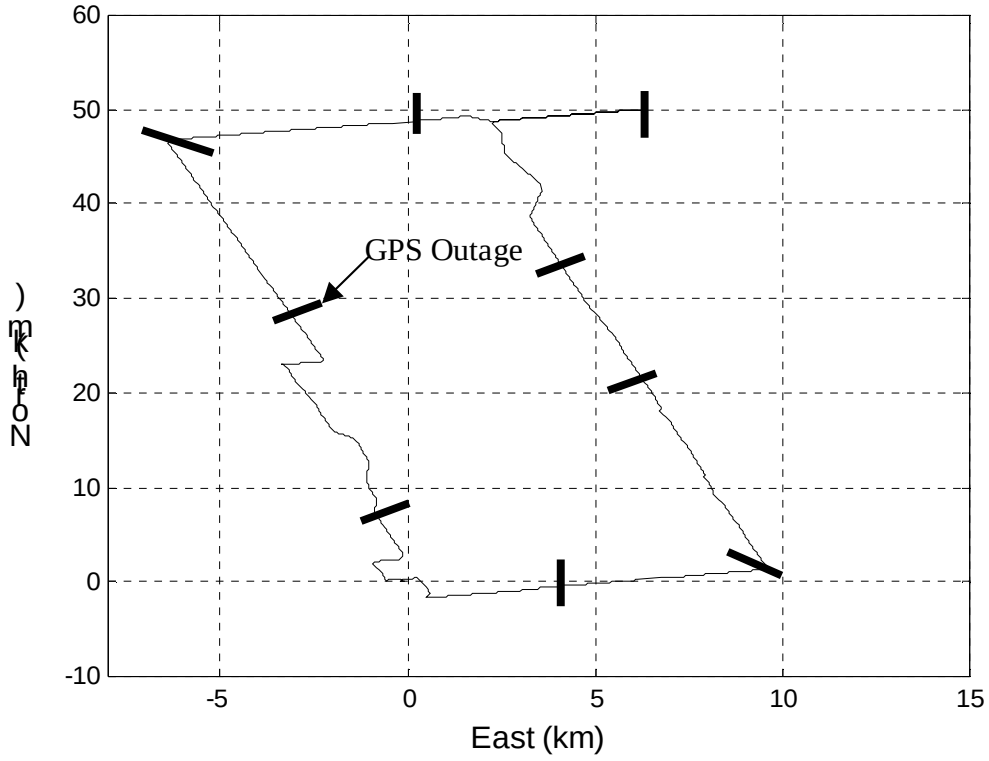

Figure 7.2 GPS Outage Locations, Van Test II

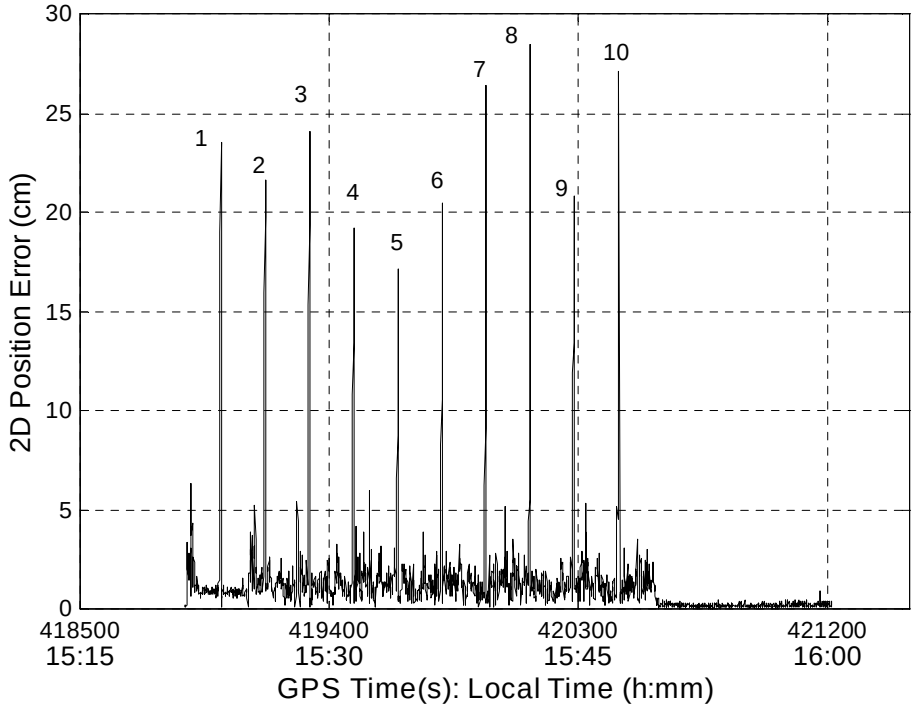

Figure 7.3 Horizontal Error, 10-second Full GPS Outage, Van Test I

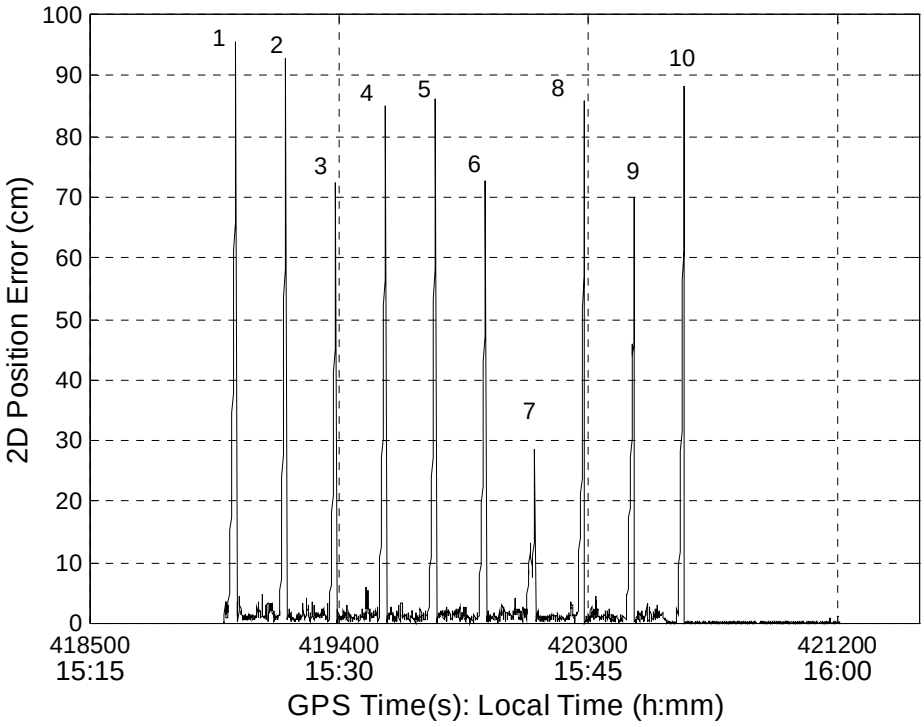

Figure 7.4 Horizontal Error, 30-second Full GPS Outage, Van Test I

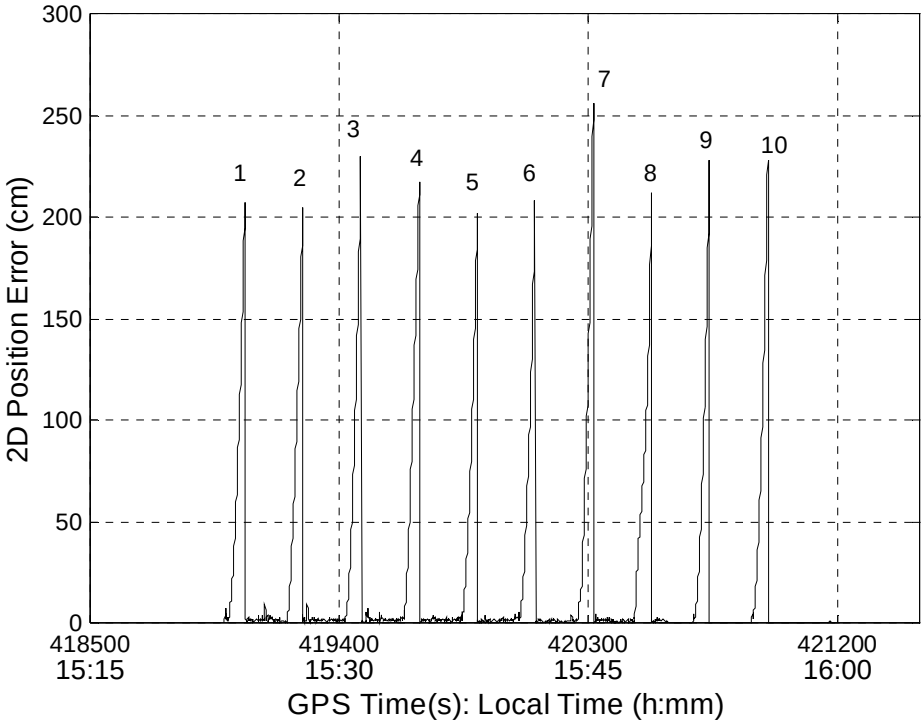

Figure 7.5 Horizontal Error, 60-second Full GPS Outage, Van Test I

Results from tight coupling integration under a partial outage (3 satellites visible) are presented in Figures 7.6 to 7.8. Three satellites with high elevations were chosen in the partial outages. Comparing to the full outage results, the 2D position drift is significantly smaller for the partial GPS outage scenario. This indicates that the filter has better prediction performance with GPS measurements as expected.

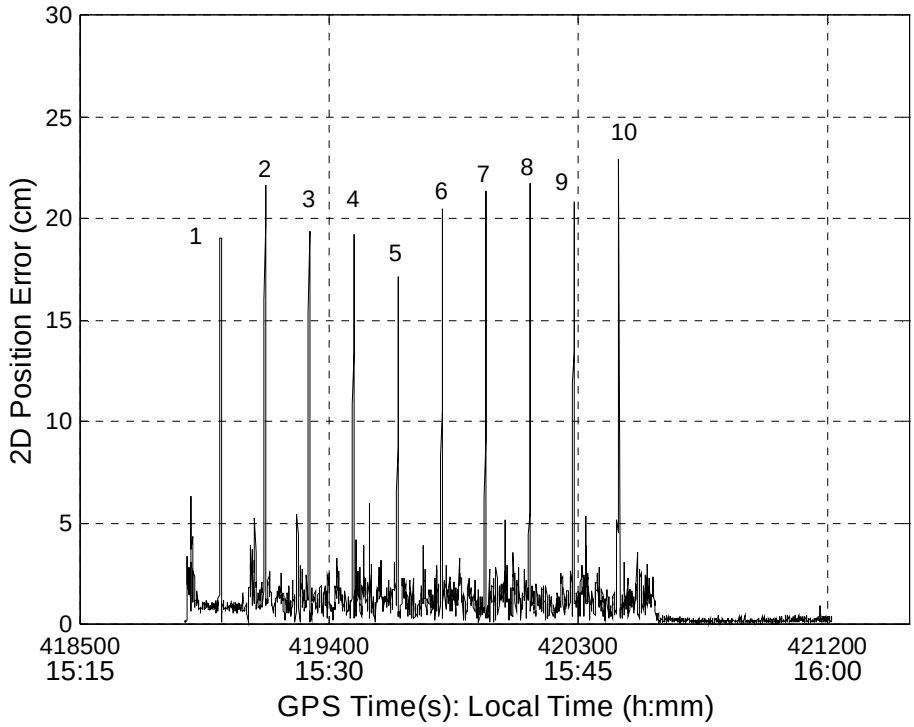

Figure 7.6 Horizontal Error, 10-second Partial GPS Outage, Van Test I

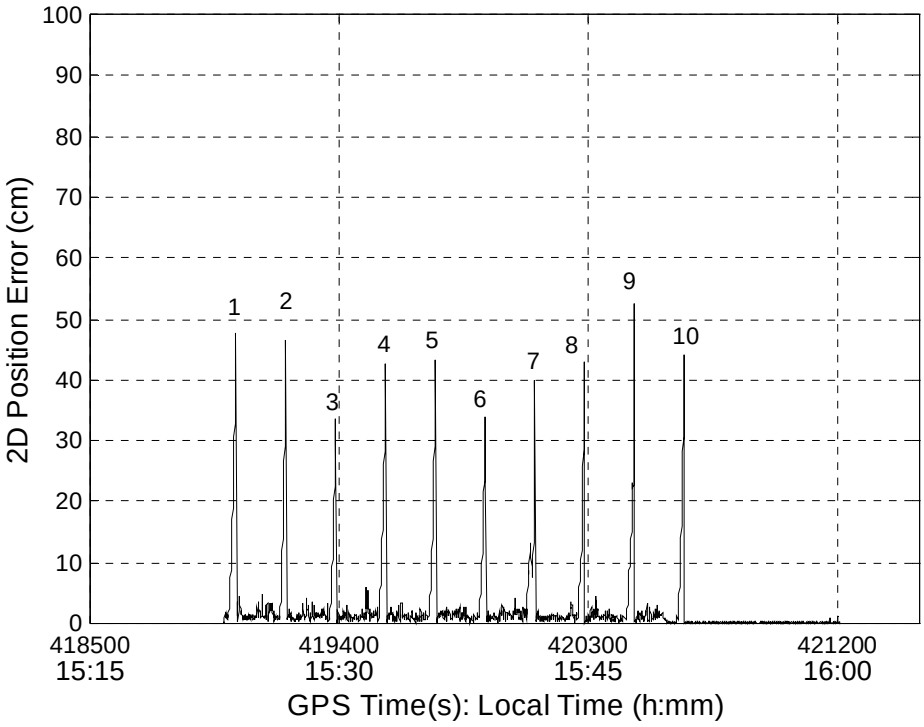

Figure 7.7 Horizontal Error, 30-second Partial GPS Outage, Van Test I

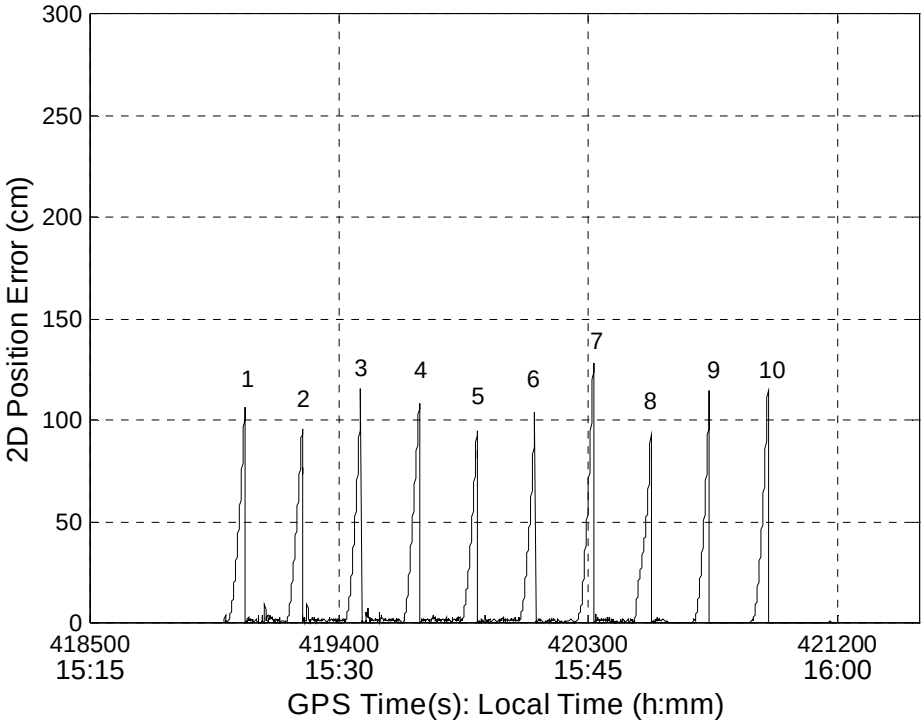

Figure 7.8 Horizontal Error, 60-second Partial GPS Outage, Van Test I

Position error statistics for the three integration scenarios under complete and partial GPS outages are summarized in Table 7.1. It can be observed that in the loose coupling position errors are the same under full and partial outages for the same outage period. As discussed before, this is because there is no GPS navigation solution available for both complete and partial outages (less than 3 satellites), which is used for correcting the INS solution. However, under tight coupling and centralized integration schemes, there are GPS measurements available for the update in the master filter. Therefore, it can be seen that, in the table, position drifts are all improved under partial outages for tight coupling and centralized integration.

Table 7.1 GPS Outage Position Error Statistics, Van Test I

GPS outage duration (Seconds)	INS Horizontal Position Error RMS (metres)					
	Loose Coupling		Tight Coupling		Centralized Intgr.	
	Full*	Partial*	Full	Partial	Full	Partial
10	0.2	0.2	0.2	0.1	0.2	0.1
30	0.8	0.8	0.8	0.4	0.8	0.4
60	2.0	2.0	2.0	0.9	2.0	1.0

*Full – full GPS outage; Partial – partial GPS outage (3 satellites visible)

The same testing scenarios are simulated for Van Test II. GPS outages of three different periods (10, 30 and 60 seconds) are simulated for ten cases. Position error statistics for Van Test II are presented in Table 7.2. Compared to Table 7.1, it can be seen that the position drift in this test gives no significant difference. This is because the IMU used in both tests was exactly the same.

Table 7.2 GPS Outage Position Error Statistics, Van Test II

GPS outage duration (Seconds)	INS Horizontal Position Error RMS (metres)					
	Loose Coupling		Tight Coupling		Centralized Intgr.	
	Full*	Partial*	Full	Partial	Full	Partial
10	0.2	0.2	0.2	0.1	0.2	0.1
30	0.9	0.9	0.9	0.5	0.8	0.5
60	2.1	2.1	2.1	1.1	2.0	1.2

*Full – full GPS outage; Partial – partial GPS outage (3 satellites visible)

7.2 Analysis of Results

7.2.1 Van Test I

The L1 ADOPs with and without INS aiding during the full ten GPS outages under tight coupling integration are shown in Figures 7.9 to 7.11. The same results for the widelane are shown in Figures 7.12 to 7.14. As discussed in Chapter 4, the ADOP is an indicator of the float ambiguity accuracy which relates to the size of the integer search space. During the 10-second outage, the ADOP is significantly reduced due to the good position accuracy maintained by the inertial solution during the outage. However as the duration of the outage increases, the position error is seriously degraded and thus the benefit of incorporating the inertial solution becomes negligible. This is particularly clear in the 60-second outage case as shown in Figures 7.11 and 7.14 where the position error drift is about 2 metres and the inertial solution integration yields no benefit. However, a reduction of the ADOP does not guarantee that integers can be fixed with INS aiding. The ADOP only indicates the size of the search space as well as the accuracy of the float ambiguities and the search within the reduced space may not yield an integer solution subject to the conditions outlined in Section 3.3.

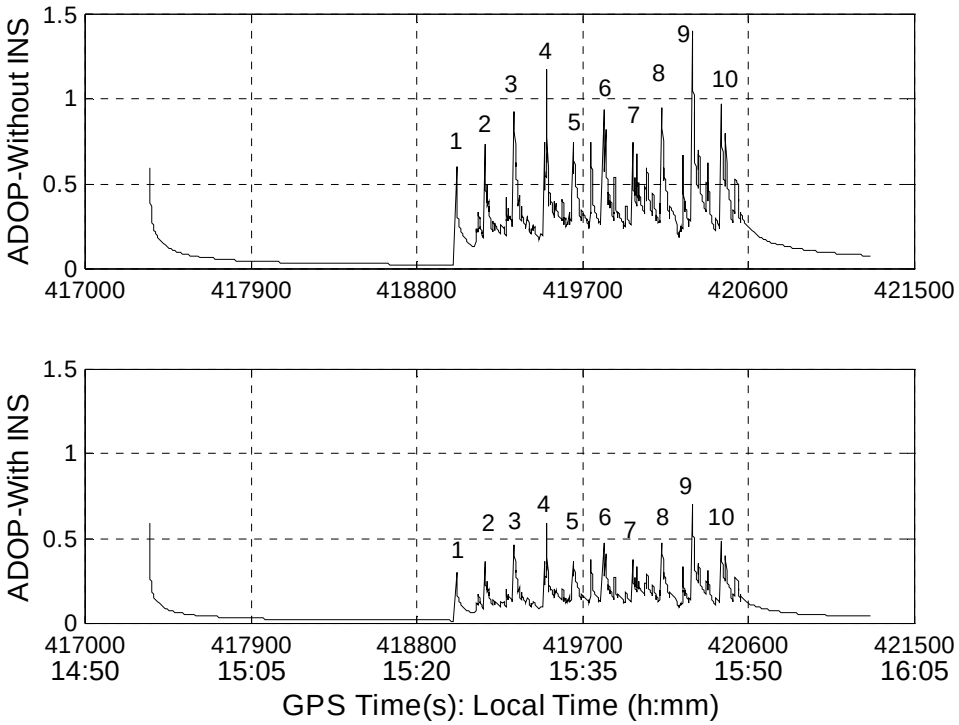

Figure 7.9 L1 ADOP, 10-second Full Outage, Van Test I

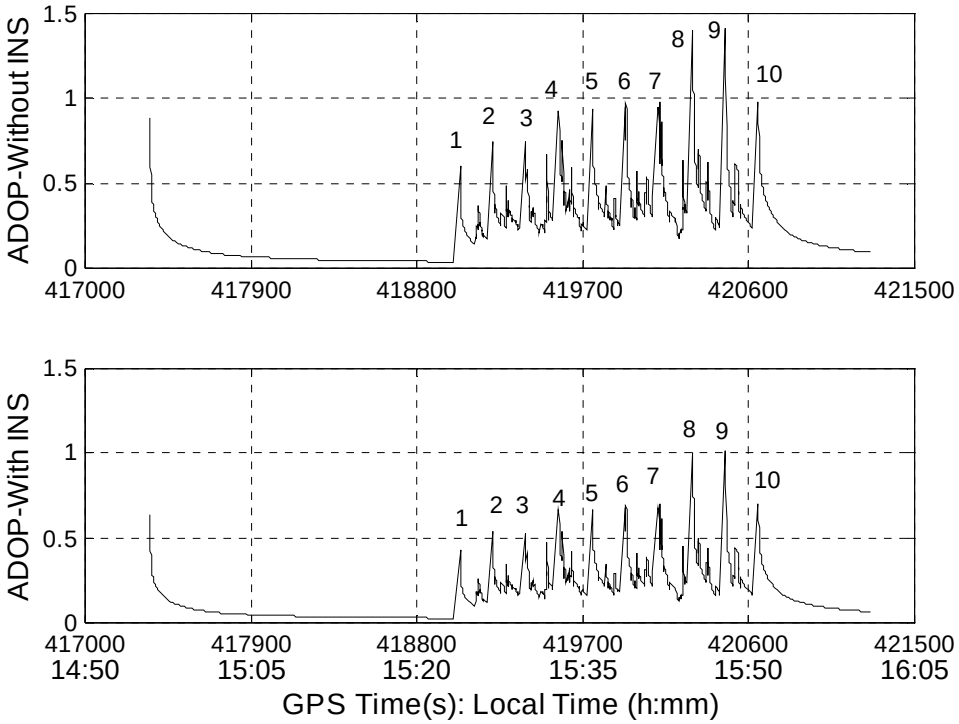

Figure 7.10 L1 ADOP, 30-second Full Outage, Van Test I

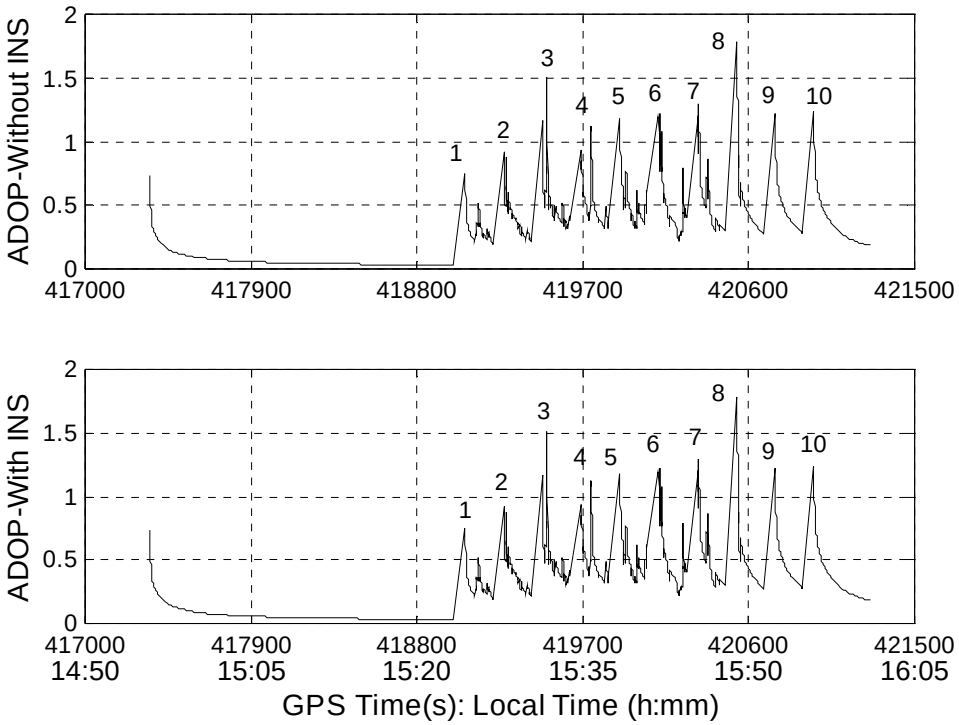

Figure 7.11 L1 ADOP, 60-second Full Outage, Van Test I

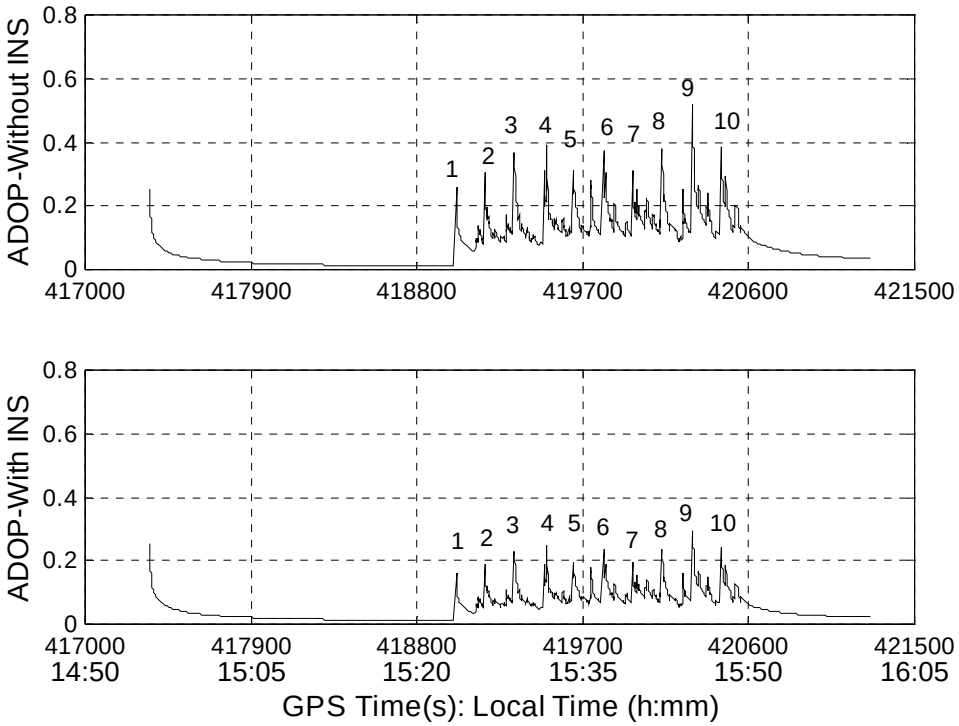

Figure 7.12 WL ADOP, 10-second Full Outage, Van Test I

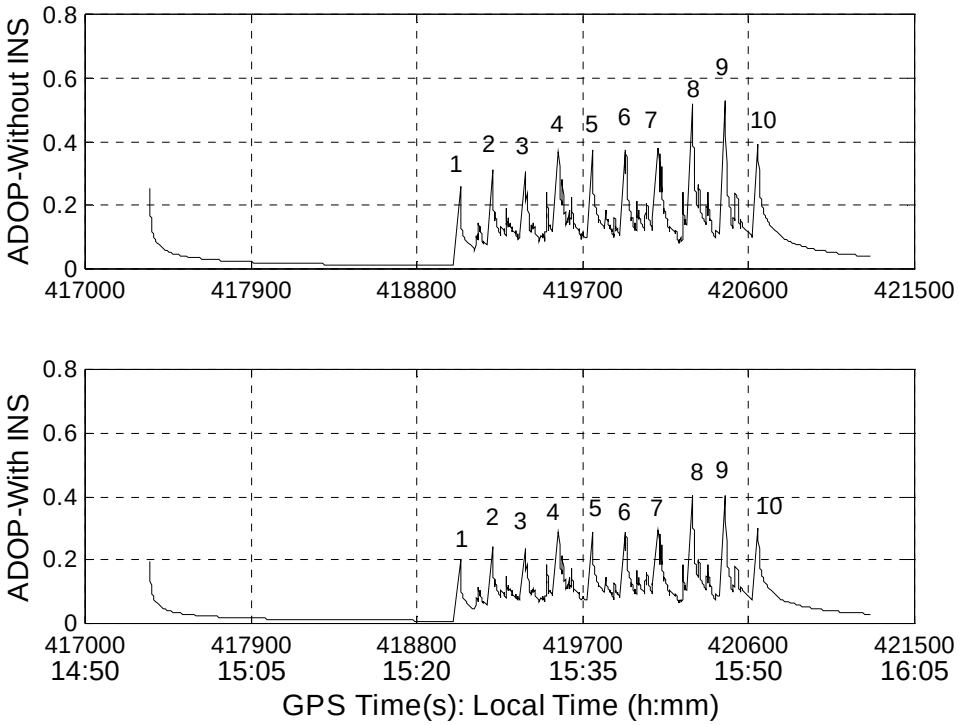

Figure 7.13 WL ADOP, 30-second Full Outage, Van Test I

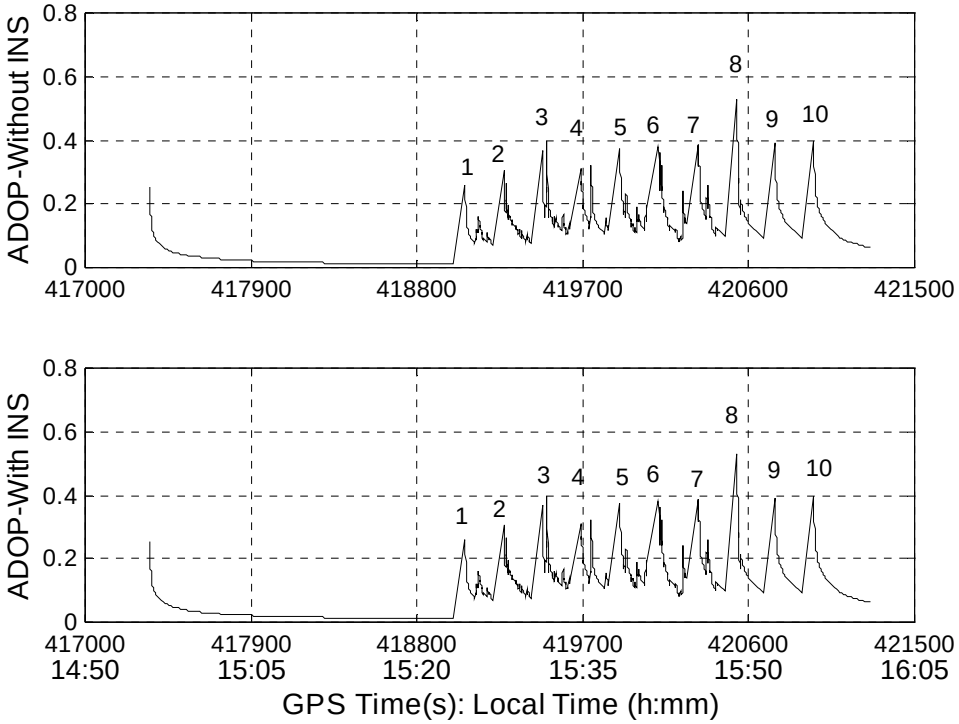

Figure 7.14 WL ADOP, 60-second Full Outage, Van Test I

The ADOP reduction shown in the above figures is used to demonstrate that the search space shrinks with INS data in the ambiguity resolution process. However, as discussed at the beginning, the ADOP is only an indicator of the search size and it cannot guarantee fixing the integers. The time to fix ambiguities is a good candidate to quantify the improvement on ambiguity resolution using INS data.

The time to fix integers in each case is recorded during the data process. Results of the 10, 30, 60 second full and partial GPS outages in Van I test are summarized in Tables 7.3 to 7.5, respectively. The outage start time for each case is slightly different because the FASF needs different intervals to fix ambiguities between outages.

Table 7.3 10-second GPS Outage, L1, Van Test I

GPS Outage Start Time(s)	TFI*, No INS aiding	TFI*, with INS aiding						Baseline (metres)
		Full Outage			Partial Outage			
		I**	II	III	I	II	III	
419001	106	56	57	40	56	30	20	60
419161	114	67	60	15	67	26	11	179
419321	108	57	45	40	57	34	9	78
419481	156	83	77	62	83	41	31	195
419641	117	65	59	41	65	27	12	204
419801	125	69	70	68	69	31	23	48
419961	135	71	69	60	71	32	17	208
420121	107	64	58	55	64	29	14	208
420281	277	150	151	145	150	41	41	86
420441	110	61	57	55	61	37	19	202

*TFI – Time to Fix Integers, seconds
**I – loose coupling integration, II – tight coupling integration, III – centralized integration

Table 7.4 30-second GPS Outage, L1, Van Test I

GPS Outage Start Time(s)	TFI*, No INS aiding RMS	TFI*, with INS aiding (RMS)						Baseline (metres)
		Full Outage			Partial Outage			
		I**	II	III	I	II	III	
419000.9316	191	121	123	101	121	84	71	60
419180.9240	104	79	62	24	79	49	51	207
419360.9937	135	94	81	67	94	60	50	106
419540.9346	145	107	82	71	107	74	61	100
419720.9355	125	87	71	65	87	57	45	194
419900.9367	124	84	75	67	84	55	47	233
420070.9372	194	138	123	102	138	104	91	65
420260.9384	198	140	134	110	140	103	93	160
420440.9394	235	161	151	129	161	131	105	164
420620.9404	147	107	97	78	107	74	65	56

*TFI – Time to Fix Integers, seconds

**I – loose coupling integration, II – tight coupling integration, III – centralized integration.

Table 7.5 60- second GPS Outage, L1, Van Test I

GPS Outage Start Time(s)	TFI*, No INS aiding RMS	TFI*, with INS aiding, RMS						Baseline (metres)
		Full Outage			Partial Outage			
		I**	II	III	I	II	III	
419001	205	206	209	207	206	187	172	60
419211	133	130	129	127	130	117	109	228
419421	168	169	167	168	169	151	147	228
419631	150	149	151	150	149	130	122	208
419841	181	181	180	179	181	159	150	132
420051	194	194	193	192	194	175	167	53
420261	136	135	132	134	135	114	109	160
420471	235	235	236	234	235	213	214	204
420681	150	151	150	149	151	130	129	56
420891	161	159	161	158	159	137	130	56

*TFI – Time to Fix Integers, seconds

**I – loose coupling integration, II – tight coupling integration, III – centralized integration.

The average time to fix ambiguities in the various scenarios is presented in Table 7.6. The performance of the ambiguity resolution improvement as a percentage is shown in Table 7.7.

The performance of INS aiding in ambiguity resolution under a full GPS outage can be seen in Figure 7.15. It can be observed that the average time to fix integers is significantly reduced when the GPS outage duration is short (10 seconds). As the outage duration increases the time reduction is decreased. While for a 30-second outage duration there is a moderate reduction, the improvement in the 60-second outage becomes almost zero. This can be explained by the large INS drift over the relatively longer time (about 2 metres after 60 seconds). It can also be seen from Table 7.6 that in loose coupling integration, the time to fix integers is the same under both full and partial outages. This is because in the partial outage there is no GPS solution available as is the case for the full outage. However, for tight coupling and centralized integration schemes, GPS measurements are available for master filter update in the partial outages.

Table 7.6 Ambiguity Resolution Time Statistics, L1, Van Test I

GPS Outage Duration (s)	TFI*, No INS aiding	TFI*, with INS aiding					
		Full Outage			Partial Outage		
		I**	II	III	I	II	III
10	135	74	70	57	74	32	19
30	151	111	99	81	111	79	67
60	161	160	161	159	160	144	135

*TFI – Time to Fix Integers, seconds
**I – loose coupling integration, II – tight coupling integration, III – centralized integration.

Table 7.7 Time to Fix Integers Improvement, L1, Van Test I

GPS Outage Duration (s)	Percentage of TFI Reduction with INS aiding					
	Full Outage			Partial Outage		
	I**	II	III	I	II	III
10	45%	48%	57%	45%	76%	85%
30	26%	34%	46%	26%	47%	55%
60	0	0	1%	0	10%	16%

**I – loose coupling integration, II – tight coupling integration, III – centralized integration.

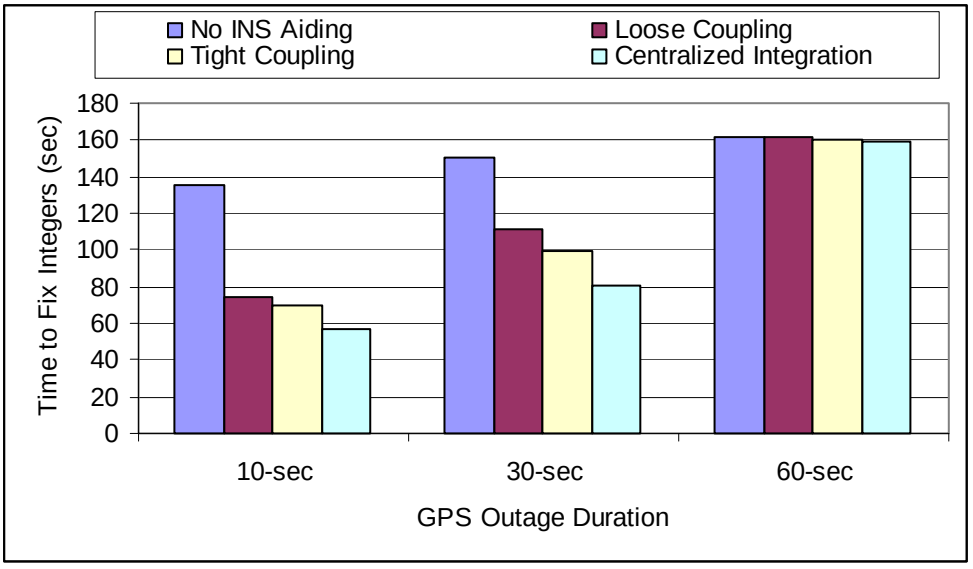

Figure 7.15 Ambiguity Resolution Performance, L1 Full Outage, Van Test I

Results under partial GPS outages are shown in Figure 7.16. Compared with the full outage scenario, the reduction of time to fix integers under partial outages is more significant in tight coupling and centralized INS/GPS integration scenarios. This is because the GPS measurements available during the outage are still used in the master filter to update the predictions. The measurement update improves the system filtering

performance and thus makes the navigation solution more accurate as indicated in Section 7.1. It is particularly obvious that under a full GPS outage the time reduction in a 60-second outage is zero while under a partial outage there is still some reduction. However, the GPS satellites in the partial outage present no improvement in the loose coupling integration. This is because there are only three satellites retained in the outage and the number of satellites is not sufficient to construct any navigation solution in the GPS filter, thus the master filter stays in pure prediction mode.

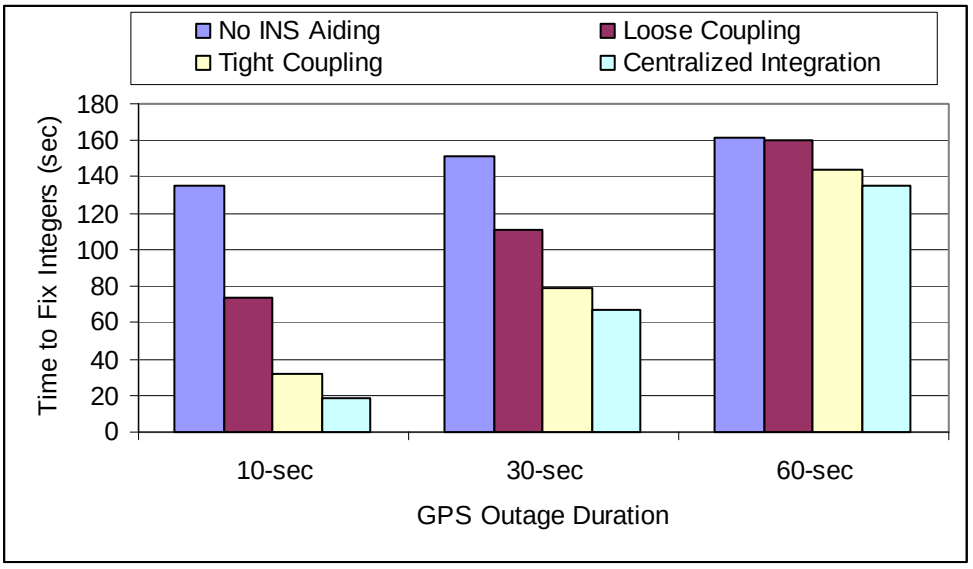

Figure 7.16 Ambiguity Resolution Performance, L1 Partial Outage, Van Test I

The overall inertial aiding performance under full outage versus partial outage in ambiguity resolution can be seen in Table 7.8. The results show that under partial outage circumstances, the improvement percentage is more significant than for the full GPS outage. The effect of a partial presence of GPS satellites in ambiguity resolution with

inertial data under a 10-second outage is shown in Figure 7.17. During the full outage, the master filter (or the augmented filter in centralized integration) performs pure prediction. The presence of GPS satellites, however, can be fed into the filter to update the predictions and the accuracy of the position from the filter can therefore be improved. The more accurate information from the master filter during the outage can then improve the system filtering performance while full satellite measurements are available and thus makes the search procedure fix the ambiguities faster. In loose coupling, the GPS filter cannot generate a position under a partial outage where there are less than four satellites visible, and thus it cannot provide navigation solutions to the master filter to update its predictions. This makes no difference in terms of the time to fix integers with inertial aiding between full and partial GPS outage case as shown in the Figure 7.16.

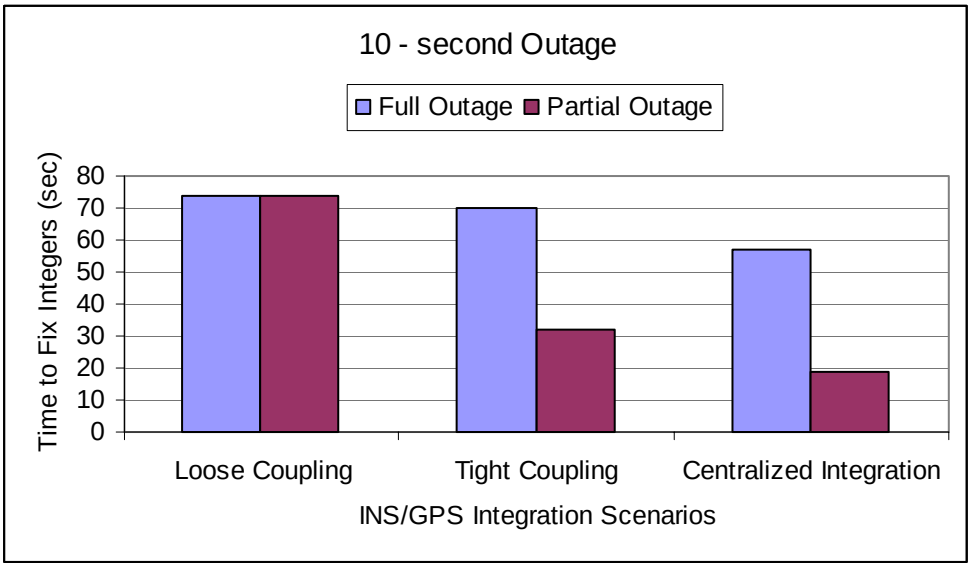

Figure 7.17 Ambiguity Resolution Performance, L1 GPS Outage, Van Test I

The results under the same testing scenarios for the widelane are summarized in Tables 7.8 and 7.9. The same improvement patterns can be observed from statistics in the widelane case. In Table 7.8, time to fix integers is the same for loose coupling integration under both full and partial outages. As discussed previously, this is because there are no GPS positions available in the partial outage as is the case for the full outage. The introduction of inertial data in the ambiguity resolution process reduces the average time to fix integers to different extents depending on the outage duration. GPS measurements in the partial outages improve the accuracy of information from the master filter prediction and thus facilitate ambiguity resolution after outages.

Table 7.8 Ambiguity Resolution Time Statistics, Widelane, Van Test I

GPS Outage Duration (s)	TFI*, No INS aiding	TFI*, with INS aiding					
		Full Outage			Partial Outage		
		I**	II	III	I	II	III
10	43	28	20	11	29	14	10
30	45	30	21	15	30	16	12
60	48	48	47	49	47	35	30

*TFI – Time to Fix Integers, seconds
**I – loose coupling integration, II – tight coupling integration, III – centralized integration.

Table 7.9 Time to Fix Integers Improvement, Wide-lane, Van Test I

GPS Outage Duration (s)	Percentage of TFI Reduction with INS aiding					
	Full Outage			Partial Outage		
	I**	II	III	I	II	III
10	34%	53%	74%	32%	67%	76%
30	33%	53%	66%	33%	64%	73%
60	0	2%	0	0	27%	37%

**I – loose coupling integration, II – tight coupling integration, III – centralized integration.

7.2.2 Van Test II

In this section the second van test is examined to determine the effect of inertial data on ambiguity resolution under relatively longer baselines and higher dynamics. As shown in Section 6.3.2, the baseline length in Van Test II reaches up to 50 km while the maximum baseline in Van Test I is less than 240 m. The effect of longer baselines is such that the atmospheric errors can be significantly larger.

Time to fix integers for L1 under the 10, 30, and 60-second outages are summarized in Tables 7.10 to 7.12. After 20 km, the search process cannot find the candidate set satisfying the ratio test and thus integers cannot be fixed. It is particularly clear that the search process fails to fix integers when the baselines are longer.

Table 7.10 10 – second GPS Outage, L1, Van Test II

GPS Outage Start Time(s)	TFI*, No INS aiding	TFI*, with INS aiding						Baseline (Metres)
		Full Outage			Partial Outage			
		I**	II	III	I	II	III	
413629	97	61	49	48	60	37	34	79
414034	132	103	95	92	102	56	55	1697
414436	220	209	197	195	202	103	101	5018
414980	321	310	308	305	310	177	170	9733
415713	592	581	579	520	581	397	390	15635
417429	--	--	--	--	--	--	--	50287
418166	--	--	--	--	--	--	--	45702
418577	--	--	--	--	--	--	--	37055
420125	211	150	151	145	151	81	78	2365
420396	102	61	57	55	67	37	35	119

*TFI – Time to Fix Integers, seconds
**I – loose coupling integration, II – tight coupling integration, III – centralized integration

Table 7.11 30 – second GPS Outage, L1, Van Test II

GPS Outage Start Time(s)	TFI*, No INS aiding	TFI*, with INS aiding						Baseline (Metres)
		Full Outage			Partial Outage			
		I**	II	III	I	II	III	
413629	97	71	60	57	69	47	45	79
414034	132	109	105	99	110	66	63	1697
414436	220	217	206	203	214	112	111	5018
414980	321	312	310	307	315	189	182	9733
415713	592	585	580	537	584	405	400	15635
417429	--	--	--	--	--	--	--	50287
418166	--	--	--	--	--	--	--	45702
418578	--	--	--	--	--	--	--	37055
420125	211	161	157	149	159	92	89	2365
420396	102	74	67	63	75	48	45	119

*TFI – Time to Fix Integers, seconds
**I – loose coupling integration, II – tight coupling integration, III – centralized integration.

Table 7.12 60 – second GPS Outage, L1, Van Test II

GPS Outage Start Time(s)	TFI*, No INS aiding	TFI*, with INS aiding						Baseline (Metres)
		Full Outage			Partial Outage			
		I**	II	III	I	II	III	
413628.9278	97	98	99	97	98	90	85	79
414033.9274	132	132	130	131	131	121	114	1697
414435.9279	220	221	219	220	221	215	206	5018
414979.9285	321	321	321	320	320	301	290	9733
415712.9349	592	593	591	590	591	580	561	15635
417428.9299	--	--	--	--	--	--	--	50287
418165.9299	--	--	--	--	--	--	--	45702
418576.9297	--	--	--	--	--	--	--	37055
420124.9286	211	212	211	210	210	198	187	2365
420395.6783	102	101	102	101	102	96	85	119

*TFI – Time to Fix Integers, seconds
**I – loose coupling integration, II – tight coupling integration, III – centralized integration.

When looking at individual simulation points in Van Test II, it can be observed that the points at longer baselines show less improvement in time to fix integers with INS aiding than shorter baseline points. Figure 7.18 shows the INS aiding effect on all simulation points versus baselines for 10-second GPS outage with loose coupling. The case is true for all other GPS outage periods and INS aiding schemes. It can be seen that the effectiveness of INS aiding in GPS ambiguity resolution decreases as the baseline increases in this test case. This may be explained by the presence of more significant atmospheric errors in the longer baselines.

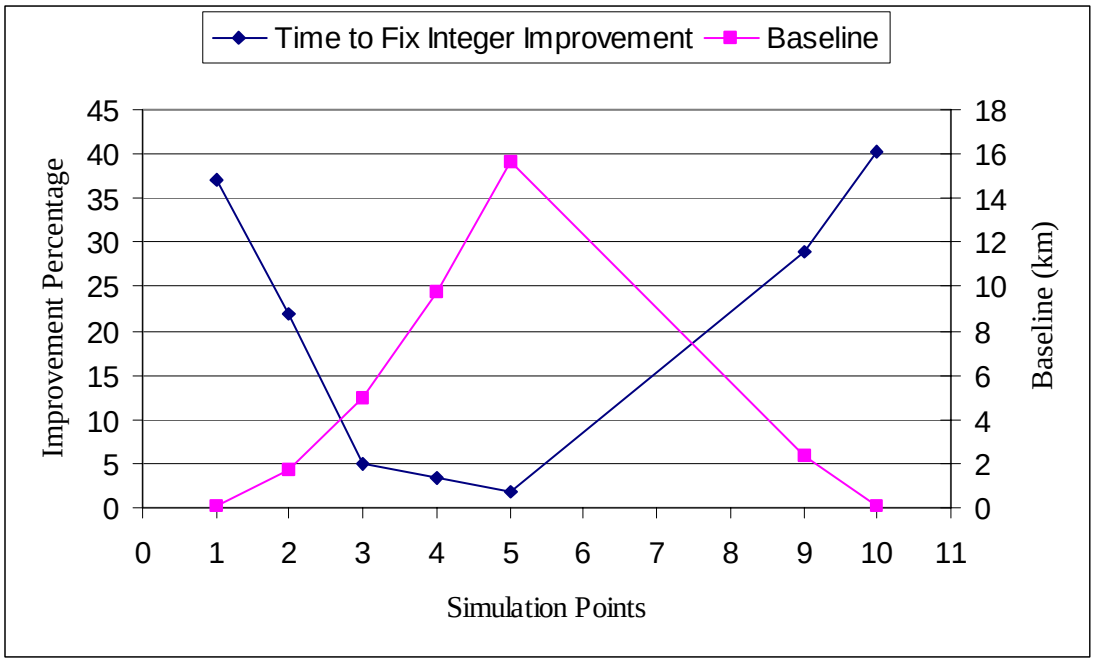

Figure 7.18 Performance of Ambiguity Resolution with INS Aiding versus baselines

The average times to fix ambiguities for the L1 and widelane measurements are summarized in Tables 7.13 and 7.14, respectively. Figure 7.19 shows the performance of ambiguity resolution with INS aiding. Basically the improvement pattern observed in Van Test I can be seen in Van Test II as well. During the 10-second GPS outage period there is an improvement in ambiguity resolution from INS aiding. As the outage period

increases, the improvement decreases. It is particularly clear that in the 60-second outage period the improvement is almost zero. The same observation exists for the partial outage cases as well as the widelane case.

When comparing Figure 7.19 to 7.16, it can be immediately seen that Van Test I has a more significant improvement than Van Test II in all outage scenarios. However, time to fix integers shown in the figures is average values. In Van Test I, all simulation points had very short baselines while simulation points in Van Test II have baselines ranging from 80 m to 50 km. Since the longer baseline points have less improvement as shown in the results, the averaged values can be larger with more long baseline points.

Table 7.13 Ambiguity Resolution Time Statistics, L1, Van Test II

GPS Outage Duration (s)	TFI*, No INS aiding	TFI*, with INS aiding					
		Full Outage			Partial Outage		
		I**	II	III	I	II	III
10	240	210	205	194	212	126	123
30	240	218	212	203	217	137	133
60	240	240	239	238	240	229	219

*TFI – Time to Fix Integers, seconds
**I – loose coupling integration, II – tight coupling integration, III – centralized integration.

Table 7.14 Ambiguity Resolution Time Statistics, Widelane, Van Test II

GPS Outage Duration (s)	TFI*, No INS aiding	TFI*, with INS aiding					
		Full Outage			Partial Outage		
		I**	II	III	I	II	III
10	104	91	80	82	92	68	64
30	104	94	85	84	94	73	68
60	104	105	104	103	104	95	93

*TFI – Time to Fix Integers, seconds

**I – loose coupling integration, II – tight coupling integration, III – centralized integration.

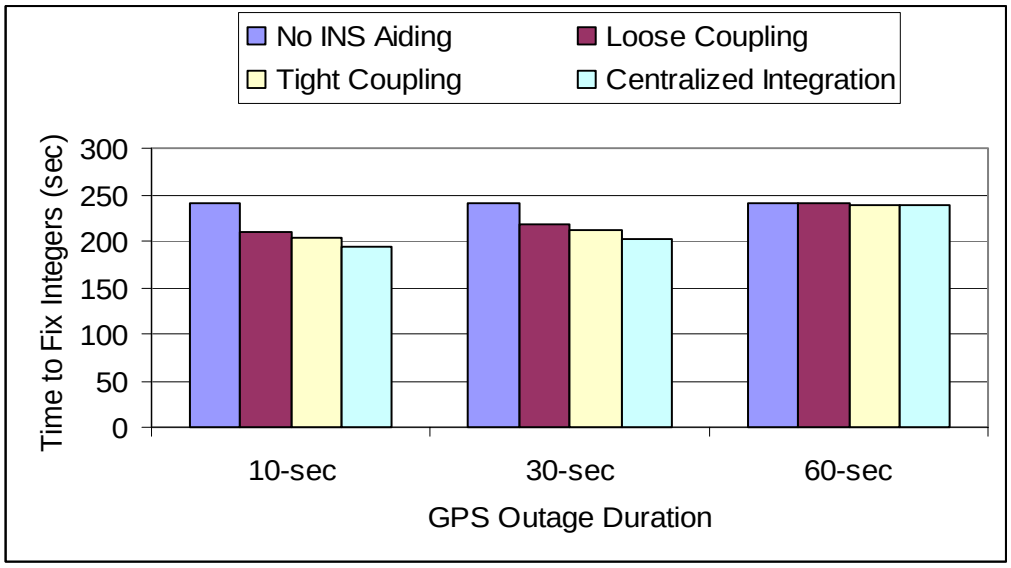

Figure 7.19 Ambiguity Resolution Performance, L1 Full Outage, Van Test II

7.2.3 Summary

The data analysis in this chapter shows that with inertial data the performance of ambiguity resolution is significantly improved. In this regard, loose coupling does not perform as well as the tight coupling and centralized integration. Better improvement is achieved under partial GPS outages, where GPS measurements are still available for updating the master filter, than complete outages, in which the master filter operates in pure prediction mode. It is also found that with longer GPS outage periods, the benefit of using inertial data in the ambiguity resolution decreases. Based on results from Van Test II, the improvement in ambiguity resolution tends to be a function of baseline, with less improvement in terms of time to fix integers as baseline increases.

Petovello (2003) also examined the impact of inertial data on GPS ambiguity resolution. Basically, the same improvement pattern was observed in the data analysis with different specific improvement percentage. It was also found that tight integration outperforms loose integration and the improvement in time to fix integers decreases as GPS outage time increases. Scherzinger (2002) also studied the impact of inertial data on ambiguity accuracy prior to the integer search procedure. The ADOP was also significantly decreased when inertial data was integrated with the tight integration. However, when comparing INS error growth, it was found that Petovello (2003) and Scherzinger (2002) had better average results under the same GPS outage period even with lower grade IMU HG1700. This is because of the shorter initial INS alignment time and thus larger alignment errors. The location of GPS outages as shown in Figures 7.2 and 7.3, where GPS outages occurred during vehicle sharp turns, can also contribute to stand-alone INS error growth.

7.3 Cycle Slip Detection with INS Aiding

As discussed in Section 4.6, the basic concept behind INS aiding in cycle slip detection during GPS outages is to use the predicted INS position in order to calculate the DD carrier phase and compare it with the measured DD carrier phase to obtain the difference (Eq. 4.15). The difference value, δ, will be close to zero and continuous with respect to time. The value of δ is monitored and a threshold is placed to determine whether cycle slip occurs, and upon a cycle slip the measured DD carrier phase is corrected by δ. Therefore the accuracy of cycle slip detection depends upon the accuracy of INS position

prediction during GPS outages. The INS position errors induced into GPS DD carrier phase measurement will cause constant biases in ambiguity determination and thus the errors should be well below a half cycle. Table 7.15 shows the statistics of δ on PRNs 11, 15 and 23 in Van Test I (i.e. difference between INS derived DD carrier phase measurement and measured DD carrier phase) over a 500-second sample size where there are no cycle slips. The base GPS satellite is PRN 12.

In order to study the efficiency of using an INS for cycle slip detection, cycle slips were simulated for ten GPS outages with 10-second outage periods. The data set used is Van Test I. INS position errors in 30 and 60-second outages are too large to perform cycle slip detection. A slip of ten cycles is created in the L1 carrier phase measurement on PRN 5 one epoch after the outage. PRN 5 is chosen because it is available during the entire test.

Table 7.15 Statistics on Diff. between INS Derived and GPS Measured DD Carrier Phase Difference, L1

PRN	Mean (cm)	RMS (cm)	Min (cm)	Max (cm)
11	0.1	0.4	-0.2	0.3
15	0	0.3	-0.1	0.2
23	0.1	0.5	-0.3	0.2

The purpose of having a one-epoch delay is to make the phase rate available and to perform a comparison between cycle slip detection with GPS phase rate and with INS aiding. Figure 7.20 shows the generation procedure.

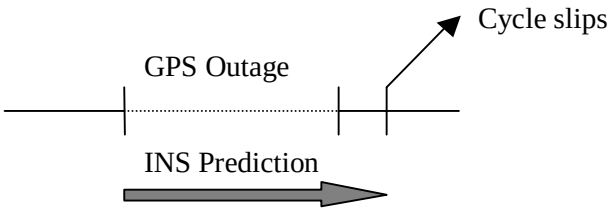

Figure 7.20 Cycle Slip Generation

Table 7.16 shows the detection results for both the full and partial GPS outages. At each epoch the same simulation is repeated 500 times in order to get RMS statistics. It can be seen that the cycle slip error defined as the difference between the detected cycle slip (δ) and true cycle slip is generally smaller for the INS/GPS integration case than in cycle slip detection with the GPS phase rate. This is because the position from the INS prediction over the short-term is very accurate and thus cycle slip detection with INS aiding has better performance. In the INS aiding case, cycle slip errors for a partial outage are smaller than for a full outage and this is because the position solution in a partial GPS outage has better accuracy. Figure 7.21 below shows a clear improvement in cycle slip detection with INS aiding.

Table 7.16 Difference between δ and True Cycle Slips (RMS, cm), L1

Outage Start Time (sec)	Full Outage (cm)	Partial Outage (cm)	GPS Phase Rate (cm)
419001	3.1	1.6	4.9
419161	2.9	2.2	5.4
419321	3.1	1.9	5.3
419481	2.7	1.5	6.1
419641	2.8	1.4	5.1
419801	3.2	2.0	5.5
419961	2.9	1.1	4.8
420121	3.0	1.7	5.7
420281	3.1	1.9	4.9
420441	2.8	1.3	5.1

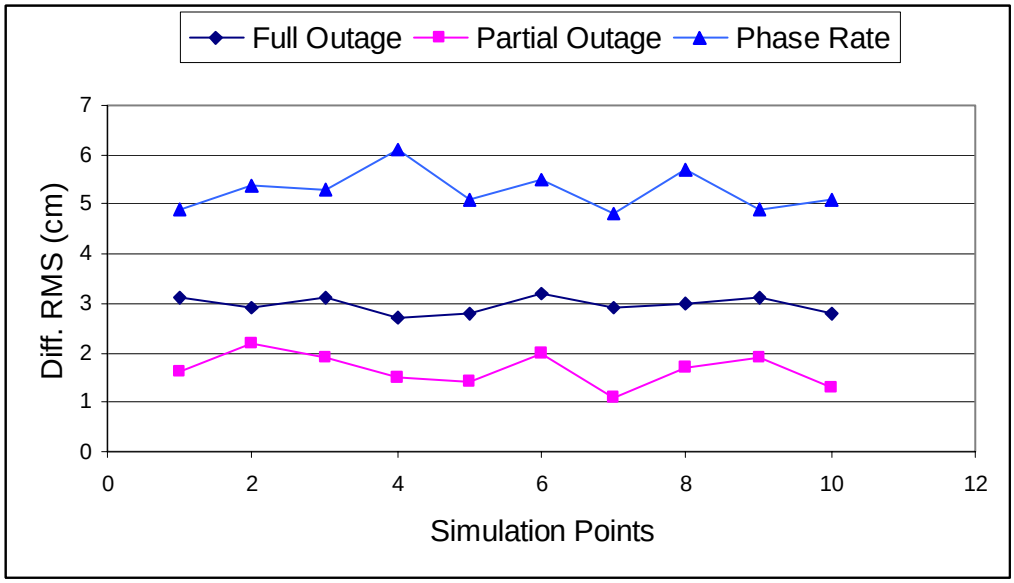

Figure 7.21 Cycle Slip Detection with INS Aiding vs. Doppler (Phase Rate)

CHAPTER 8

CONCLUSIONS AND RECOMMENDATIONS

The objective of this research was to investigate the feasibility of integrating high quality inertial data into GPS carrier phase ambiguity resolution. The research was comprised of three major components. The relevant theory on GPS and INS and INS/GPS integration was presented in the first part, combined with a detailed study on three INS/GPS integration filter structures and a brief overview on GPS ambiguity resolution principles. In the second part, the methodology of integrating inertial data into GPS ambiguity resolution was developed. The inertial aiding scheme was studied under three INS/GPS integration scenarios: loose coupling, tight coupling and the augmented master filter integration. The third part consisted of a description of the software package that implements the methodology and results from processing two data sets with short and longer baselines. In the following sections conclusions are drawn from the research carried out in this thesis and recommendations are given for the future research on this topic.

8.1 Conclusions

1. Three INS/GPS integration strategies proposed in the research have different advantages. The first approach, so-called INS navigation aiding, is primarily useful in GPS outages where there are no GPS positions available or the number of satellites available is insufficient (e.g. less than four) such that the GPS navigation stand-alone

module can not resolve the receiver's position. This approach is simplistic and easy to implement since it does not require any change in the system model. INS measurement aiding is suitable for instant or very short-period GPS outages. It is also useful for cases where the GPS filter loses the integers because of cycle slips or failure of residual checks invalidating the integers. The third approach, the augmented master filter, reduces the complexity of having two parallel Kalman filters. The INS aiding in the ambiguity resolution is automatically accomplished through the float ambiguity estimation in the augmented state vector. This approach is also subject to the INS drift during stand-alone navigation mode.

2. The LAMBDA technique reduces the correlation among ambiguities. The process of applying LAMBDA transformation to the VCV matrix of initial float ambiguities is a process of performing conditional least squares adjustment. After the adjustment the accuracy of transformed ambiguities is improved. The presence of high-quality inertial data in the measurement update further improves the accuracy of float ambiguity estimation. The theoretical analysis of ADOP in least squares framework as well as results from the data analysis shows that with additional inertial data the accuracy of float ambiguities is improved and the size of ambiguity search space is reduced.

3. The performance of INS aiding in ambiguity resolution is examined by processing two data sets. 10, 30 and 60-second GPS outages were simulated in each data set and the time to fix integers after the outages were recorded. Results from both data sets

showed that during short-term GPS outages, incorporation of INS data reduced the time to fix ambiguities quite significantly (average 40 – 70% improvement in 10 – second GPS outage case). The INS aiding in the augmented master filter integration has the best performance. The INS aiding mechanism for long baseline case showed almost the same percentage improvement in terms of average time to fix integers after the outages. However the feasibility of using INS data in the long baseline case eventually depends on the significance of GPS atmospheric errors. Results showed that in the circumstances where GPS-only cannot resolve integers due to atmospheric errors in long baselines inertial data integration cannot improve the situation to fix integers either.

4. The efficiency of using inertial data in cycle slip detection and recovery is also examined by processing the short baseline test data. Cycle slips are simulated at various epochs with 10 – second GPS outages and slip detections with INS and GPS-only are performed at these epochs. Results show that cycle slips recovered with INS is more accurate than with GPS-only. The efficiency of using INS/GPS integration to detect and recover cycle slips primarily depends on the INS bridging time. Over a long-term bridge, such that the INS error drift exceeds one half cycle, there is no benefit of using inertial data to perform cycle slip detection and recovery.

8.2 Recommendations

1. The data process in the software is for post-mission data sets. Further evaluation on real time data process should be performed in the future work.

2. Two van data sets were used. Data sets from aircraft tests should be processed to evaluate the performance of INS aiding in ambiguity resolution under higher dynamics.

3. The IMU used in the tests is very high quality. Other grades and low-cost IMUs can be used to further evaluate the feasibility of using inertial data in fixing integers and detecting cycle slips.

4. In post-mission data processing the technique of forward - backward prediction and smoothing can be applied to extend INS bridging time in ambiguity resolution and cycle slip detection.

REFERENCES

Britting, K.R. (1971), Inertial Navigation System Analysis, Wiley – Interscience, New York.

Brown, R.G. and Patrick Y.C. Hwang (1995), Introduction to Random Signals and Applied Kalman Filtering, Second Edition, John Willey & Sons, Inc., pp. 231 – 235.

Cannon, M.E. (1987), Kinematic Positioning Using GPS Pseudorange and Carrier Phase Observations, Report No. 20019, Department of Geomatics Engineering, University of Calgary, Canada.

Cannon, M.E. (1991), Airborne GPS/INS with an Application to Aerotriangulation, UCSE Report No. 20040, Department of Geomatics Engineering, University of Calgary, Canada.

Cannon, M.E. and Lachapelle, G. (1992), Analysis of a High Performance C/A Code GPS Receiver in Kinematic Mode, Proceedings of the National Technical Meeting, San Diego, Jan. 27-29, The Institute of Navigation, Washington D.C., pp. 49-58.

Cannon, M.E. (2002), Satellite Positioning, ENG 561 Lecture Notes, Department of Geomatics Engineering, University of Calgary, Canada.

Cannon, M.E., Lachapelle, G., Sun, H., Fletcher T., Caballero R. and Hawes I. (1999), Development and Testing of an Integrated INS/GPS Cross – linked System for Sub – meter Positioning of CF – 188 Jet Fighter, Proceedings of ION Annual Meeting, Cambridge, June 28-30, pp. 463 – 474.

Chen, D. (1993), Fast Ambiguity Search Filter (FASF): A Novel Concept for GPS Ambiguity Resolution, Proceedings of the sixth International Technical Meeting of the Satellite Division of the ION, GPS – 93, Salt City, September 22 - 24.

Chen, D. and Lachapelle, G. (1994), A Comparison of the FASF and Least – Squares Search Algorithms for Ambiguity Resolution On The Fly, Proceedings of International Symposium on Kinematic Systems – KIS 94, pp. 241 – 253, Banff, Canada, August 30 – September 2.

Chen, D. (1994), Development of a FAst Ambiguity Search Filtering (FASF) Method for GPS Carrier Phase Ambiguity Resolution, UCGE Reports No. 20071, Dept. of Geomatics Engineering, University of Calgary.

Counselman C.C. and Gourevitch S.A. (1981), Miniature interferometer terminals for earth surveying: ambiguity and multipath with the Global Positioning System, IEEE Transactions on Geoscience and Remote Sensing, GE-19 (4), pp. 224 – 252

Gao, Y., Krakiwsky, E.J., Abousalem, M.A. and Mclellan, J.F. (1993), Comparison and Analysis of Centralized, Decentralized, and Federated Filters, Navigation, Vol. 40, No. 1, pp. 69 – 86.

Golub, G.H. and Loan C.F.V. (1989), Matrix Computations, Second Edition, The Johns Hopkins University Press, Baltimore, Maryland, USA.

GPS Standard Positioning Service (SPS) Performance Standard (2001), Assistant Secretary of Defense for Command, Control, Communications, and Intelligence, October, 2001.

Erickson, C (1992), Investigations of C/A Code and Carrier Measurements and Techniques for Rapid Static GPS Surveys, UCGE Reports, No. 20044, Department of Geomatics Engineering, University of Calgary, Canada.

Hopfield, H. (1969), Two – quartic Tropospheric Refractivity Profile for Correction Satellite Data, Journal of Geophysical Research, Vol. 74, No. 18, pp. 4487 – 4499.

Hofmann-Wellenhof B., Lichtenegger H., and Collins J. (1997), GPS Theory and Practice, Third Revised Edition, Spring – Verlag, Wien New York.

Klobuchar, J.A. (1995), Potential Ionospheric Limitations to GPS Wide Area Augmentation System. Navigation, Journal of the Institute of Navigation, Vol 42, 1995.

Klobuchar , J.A. (1996), Ionospheric Effects on GPS. Global Positioning System, Theory and Application, Vol. 1, American Institute of Aeronautics and Astronautics, Inc., pp. 485-514.

Krakiwsky, E.J. (1990), The Method of Least Squares: A Synthesis of Advances, UCGE Reports 10003, Department of Geomatics Engineering, University of Calgary, Canada.

Lachapelle, G., Cannon, M.E. and Lu G. (1992), Ambiguity Resolution on the Fly – A Comparison of P Code and High Performance C/A Code Technologies, Proceedings of ION GPS – 92, Albuquerque, pp. 1025 – 1032

Lachapelle, G., Cannon, M.E. and Lu G. (1992), High-Precision GPS Navigation with Emphasis on Carrier – Phase Ambiguity Resolution, Marine Geodesy, Vol. 15, No. 4, pp. 253 – 269.

Lachapelle, G., C. Liu, G. Lu (1993), Quadruple Single Frequency Receiver System for Ambiguity Resolution On The Fly, Proceedings of ION GPS – 93, Salt Lake City, pp. 1167 – 1172.

Lachapelle, G. (1998), GPS Theory and Applications, ENGO625 Lecture Notes, Department of Geomatics Engineering, University of Calgary, Canada.

Liao, X. (2000), Carrier Phase Based Ionosphere Recovery over a Regional Area GPS Network, UCGE Report No. 20143, Department of Geomatics Engineering, University of Calgary, Canada.

Lu, G. (1995), Development of a GPS Multi – Antenna System for Attitude Determination, UCGE Reports 20073, Department of Geomatics Engineering, The University of Calgary.

Mader, G.L. (1990), Ambiguity Function Techniques for GPS Phase Initialization and Kinematic Solutions, Proceedings of the Second International Symposium on Precise Positioning with the Global Positioning System, Ottawa, Canada, September 3 – 7, pp.1233 – 1247.

Parkinson, B.W., T. Stansell, R. Bread, and K. Gromov (1995), A History of Satellite Navigation, Navigation Journal of the Institute of Navigation, Vol . 42, No. 1, pp. 109-164.

Paul de Jonge and Christian Tiberius (1996), The LAMBDA Method for Integer Ambiguity Estimation: Implementation Aspects, LGR Series No., 12, Delft Geodetic Computing Center.

Petovello, M.G. (2003), Real-Time Integration of a Tactical-Grade IMU and GPS for High-Accuracy Positioning and Navigation, Ph.D. thesis, UCGE Reports 20173, Department of Geomatics Engineering, The University of Calgary.

Petovello, M.G., M.E. Cannon, G. Lachapelle, J. Wang, C.K.H. Wilson, O.S. Salychev and V.V. Voronov, Development and Testing of a Real – Time GPS/INS Reference System for Autonomous Automobile Navigation, Proceedings of ION GPS – 01, Salt Lake City, UT, pp. 1-8.

Raquet, J. (1998), Development of a Method for Kinematic GPS Carrier-Phase Ambiguity Resolution Using Multiple Reference Receiver. Ph.D. thesis, UCGE Report No. 20116, May 1998, Department of Geomatics Engineering, University of Calgary.

Raquet, J., G. Lachapelle, and T.E. Melgard (1998), Test of A 400km X 600km Network of Reference Receivers for Precise Kinematic Carrier-Phase Positioning in Norway. Proceedings of ION GPS-98, The 11th International Technical Meeting of the Satellite Division of the Institute of Navigation, Nashville, Tennessee, September 15-19, pp. 407-416.

Ray, J. K. (2000), Mitigation of GPS Code and Carrier Phase Multipath Effects using a Multi-Antenna System**,** Ph.D. thesis, UCGE Report No. 20136, Department of Geomatics Engineering, University of Calgary.

Remondi, B.W. (1984), Using the Global Positioning System (GPS) Phase Observable for Relative Geodesy: Modeling, Processing and Results. University of Texas at Austin, Center for Space Research.

Remondi, B.W. (1990), Pseudo – Kinematic GPS Results Using the Ambiguity Function Method. NOAA Technical Memorandum NOS NGS – 52, National Information Center, Rockville, Maryland.

Remondi, B.W. (1991), Kinematic GPS Results without Static Initialization, NOAA Technical Memorandum NOS NGS – 55, National Information Center, Rockville, Maryland.

Saastamoinen, J. (1973), Contribution to the Theory of Atmospheric Refraction, Bulletin Geodesique, 107, pp. 13 – 34.

Salychev, O. S. (1998), Inertial Systems in Navigation and Geophysics, Bauman MSTU Press, Moscow.

Salychev, O.S. (1999), Applied Estimation Theory in Geodetic and Navigation Application, ENGO 699.52, Department of Geomatics Engineering, University of Calgary, Canada.

Salychev, O.S., V.V. Voronov, M.E. Cannon, R. Nayak and G. Lachapelle (2000), Low Cost INS/GPS Integration: Concepts and Testing. Proceedings of the National Technical Meeting, The Institute of Navigation, Alexandria, VA., pp. 98 – 105.

Schmidt, G.T. (1978), Introduction and Overview of Strapdown Inertial System, AGARD Lecture Series No. 95, Neuily sur Seine, France.

Scherzinger, B. M. (2000), Precise Robust Positioning with Inertial/GPS RTK, Proceedings of GPS – 2000, The Institute of Navigation, Alexandria, VA., pp. 155 – 162.

Scherzinger, B. M. (2002), Robust Positioning with Single Frequency Inertially Aided RTK, Proceedings of the 2002 National Technical Meeting, The Institute of Navigation, San Diego, CA, pp. 911 – 917.

Schwarz, K. P., M. Wei and M.V. Gelderen (1994), Aided Versus Embedded – a Comparison of Two Approaches to GPS/INS Integration, Proceedings of IEEE Position Location and Navigation Symposium, 1994, pp. 314 - 322

Schwarz, K. P. and M. Wei (1999), INS/GPS Integration for Geodetic Applications, ENG623 Lecture Notes, Department of Geomatics Engineering, University of Calgary, Canada.

Schwarz, K.P., N. El-Sheimy, and Z. Liu (1994), Fixing GPS Cycle Slips by INS/GPS – Methods and Experiences, International Symposium on Kinematic Systems in Geodesy, Gematics and Navigation – KIS 94, Banff, Canada, pp. 265 – 274.

Schwarz K.P. and G. Zhang (1994), Development and Testing a Low Cost Integrated GPS/INS, Proceedings of GPS – 1994, The Institute of Navigation, Alexandria, VA., pp. 1137 – 1144.

Shi, J. and M.E. Cannon (1995), Critical Error Effects and Analysis in Carrier Phase Based Airborne GPS Positioning Over Larger Areas, Bulletin Geodesique, 69, pp. 261 – 273.

Skaloud, J. (1999), Optimizing Georeferencing of Airborne Survey Systems by INS/GPS, PhD Thesis, UCGE Reports No. 20126, pp. 90 - 103, Department of Geomatics Engineering, University of Calgary.

Skone, S. (1998), Wide Area Ionosphere Grid Modelling in the Auroral Region, UCGE Reports No. 20123, Department of Geomatics Engineering, University of Calgary, Canada.

Spilker, J.J. Jr. (1994), GPS Navigation Data, Overview of GPS Operation and Design, Global Positioning System: Theory and Applications, Vol. I, ed. B.W. Parkinson and J.J. Jr. Spilker, America Institute of Aeronautics and Astronautics, Inc., Washington DC, pp. 121 – 176.

Sun, H. (1994), GPS/INS Integration for Airborne Applications, Master Thesis, UCGE Reports No. 20069, Department of Geomatics Engineering, University of Calgary, Canada.

Teunissen, P. J. G. (1993), Least - Squares Estimation of the Integer GPS Ambiguities, Invited lecture, Section IV Theory and Methodology, IAG General Meeting, Beijing, China, August 1993.

Teunissen, P. J. G. (1995), The Invertible GPS Ambiguity Transformations. Manuscr Geodaetica, Vol. 20, No. 6, pp. 489 – 497.

Teunissen, P. J. G., P. J. de Jonge and C. C. J. M. Tiberius (1997), Performance of the LAMBDA Method for Fast GPS Ambiguity Resolution, Journal of ION, Fall, pp.373 – 383.

Teunissen, P. J. G. (1997a), A Canonical Theory for Short GPS baselines. Part II: the Ambiguity Precision and Correlation. Journal of Geodesy, Vol. 71, No. 7, pp. 389 – 401.

Teunissen, P and D. Odijk (1997), Ambiguity Dilution of Precision: Definition, Properties and Applications, ION – GPS – 97 Proceedings, pp. 891 – 899.

Wang, J., M.P. Stewart, M.P. and M. Tsakiri (2000), A Comparative Study of the Integer Ambiguity Validation Procedures, Earth Planets Space, 52, 2000, pp. 813 – 817

Wei, M. and K.P. Schwarz (1990), Testing a Centralized Filter for GPS/INS Integration, Proceedings of the IEEE 1990 PLANS – Position, Location and Navigation Symposium, Las Vegas, Nevada, March.

Wells, D., N. Beck, N., D. Delikaraoglou, A. Kleusberg, E.J. Krakiwsky , G. Lachapelle, R.B. Lamgley, M. Nakiboglu, K.P. Schwar, J.M. Tranquilla, and P. Vanicek (1987), Guide to GPS Positioning, Canadian GPS Associates, Federicton, New Brunswick, Canada.

Weisenburger, S. D. (1997), Effect of Constraints and Multiple Receivers for On – The – Fly Ambiguity Resolution, Master Thesis, UCGE Reports No. 20109, Department of Geomatics Engineering, University of Calgary, Canada.

Wolf, R., G.W. Hein, B. Eissfeller, and E. Loehnert (1996), An Integrated Low Cost GPS/INS Attitude Determination and Position Location System, Proceedings of ION GPS – 96, Alexandria, VA., pp. 975 - 981.

Wong R.V.C. (1985), A Kalman Filter – Smoother For An Inertial Survey System of Local Level Type, Master Thesis, UCSE Reports No. 20001, Department of Geomatics Engineering, University of Calgary, Canada.

Zumberge, J.F. and W.I., Bertiger (1996), Ephemeris and Clock Navigation Message Accuracy, Global Positioning System: Theory and Applications, Vol. 1, American Institute of Aeronautics and Astronautics Inc., Washington DC, pp. 585-600.

APPENDIX A

Derivation of DD ambiguity VCV Matrix

Rewriting equation (3.6) gives:

$$\begin{bmatrix} Q_{\delta\hat{r}} & Q_{\delta\hat{r},\nabla\Delta N} \\ Q_{\nabla\Delta N,\delta\hat{r}} & Q_{\nabla\Delta N} \end{bmatrix} = \left(B' R_{\varepsilon}^{-1} B\right)^{-1} \tag{A.1}$$

Notice that R_{ε}^{-1} and B take the following forms:

$$R_{\varepsilon}^{-1} = \begin{bmatrix} R_{ins} & & \\ & R_{\nabla\Delta\rho} & \\ & & R_{\nabla\Delta\varphi} \end{bmatrix}^{-1} = \begin{bmatrix} R_{ins}^{-1} & & \\ & R_{\nabla\Delta\rho}^{-1} & \\ & & R_{\nabla\Delta\varphi}^{-1} \end{bmatrix} \tag{A.2}$$

$$B = \begin{bmatrix} H & O \\ A & O \\ A & \lambda B \end{bmatrix} \tag{A.3}$$

Substituting above expressions (A.2) and (A.3) into (A.1) yields:

$$\begin{aligned} (B' R_{\varepsilon}^{-1} B)^{-1} &= \left(\begin{bmatrix} H' & A' & A' \\ O & O & \lambda B' \end{bmatrix} \begin{bmatrix} R_{ins}^{-1} & & \\ & R_{\nabla\Delta\rho}^{-1} & \\ & & R_{\nabla\Delta\varphi}^{-1} \end{bmatrix} \begin{bmatrix} H & O \\ A & O \\ A & \lambda B \end{bmatrix} \right)^{-1} \\ &= \left(\begin{bmatrix} H' R_{ins}^{-1} & A' R_{\nabla\Delta\rho}^{-1} & A' R_{\nabla\Delta\varphi}^{-1} \\ O & O & \lambda B' R_{\nabla\Delta\varphi}^{-1} \end{bmatrix} \begin{bmatrix} H & O \\ A & O \\ A & \lambda B \end{bmatrix} \right)^{-1} \\ &= \begin{pmatrix} H' R_{ins}^{-1} H + A' R_{\nabla\Delta\rho}^{-1} A + A' R_{\nabla\Delta\varphi}^{-1} A & \lambda A' R_{\nabla\Delta\varphi}^{-1} B \\ \lambda B' R_{\nabla\Delta\varphi}^{-1} A & \lambda^2 B' R_{\nabla\Delta\varphi}^{-1} B \end{pmatrix}^{-1} \end{aligned}$$

i.e.:

$$\begin{bmatrix} Q_{\hat{r}} & Q_{\hat{r},\nabla\Delta\hat{N}} \\ Q_{\nabla\Delta\hat{N},\hat{r}} & Q_{\nabla\Delta\hat{N}} \end{bmatrix} = \begin{pmatrix} H'R_{ins}^{-1}H + A'R_{\nabla\Delta\rho}^{-1}A + A'R_{\nabla\Delta\varphi}^{-1}A & \lambda A'R_{\nabla\Delta\varphi}^{-1}B \\ \lambda B'R_{\nabla\Delta\varphi}^{-1}A & \lambda^2 B'R_{\nabla\Delta\varphi}^{-1}B \end{pmatrix}^{-1} \tag{A.4}$$

The matrix algebra theory indicates that the following formula exists for the partitioned inverse (Golub et al., 1989):

$$\begin{bmatrix} A_{11} & A_{12} \\ A_{21} & A_{22} \end{bmatrix}^{-1} = \begin{bmatrix} * & * \\ * & F_2 \end{bmatrix}$$

$$F_2 = (A_{22} - A_{21}A_{11}^{-1}A_{12})^{-1}$$

Applying above partitioned inverse to (A.4) gives:

$$Q_{\nabla\Delta\hat{N}} = \left[\lambda^2 B'R_{\nabla\Delta\varphi}^{-1}B - \lambda^2 C'R_{\nabla\Delta\varphi}^{-1}A\left(H'R_{ins}^{-1}H + A'R_{\nabla\Delta\rho}^{-1}A + A'R_{\nabla\Delta\varphi}^{-1}A\right)^{-1}A'R_{\nabla\Delta\varphi}^{-1}B\right]^{-1} \tag{A.5}$$

With the updating formula in the matrix algebra (Golub et al., 1989):

$$[A - BCB']^{-1} = A^{-1} + A^{-1}B[C^{-1} - B'A^{-1}B]^{-1}B'A^{-1}$$

Another form of equation (A.5) can be obtained:

$$\begin{aligned} Q_{\nabla\Delta\hat{N}} = \frac{1}{\lambda^2}[&\left(B'R_{\nabla\Delta\varphi}^{-1}B\right)^{-1} + \left(B'R_{\nabla\Delta\varphi}^{-1}B\right)^{-1}BR_{\nabla\Delta\varphi}^{-1}A(H'R_{ins}^{-1}H + A'R_{\nabla\Delta\rho}^{-1}A + A'R_{\nabla\Delta\varphi}^{-1}A \\ &- A'R_{\nabla\Delta\varphi}^{-1}B)A'R_{\nabla\Delta\varphi}^{-1}B] \end{aligned}$$

i.e.:

$$Q_{\nabla\Delta\hat{N}} = \frac{1}{\lambda^2}[R_{\nabla\Delta\varphi}^{*} + R_{\nabla\Delta\varphi}^{*}B'R_{\nabla\Delta\varphi}^{-1}[H'R_{ins}^{-1}H + A'R_{\nabla\Delta\rho}^{-1}A]^{-1}A'R_{\nabla\Delta\varphi}^{-1}BR_{\nabla\Delta\varphi}^{*}] \tag{A.6}$$

where

$$R^{*}_{\nabla\Delta\varphi} = \left(B' R^{-1}_{\nabla\Delta\varphi} B\right)^{-1} \tag{A.7}$$

From the special form of C as indicated by equation (3.5) it can be seen that $R^{*}_{\nabla\Delta\varphi}$ is a $k \times k$ matrix that is the linear combinations of columns and rows in $R^{-1}_{\nabla\Delta\varphi}$.

APPENDIX B

GPS Data Specification (Lines 1 – 10)

Table B.1 GPS Data Specifications

Line	Description	Contents
1	-	GPS start time (seconds), GPS end time (seconds), Base satellite PRN,
2	-	Code measurement type (0 – CA, 1-L1, 2-L2), carrier phase measurement type (0,1 – L1, 2 – L2, 3 – widelane), GPS time type (1 – transmit time, 2 – receive time)
3	-	Cut off evaluation (degree), tropospheric correction flag (0 – NO, 1 - YES)
4	Coordinates of the monitor station	Coordinate type (0 – geocentric, 1 – ellipsoidal), x (latitude), y (longitude), z (height)
5	Approximate coordinates of the remote station	Coordinate type (0 – geocentric, 1 – ellipsoidal), x (latitude), y (longitude), z (height)
6	-	Satellites to be rejected in the data process, space delimited
7	-	GPS static start time (seconds), GPS static end time (seconds)
8	-	A full file path to the GPS data of the base station
9	-	A full file path to the GPS data of the remote station
10	-	A full file path to the GPS ephemeris data

INS Data Specification(lines 11 – 17)

Table B.2 INS Data Specification

Line	Description	Contents
11	-	A full path to the IMU data
12	-	INS start time (seconds), fine alignment period (seconds) , frequency (HZ)
13	Initial variances for the KALMAN filter	Misalignment x (degree^2), y (degree^2), z (degree^2), latitude (m^2), longitude (m^2), north velocity (m/s)^2, south velocity (m/s)^2, height (meter^2), vertical velocity(m/s)^2, gyro drift x (degree/hr)^2, drift y (degree/hr)^2, drift z (degree/hr)^2, accl. bias x (m/s^2)^2, bias y (m/s^2)^2, bias z(m/s^2)^2,
14	System disturbance specification (spectral densities)	Misalignment x (degree^2), y (degree^2), z (degree^2), latitude (m^2), longitude (m^2), north velocity (m/s)^2, south velocity (m/s)^2, height (meter^2), vertical velocity (m/s)^2, gyro drift x (degree/hr)^2, drift y (degree/hr)^2, drift z (degree/hr)^2, accl. bias x (m/s^2)^2, bias y (m/s^2)^2, bias z(m/s^2)^2,
15	ZUPT variances	Variance (m/s)^2
16	Lever arm configuration	X (m), y (m), z (m)
17	Correlation time of gyro drift and accelerometer bias	Gyro x (seconds), y (seconds), z (seconds), accelerometer x (seconds), y (seconds), z (seconds)

Miscellaneous(lines 18 – 20)

Table B.3 Miscellaneous Specifications

Line	Description	Contents
18	Data process mode	Data process mode (0 – INS Only, 1 – GPS Only, 2 – INS/GPS loose coupling, 3 – INS/GPS tight coupling 1, 4 - INS/GPS integration with centralized filter structure)
19	INS Aiding Flag	INS aiding mode (0 – No aiding, 1 – YES)
20	Output file prefix	Prefix (e.g. van, aircraft etc.)

Table B.4 Formats of Output Files

Output File	Description	Format
*.GPS	GPS navigation solution	GPS time (seconds), latitude (degree), variance (m), longitude (degree), variance (m2), height (m^2), variance (m^2), north velocity (m/s), variance $(m/s)^2$, south velocity (m/s), variance $(m/s)^2$, vertical velocity (m/s), variance $(m/s)^2$
*.AMB	GPS ambiguity resolution results	GPS time (seconds), integer flag (0 – float, 1 – fixed), number of integer candidates, ADOP (cycles), PRN#1, residual (cm), PRN#2, residual (cm), ……
*.SLP	Cycle slip detection summary	GPS time (seconds), PRN#1, cycle slips (cycles), PRN#2, cycle slips (cycles),……
*.ALG	INS coarse alignment results	GPS time (seconds), roll (degree), pitch (degree), yaw (degree)
*.ALG	INS fine alignment results (presented after coarse alignment results)	GPS time (seconds), roll (degree), variance ($degree^2$), pitch (degree), variance ($degree^2$), yaw (degree), variance ($degree^2$)
*.INS	INS navigation or INS/GPS integration results	GPS time (seconds), latitude (degree), variance (m), longitude (degree), variance (m^2), height (m^2), variance (m^2), north velocity (m/s), variance $(m/s)^2$, south velocity (m/s), variance $(m/s)^2$, vertical velocity (m/s), variance $(m/s)^2$, roll (degree), variance ($degree^2$), pitch (degree), variance ($degree^2$), yaw (degree), variance ($degree^2$)